

**PREMATURE ASPHALT CONCRETE
PAVEMENT CRACKING**

Final Report

SPR 734

PREMATURE ASPHALT CONCRETE PAVEMENT CRACKING

Final Report

SPR 734

by
R. Christopher Williams, Professor
and R. Shaidur
Institute for Transportation
Iowa State University
2711 South Loop Drive, Suite 4700
Ames, Iowa 50010

for

Oregon Department of Transportation
Research Section
555 13th Street NE, Suite 1
Salem OR 97301

and

Federal Highway Administration
400 Seventh Street, SW
Washington, DC 20590-0003

June 2015

1. Report No. FHWA-OR-RD-15-16		2. Government Accession No.		3. Recipient's Catalog No.	
4. Title and Subtitle Premature Asphalt Concrete Pavement Cracking				5. Report Date -June 2015-	
				6. Performing Organization Code	
7. Author(s) R. Christopher Williams, Professor and R. Shaidur				8. Performing Organization Report No.	
9. Performing Organization Name and Address Institute for Transportation Iowa State University 2711 South Loop Drive, Suite 4700 Ames, Iowa 50010				10. Work Unit No. (TRAIS)	
				11. Contract or Grant No.	
12. Sponsoring Agency Name and Address Oregon Dept. of Transportation Research Section and Federal Highway Admin. 555 13 th Street NE, Suite 1 400 Seventh Street, SW Salem, OR 97301 Washington, DC 20590-0003				13. Type of Report and Period Covered Final Report	
				14. Sponsoring Agency Code	
15. Supplementary Notes					
16. Abstract-Recently, the Oregon Department of Transportation (ODOT) has identified hot mix asphalt concrete (HMAC) pavements that have displayed top-down cracking within three years of construction. The objective of the study was to evaluate the top-down cracked pavement sections and compare the results with the non-cracked pavement sections. Research involved evaluating six surface cracked pavements and four non-cracked pavement sections. The research included extensive field and laboratory investigations of the 10 pavement sections by conducting distress surveys, falling weight deflectometer (FWD) testing, dynamic cone penetrometer (DCP) testing, and coring from the cracked and non-cracked pavement sections. Cores were then subjected to a full laboratory-testing program to evaluate the HMAC mixtures and binder rheology. The laboratory investigation included dynamic modulus, indirect tensile (IDT) strength, and specific gravity testing on the HMAC cores, binder rheological tests on asphalt binder and aggregate gradation analysis. The FWD and DCP tests indicated that top-down cracked pavement sections were structurally sound, even some of the sections with top-down cracking showed better structural capacity compared to non-cracked sections. The study also found that top-down cracking initiation and propagation were independent of pavement cross-section or the HMAC thickness. The dynamic modulus testing indicated that cores from all the top-down cracked pavement sections except one section (OR 140) possessed stiffer mixtures than that of non-cracked pavement sections. All four non-cracked pavement areas were found to be exhibiting fairly high IDT strength, and low variability in IDT strength and HMAC density when compared to top-down cracked sections as indicated by the IDT strength tests and air void analysis. Asphalt binder rheological test result indicated that asphalt binders from all the top-down cracked sections except OR140 showed higher complex shear modulus (stiffer binder) compared to non-cracked pavement sections. The study concluded that top-down cracking could be caused by a number of contributors such as stiffer HMAC mixtures, mixture segregation, binder aging, low HMAC tensile strength, and high variability in tensile strength or by combination of any.					
17. Key Words			18. Distribution Statement Copies available from NTIS, and online at http://www.oregon.gov/ODOT/TD/TP_RES/		
19. Security Classification (of this report)- Unclassified		20. Security Classification (of this page)- Unclassified		21. No. of Pages 182	22. Price

SI* (MODERN METRIC) CONVERSION FACTORS

APPROXIMATE CONVERSIONS TO SI UNITS					APPROXIMATE CONVERSIONS FROM SI UNITS				
Symbol	When You Know	Multiply By	To Find	Symbol	Symbol	When You Know	Multiply By	To Find	Symbol
<u>LENGTH</u>					<u>LENGTH</u>				
in	inches	25.4	millimeters	mm	mm	millimeters	0.039	inches	in
ft	feet	0.305	meters	m	m	meters	3.28	feet	ft
yd	yards	0.914	meters	m	m	meters	1.09	yards	yd
mi	miles	1.61	kilometers	km	km	kilometers	0.621	miles	mi
<u>AREA</u>					<u>AREA</u>				
in ²	square inches	645.2	millimeters squared	mm ²	mm ²	millimeters squared	0.0016	square inches	in ²
ft ²	square feet	0.093	meters squared	m ²	m ²	meters squared	10.764	square feet	ft ²
yd ²	square yards	0.836	meters squared	m ²	m ²	meters squared	1.196	square yards	yd ²
ac	acres	0.405	hectares	ha	ha	hectares	2.47	acres	ac
mi ²	square miles	2.59	kilometers squared	km ²	km ²	kilometers squared	0.386	square miles	mi ²
<u>VOLUME</u>					<u>VOLUME</u>				
fl oz	fluid ounces	29.57	milliliters	ml	ml	milliliters	0.034	fluid ounces	fl oz
gal	gallons	3.785	liters	L	L	liters	0.264	gallons	gal
ft ³	cubic feet	0.028	meters cubed	m ³	m ³	meters cubed	35.315	cubic feet	ft ³
yd ³	cubic yards	0.765	meters cubed	m ³	m ³	meters cubed	1.308	cubic yards	yd ³
NOTE: Volumes greater than 1000 L shall be shown in m ³ .									
<u>MASS</u>					<u>MASS</u>				
oz	ounces	28.35	grams	g	g	grams	0.035	ounces	oz
lb	pounds	0.454	kilograms	kg	kg	kilograms	2.205	pounds	lb
T	short tons (2000 lb)	0.907	megagrams	Mg	Mg	megagrams	1.102	short tons (2000 lb)	T
<u>TEMPERATURE (exact)</u>					<u>TEMPERATURE (exact)</u>				
°F	Fahrenheit	(F-32)/1.8	Celsius	°C	°C	Celsius	1.8C+32	Fahrenheit	°F

*SI is the symbol for the International System of Measurement

ACKNOWLEDGEMENTS

This research was sponsored by the Oregon Department of Transportation (ODOT) and the Federal Highway Administration (FHWA) under this project titled “Premature Asphalt Concrete Pavement Cracking”. The authors gratefully acknowledge ODOT engineers for all the technical assistance and data provided. This research study would not have been possible without the contribution of a number of individuals. The authors would like to acknowledge the significant efforts of Paul Ledtje and Andy Cascione from ISU and the technical advisory panel members Justin G. Moderie, John Coplantz, Larry Ilg, and Anthony Bosen. The authors would also like to extend their gratitude toward Norris Shippen (project coordinator) for his cooperation and assistance provided throughout this research. The contents of this paper reflect the views of the authors, who are responsible for the accuracy of the facts and data presented herein, and do not necessarily reflect the official policies of the ODOT and FHWA. This paper does not constitute a standard, specification, or regulation.

DISCLAIMER

This document is disseminated under the sponsorship of the Oregon Department of Transportation and the United States Department of Transportation in the interest of information exchange. The State of Oregon and the United States Government assume no liability of its contents or use thereof.

The contents of this report reflect the view of the authors who are solely responsible for the facts and accuracy of the material presented. The contents do not necessarily reflect the official views of the Oregon Department of Transportation or the United States Department of Transportation.

The State of Oregon and the United States Government do not endorse products of manufacturers. Trademarks or manufacturers’ names appear herein only because they are considered essential to the object of this document.

This report does not constitute a standard, specification, or regulation.

TABLE OF CONTENTS

1.0	INTRODUCTION.....	1
1.1	BACKGROUND	1
1.2	RESEARCH PROBLEM STATEMENT.....	2
1.3	RESEARCH OBJECTIVES.....	2
1.4	REPORT ORGANIZATION	3
2.0	LITERATURE REVIEW	2
2.1	BACKGROUND AND INTRODUCTION	2
2.2	STAGES OF TOP-DOWN CRACKING	4
2.3	CAUSES AND MECHANISMS OF TOP-DOWN CRACKING.....	5
2.4	TOP-DOWN CRACKING MODEL USED IN MEPDG.....	9
2.5	ENERGY RATIO CONCEPT	12
2.6	PREVENTION AND REHABILITATION OF TOP-DOWN CRACKING.....	14
3.0	RESEARCH PLAN DEVELOPMENT	16
3.1	EXPERIMENTAL PLAN AND SITE SELECTION	16
3.2	FIELD WORK PLAN	17
3.3	LABORATORY TESTING PLAN	17
4.0	FIELD AND LABORATORY INVESTIGATION	20
4.1	FIELD INVESTIGATION	20
4.1.1	<i>Distress Survey</i>	20
4.1.2	<i>Falling Weight Deflectometer Testing</i>	23
4.1.2.1	Temperature Correction for HMA Modulus.....	25
4.1.2.2	HMA Pavement Temperature Prediction	25
4.1.2.3	Temperature Correction for HMA Modulus.....	26
4.1.2.4	Structural Capacity.....	26
4.1.3	<i>Dynamic Cone Penetrometer Test</i>	28
4.2	LABORATORY TESTING.....	31
4.2.1	<i>Dynamic Modulus Testing</i>	31
4.2.1.1	Dynamic Modulus.....	31
4.2.1.2	Dynamic Modulus Testing.....	33
4.2.1.3	Dynamic Modulus Master Curve	35
4.2.2	<i>Indirect Tensile Strength</i>	37
4.2.3	<i>Specific Gravity Tests</i>	39
4.2.4	<i>Binder Rheological Properties Test</i>	40
4.2.4.1	Dynamic Shear Rheometer Test.....	40
4.2.4.2	Bending Beam Rheometer	41
5.0	RESULTS AND DISCUSSION	44
5.1	FIELD INVESTIGATION RESULTS.....	44
5.1.1	<i>Falling Weight Deflectometer Test Results</i>	44
5.1.1.1	Deflection Data	44
5.1.1.2	Backcalculated Layer Moduli	51
5.1.1.3	Structural Capacity.....	63
5.1.2	<i>Dynamic Cone Penetrometer Test Results</i>	64
5.1.3	<i>Core Thickness Data</i>	70
5.2	LABORATORY TEST RESULTS	71

5.2.1	<i>Dynamic Modulus Test Results</i>	71
5.2.2	<i>Indirect Tensile Strength Test Results</i>	76
5.2.3	<i>Air Void Analysis Results</i>	77
5.2.4	<i>Binder Rheological Test Results</i>	78
5.2.4.1	DSR Test Results at High Temperature.....	79
5.2.4.2	DSR Test Results at Intermediate Temperature.....	80
5.2.4.3	Frequency Sweep Tests Results.....	81
5.2.4.4	BBR Test Results.....	89
5.2.5	<i>Aggregate Gradation and Binders</i>	90
6.0	SUMMARY, CONCLUSION AND RECOMMENDATIONS	94
6.1	SUMMARY AND CONCLUSIONS.....	94
6.2	RECOMMENDATIONS.....	95
6.3	RECOMMENDATIONS FOR FUTURE STUDY.....	96
7.0	REFERENCES	98

APPENDIX A: FWD DEFLECTION DATA

APPENDIX B: BACKCALCULATED STIFFNESS MODULUS

APPENDIX C: DYNAMIC MODULUS TEST RESULTS DATA

APPENDIX D: DSR FREQUENCY TEST RESULTS DATA

APPENDIX E: CORE PICTURES OF TOP-DOWN CRACKED SECTIONS

APPENDIX F: CORES INFORMATION OF VISUAL OBSERVATION

LIST OF TABLES

Table 4.1:	Summary of Field Condition Distress Surveys.....	21
Table 4.2:	Geophone Spacing Used in FWD Testing.....	25
Table 4.3:	Temperatures and Frequencies used in Frequency Sweep Procedure.....	41
Table 5.1:	Coefficient of Variation of the Measured Deflection Data.....	50
Table 5.2:	Input Used in the Backcalculation Process.....	51
Table 5.3:	Temperature Corrected Backcalculated Moduli.....	53
Table 5.4:	Coefficients of Variation of the Backcalculated Layer Moduli.....	55
Table 5.5:	Subgrade Resilient Modulus, Effective Modulus and Effective Structural Number Backcalculated from FWD Test Results.....	64
Table 5.6:	CBR and Modulus Values Estimated from PR through Empirical Correlations.....	69
Table 5.7:	Variation in Core Thickness.....	70
Table 5.8:	Summary of Dynamic Modulus (E*) Test Results.....	72
Table 5.9:	Indirect Tensile (IDT) Strength Test Results.....	76
Table 5.10:	Air Voids Analysis Results.....	78
Table 5.11:	High Temperature Performance Grade (PG).....	80
Table 5.12:	Minimum Temperature for Fatigue Cracking in Asphalt Binder.....	81
Table 5.13:	BBR Test Results.....	89
Table 5.14:	Low Temperature Performance Grade (PG).....	90
Table 5.15:	PG Grade and % Rap.....	90

LIST OF FIGURES

Figure 1.1:	Pictures Showing the Development of Top-Down Cracking.....	2
Figure 2.1:	Lane Exhibiting Surface Initiated Top-Down Cracking in Both Wheelpaths (<i>Myers et al. 2001</i>).....	3
Figure 2.2:	Core Extracted from Wheelpath Shows Top-Down Cracking (<i>Myers et al. 2001</i>).....	3
Figure 2.3:	Photographs Illustrating the Development of Top-Down Cracking (<i>Svasdisant et al. 2002</i>).....	4

Figure 2.4: Segregation at the Bottom of Pavement lift (<i>Harmelink et al. 2008</i>).....	7
Figure 2.5: Paver Top View and Associated top-Down Longitudinal cracks (<i>Harmelink et al. 2008</i>)	8
Figure 2.6: Energy Ratio for 27 Field Test Sections in Florida (<i>Kim et al. 2009</i>).....	12
Figure 2.7: Description of Parameters Obtained from (a) Resilient Modulus, (b) Creep Compliance, and (c) Strength Tests (<i>Kim et al. 2009</i>).....	13
Figure 2.8: Inverse Tensile Strain at Top of the Asphalt Layer versus Energy Ratio (<i>Kim et al. 2009</i>)	14
Figure 3.1: Proposed Experimental Plan	16
Figure 3.2: Designation of the Test Sections in the Study.....	17
Figure 3.3: Tests on Asphalt Mix Cores and Asphalt Binder	18
Figure 4.1: Top-Down and Transverse Cracking on Section OR238-C	21
Figure 4.2: Top-Down Cracking on Section OR221-C	22
Figure 4.3: Top-Down Cracking on Section OR99*-C	22
Figure 4.4: Top-Down and Transverse Cracking on Section OR99EB-C	23
Figure 4.5: FWD Testing Used by ODOT	24
Figure 4.6: Schematic of standard loading configuration and deflection basin (<i>Pellinen et al. 2004</i>)	24
Figure 4.7: Schematic of Dynamic Cone Penetrometer (<i>Deepika and Chakravarthi 2012</i>).....	30
Figure 4.8: Photos of Dynamic Cone Penetrometer Testing	31
Figure 4.9: Stress and Strain of Typical Viscoelastic Materials under Sinusoidal Loading (<i>Garcia and Thompson 2007</i>).....	32
Figure 4.10: Specimen Set-Up for Dynamic Modulus Testing in IDT Mode.....	34
Figure 4.11: UTM-25 Machine for Dynamic Modulus Testing	35
Figure 4.12: Results of Dynamic Modulus Test and Data Shifting.....	37
Figure 4.13: Test Data Shifted to Form Master Curve	37
Figure 4.14: Specimen Set-Up for IDT Strength Test.....	38
Figure 4.15: Failure Mode in IDT Strength Test.....	39
Figure 4.16: AR1500 Dynamic Shear Rheometer	41
Figure 5.1: Deflection Profiles, OR22-U.....	45
Figure 5.2: Deflection Profiles, US97-U	45
Figure 5.3: Deflection Profiles, US20-U	46
Figure 5.4: Deflection Profiles, OR99-U.....	46
Figure 5.5: Deflection Profiles, OR238-C	47
Figure 5.6: Deflection Profiles, OR99W-C	47
Figure 5.7: Deflection Profiles, OR221-C.....	48
Figure 5.8: Deflection Profiles, OR99EB-C	48
Figure 5.9: Deflection Profiles, OR140-C.....	49
Figure 5.10: Deflection Profiles, OR99*-C.....	49
Figure 5.11: Normalized Center Deflection.....	51
Figure 5.12: Variations of Normalized Center Deflection across the Pavement Sections.....	51
Figure 5.13: Average Backcalculated Moduli (a) AC Moduli, (b) Base Moduli, and (c) Subgrade Moduli.....	56
Figure 5.14: Correlation between Elmod and BAKFAA for (a) AC Moduli, (b) Base Moduli, and (c) Subgrade Moduli.....	57
Figure 5.15: Variations of Backcalculated Layer Moduli, OR22-U	58
Figure 5.16: Variations of Backcalculated Layer Moduli, US97-U	58
Figure 5.17: Variations of Backcalculated Layer Moduli, US20-U	59
Figure 5.18: Variations of Backcalculated Layer Moduli, OR99-U.....	59
Figure 5.19: Variations of Backcalculated Layer Moduli, OR238-C	60
Figure 5.20: Variations of Backcalculated Layer Moduli, OR99W-C	60
Figure 5.21: Variations of Backcalculated Layer Moduli, OR221-C.....	61
Figure 5.22: Variations of Backcalculated Layer Moduli, OR99EB-C.....	61
Figure 5.23: Variations of Backcalculated Layer Moduli, OR99EB-C.....	62
Figure 5.24: Variations of Backcalculated Layer Moduli, OR140-U.....	62
Figure 5.25: Variations of Backcalculated Layer Moduli, OR99*-C	63
Figure 5.26: Average Penetration Resistance (PR) of the Test Sections	65
Figure 5.27: DCP Penetration Resistance, OR22-U	65
Figure 5.28: DCP Penetration Resistance, US97-U.....	66
Figure 5.29: DCP Penetration Resistance, US20-U.....	66

Figure 5.30: DCP Penetration Resistance, OR99-U	67
Figure 5.31: DCP Penetration Resistance, OR238-C	67
Figure 5.32: DCP Penetration Resistance, OR221-C	68
Figure 5.33: DCP Penetration Resistance, OR99EB-C	68
Figure 5.34: DCP Penetration Resistance, OR99*-C	69
Figure 5.35: Average Core Thickness of the Sections	71
Figure 5.36: Dynamic Modulus Master Curves of All the Projects	74
Figure 5.37: Comparison of Average Dynamic Modulus for (i) Frequency 0.00001 Hz, (ii) Frequency 0.1 Hz, and (iii) Frequency 10 Hz	75
Figure 5.38: Comparison of IDT Strength Test Results	77
Figure 5.39: Comparison of Air Voids (%) Test Results	78
Figure 5.40: Variation of Binder Complex Shear Modulus at High Temperatures	80
Figure 5.41: Variation of $ G^* \sin(\delta)$ at Intermediate Temperatures	81
Figure 5.42: Master Curves, OR22-U	82
Figure 5.43: Master Curves, US97-U	82
Figure 5.44: Master Curves, US20-U	83
Figure 5.45: Master Curves, OR99-U	83
Figure 5.46: Master Curves, OR238-C	84
Figure 5.47: Master Curves, OR99W-C	84
Figure 5.48: Master Curves, OR221-C	85
Figure 5.49: Master Curves, OR99EB-C	85
Figure 5.50: Master Curves, OR140-C	86
Figure 5.51: Master Curves, OR99*-C	86
Figure 5.52: Complex Shear Modulus Master Curves	87
Figure 5.53: Master Curves for Phase Angle	88
Figure 5.54: Gradation Analysis	91
Figure 5.55: Original Mix Design % Passing #200 Sieve	91
Figure 5.56: Binder Content by Weight	92

1.0 INTRODUCTION

1.1 BACKGROUND

It has been well recognized that cracking of hot-mix asphalt concrete (HMAC) pavements is a major mode of premature failure. Currently, four major mode of failure associated with HMAC cracking are identified: (*Birgisson et al., 2002, Von Quintus and Moulthrop, 2007*) 1) fatigue cracking, also known as bottom-up cracking, which starts at the bottom of the HMAC pavement and propagates upward to the surface of the pavement, 2) top-down cracking, also known as longitudinal cracking, initiating at the top of the asphalt pavement layer in a direction along the wheel path and propagating down-ward, 3) thermal cracking, and 4) reflective cracking, in which existing cracks or joints cause stress concentrations that result in crack propagation through an HMAC overlay.

Notional investigations into cracking have identified areas where the cracking is top-down versus bottom-up. While both are serious, bottom-up cracking typically indicates the pavement structure was under designed indicating a need to change structural design practices. Top-down cracking, however, may indicate that material selection process can be fine-tuned. The only means to differentiate between top-down versus bottom-up cracking is through coring.

Traditionally, most flexible pavement design methods consider fatigue cracking initiating at the bottom of the HMA layer and propagating upward as the most critical criteria for the fatigue failure of HMA pavements. However, recent research has suggested that premature pavement fatigue failure initiates at the surface of HMA pavement and propagates downward, which is known as top-down cracking (shown in Figure 1.1). The only way to differentiate top-down cracking from bottom-up cracking is to take cores and trench sections. For years pavement engineers within the Washington State Department of Transportation (WSDOT) have observed that asphalt concrete pavements in the State of Washington have displayed longitudinal and fatigue cracks (multi-connected) that appear to crack from the top of the pavement and propagate downward. Often, the cracks stop at the interface between the wearing course and the underlying bituminous layers (a depth of about 50 mm). The top-down cracking was observed in thicker sections with thinner sections cracking full depth. Top-down cracking generally started within three to eight years of paving for pavement sections that were structurally adequate and were designed for adequate ESALs (*Uhlmeier et al., 2000*).



Figure 1.1: Pictures Showing the Development of Top-Down Cracking

1.2 RESEARCH PROBLEM STATEMENT

For over a century, highways have been paved using asphalt concrete mixes in State of Oregon as well as across the United States. However, a major problem still exists involving premature pavement failures caused by cracking, rutting, potholes etc. Recently Oregon Department of Transportation (ODOT) has constructed hot mix asphalt concrete (HMAC) pavements that have displayed premature cracking within three years of construction. Early cracking allows moisture to penetrate the pavement structure reducing the pavement section's design life and significantly increasing the life cycle cost. Also within the last several years, design and material changes occurred that may or may not have contributed to the early cracking. The changes include the continued use of relatively high recycled asphalt pavement (RAP) percentages allowed in the wearing surface; the potential use of acids recently and polymers as a binder modifications; and a shift in mix gradation levels. Construction factors like properties of the produced mix (volumetrics) and placement also play a part of the pavement performance.

1.3 RESEARCH OBJECTIVES

The objectives of the research are to determine the causes of early cracking on the State of Oregon highways system. The results of the study will be used to modify the pavement design process including modifications to the Pavement Design Guide and Mix Design Guidelines. By doing so, the ODOT will be able to design pavements that are long lasting, resulting in significant benefits to the department by reducing the life cycle cost needed to maintain the state highway system.

1.4 REPORT ORGANIZATION

The overall objective of the research is to evaluate the premature asphalt pavement cracking. The tasks toward the accomplishment of the objective are presented step by step in the next six chapters. The background and the research problem statement and objectives were presented in Chapter 1. Chapter 2 summarizes literature review with regard to premature asphalt concrete pavement cracking. Chapter 3 discusses the development of experimental plan. Chapter 4 describes the field and laboratory testing procedures employed in this study. The results of field and laboratory tests are summarized and discussed in Chapter 5. Finally, the conclusions and recommendations for future research are given in Chapter 6.

2.0 LITERATURE REVIEW

2.1 BACKGROUND AND INTRODUCTION

It has been well recognized that cracking of hot-mix asphalt (HMA) pavements is a major mode of premature failure. Currently, four major modes of failure associated with HMA cracking are identified: (Birgisson et al., 2002, Von Quintus and Moulthrop, 2007) 1) fatigue cracking, which starts at the bottom of the HMA pavement and propagates upward to the surface of the pavement, 2) top-down cracking, initiating at the top of the asphalt pavement layer in a direction along the wheel path and propagating upward, 3) thermal cracking, and 4) reflective cracking, in which existing cracks or joints cause stress concentrations that result in crack propagation through an HMA overlay.

Traditionally, most flexible pavement design methods consider fatigue cracking initiating at the bottom of the HMA layer and propagating upward as the most critical criteria for the fatigue failure of HMA pavements. However, recent research has suggested that premature pavement fatigue failure initiates at the surface of HMA pavement and propagates downward, which is known as top-down cracking (shown in Figure 2.1). A core from this pavement shown in Figure 2.2 illustrates the crack from the top and terminating in the core (Myers et al., 2001). The only way to differentiate top-down cracking from bottom-up cracking is to take cores and trench sections. For years pavement engineers within the Washington State Department of Transportation (WSDOT) have observed that asphalt concrete pavements in State of Washington have displayed longitudinal and fatigue cracks (multi-connected) that appear to crack from the top of the pavement and propagate downward. Often, the cracks stop at the interface between the wearing course and the underlying bituminous layers (a depth of about 50 mm). The top-down cracking was observed in thicker sections with thinner sections cracking full depth. Top-down cracking generally started within three to eight years of paving for pavement sections that were structurally adequate and were designed for adequate ESALs (Uhlmeier et al., 2000).

In July 1997, a section of I-25 between Colorado State Highway 7 and 120th Avenue near Denver was rehabilitated by cold milling the existing surface to a depth of 3 inch. and replacing with 3 inch. new hot mix asphalt. The 3/4 inch. (19 mm) mixture contained asphalt content of 4.8% and asphalt grade of PG 76-28. It is important to note that the project received bonus for material quality and smoothness and the mixture passed all torture tests (Hamburg and French Wheel Rutter) in the Colorado Department of Transportation's European Laboratory. Longitudinal cracks appeared in the outside lanes of both the north and southbound directions within 1 year of the project completion. The severity of the cracking ranged from low to medium and in some locations high. The occurrence of this premature cracking followed a series of investigations. The first investigation revealed that two of three cores taken over the top of existing longitudinal cracks were observed reflecting cracks through from the underlying pavement. It was identified that the reflecting cracks were due to the presence of moisture and traffic. After the first project, a statewide evaluation was conducted to identify the extent of this distress in other pavements. As a result, 28 projects were evaluated throughout the state of Colorado and 18 projects displayed top-down cracking (Harmelink et al., 2008).

A study by Myers et al. (Myers et al. 1998) in Florida reported that fatigue failure of HMA pavement in Florida was mainly caused by top-down cracking. A more recent study by Wang et al. (Wang et al. 2007) revealed that 90% cracking encountered in Florida HMA pavements were recognized as top-down cracking. This scenario is not unique to Florida. Similar results have been reported in other states and countries, including Indiana, Washington, India, Japan, Kenya, South Africa, France, Netherlands, and United Kingdom (Kim and Underwood, 2003).



Figure 2.1: Lane Exhibiting Surface Initiated Top-Down Cracking in Both Wheelpaths (Myers et al. 2001)



Figure 2.2: Core Extracted from Wheelpath Shows Top-Down Cracking (Myers et al. 2001)

2.2 STAGES OF TOP-DOWN CRACKING

Top-down cracking in hot mix asphalt pavements initiates at the pavement surface and propagates downward, sometimes throughout the entire depth of the asphalt pavement. There are three stages recognized associated with initiation and propagation of top-down cracks. (Svasdisant *et al.*, 2002). At initial stage, a single short longitudinal crack appears just outside the wheelpath. Over time, the top-down cracks grow into a second stage where the longitudinal short cracks grow longer and sister cracks develop parallel to and within 0.3 to 1 meter (1 to 3 feet) from the original cracks. Finally, the top-down cracks merge into a third stage where the parallel longitudinal cracks are connected through short transverse top-down cracks. Figure 2.3 illustrates the three stages mentioned earlier where A, B, and C represent first, second and third stages, respectively.



Figure 2.3: Photographs Illustrating the Development of Top-Down Cracking (Svasdisant *et al.*, 2002)

2.3 CAUSES AND MECHANISMS OF TOP-DOWN CRACKING

It is important that the causes and mechanisms associated with top-down cracking should be better understood to improve the cracking resistance of mixtures. This will prevent premature pavement failure, reduce significant costs incurred on highway state agencies and eventually, provide a cost-effective, long lasting pavement. There are various opinions related to mechanisms that causes top-down cracking, but there are no conclusive data to suggest that one is more applicable than the other one.

Svasdisant et al. (*Svasdisant et al. 2002*) conducted field and laboratory investigations on flexible and rubblized pavements exhibiting top down cracking. Detailed mechanistic analyses were conducted using the engineering characteristics obtained from field and laboratory test results to determine the potential for top down cracking. In the mechanistic analysis, 3-D finite element method using the ABAQUS, the CHEVRONX (a closed-form solution) and the MICHPAVE (a liner/nonlinear 2-D finite element) computer programs were used. The conclusions of the study are as follows:

- Most top down cracking are observed just outside the wheelpaths and progress in three stages.
- Surface radial tensile stress induced by wheel load and enhanced by differential stiffness due to construction (poor compaction and segregation), temperature and aging can cause top down cracking,
- Aging of asphalt binder reduces the tensile strength and tensile strain at failure of the asphalt mixture, and
- The locations of the maximum surface tensile stress predicted by the mechanistic analysis correspond very well to the locations of the filed observed top down cracking.

Baladi et al. (*Baladi et al. 2002*) studied the effects of segregation on the initiation and propagation of top down cracking in flexible pavements. Both field and forensic investigation were conducted and it was confirmed that top down cracking initiates in segregated areas. The results from the mechanistic analysis revealed that segregated areas are susceptible to fatigue cracking manifested as top down cracking.

Nunn (*Nunn 1998*) reported that surface initiated cracks, either longitudinal or transverse, were observed about 10 years after construction in UK motorways. He observed that there was no evidence of fatigue cracking in the lower bituminous base layers with thickness exceeding 180 mm-only the wearing course. The transverse cracks were related to low binder penetration values (typically about 15). He noted that the surface initiated cracking was due to horizontal tensile stresses generated by truck tires at the top of asphalt surface. Wide based tires generated the highest tensile stresses. Nunn (*Nunn 1998*) concluded based on the work performed in the Netherlands that for asphalt thickness greater than 160 mm, cracks initiated at the pavement surface and eventually penetrated to a depth of about 100 mm. He also stated that full depth cracks were observed with thinner pavement sections.

Myers et al. (*Myers et al. 1998*) observed that surface initiated cracking predominates in Florida five to ten years after construction. Based on the computer modeling, they found out that tensile stresses under the treads of the tire-not the tire edges-were the primary cause of the cracks. Further, they stated that wide based tires caused the highest tensile stresses, which confirmed the results conducted by Nunn (*Nunn 1998*). They concluded that surface initiated cracking is not a structural design issue but more related to mixture composition. They suggested that more fracture resistant mixtures be used to improve the surface initiated cracking performance of the pavement.

Gerritsen et al. (*Gerritsen et al. 1987*) observed that pavements in Netherlands were experiencing premature cracking in the wearing course. These surface cracks which did not extend into the lower bituminous base layers, occurred both inside and outside the wheelpath areas, and in some cases, soon after the construction. They reported that the surface cracking outside of the wheelpaths had low mix strength characteristics at low temperature and the surface cracks in the wheelpaths areas were largely due to radial shear forces under truck tires near the tire edges. They concluded that both load and thermal related effects could be attributed to the observed surface cracking. Their recommendation was to increase the binder film thickness to reduce early age hardening of the mixtures.

Dauzats et al. (*Dauzats et al. 1987*) reported that surface initiated cracks, either longitudinal or transverse, were observed in France and occurred typically three to five years after paving. They found that these types of surface cracks were initially caused by thermal stresses and then further propagated by traffic loads. They noted that a rapid hardening of the mix binder likely contributed to this type of pavement distress.

Studies based on measured tire/pavement contact pressures by De Beer et al. (*DeBeer et al. 1997*) and Himeno et al. (*Himeno et al. 1997*) and instrumented pavements by Dai et al. (*Dai et al. 1997*) in MinnRoad supported the view that truck tires were a primary cause of top-down cracking in asphalt concrete wearing courses.

In a study by Harmelink et al. (*Harmelink et al. 2008*), 28 projects were evaluated from a wide geographical area of Colorado and 18 sites out of 28 sites were judged exhibiting top down cracking. Of these 18 sites, 12 had visual evidence of segregation observed at the bottom of the upper pavement lift as illustrated in Figure 2.4 from mix placement, that was not visible on the surface. Other factors included percentage of air voids in the pavement, volume of effective asphalt binder, and physical properties of the asphalt binder. Figure 2.5 illustrates the segregation of the mix during placement by Harmelink et al. (2008).

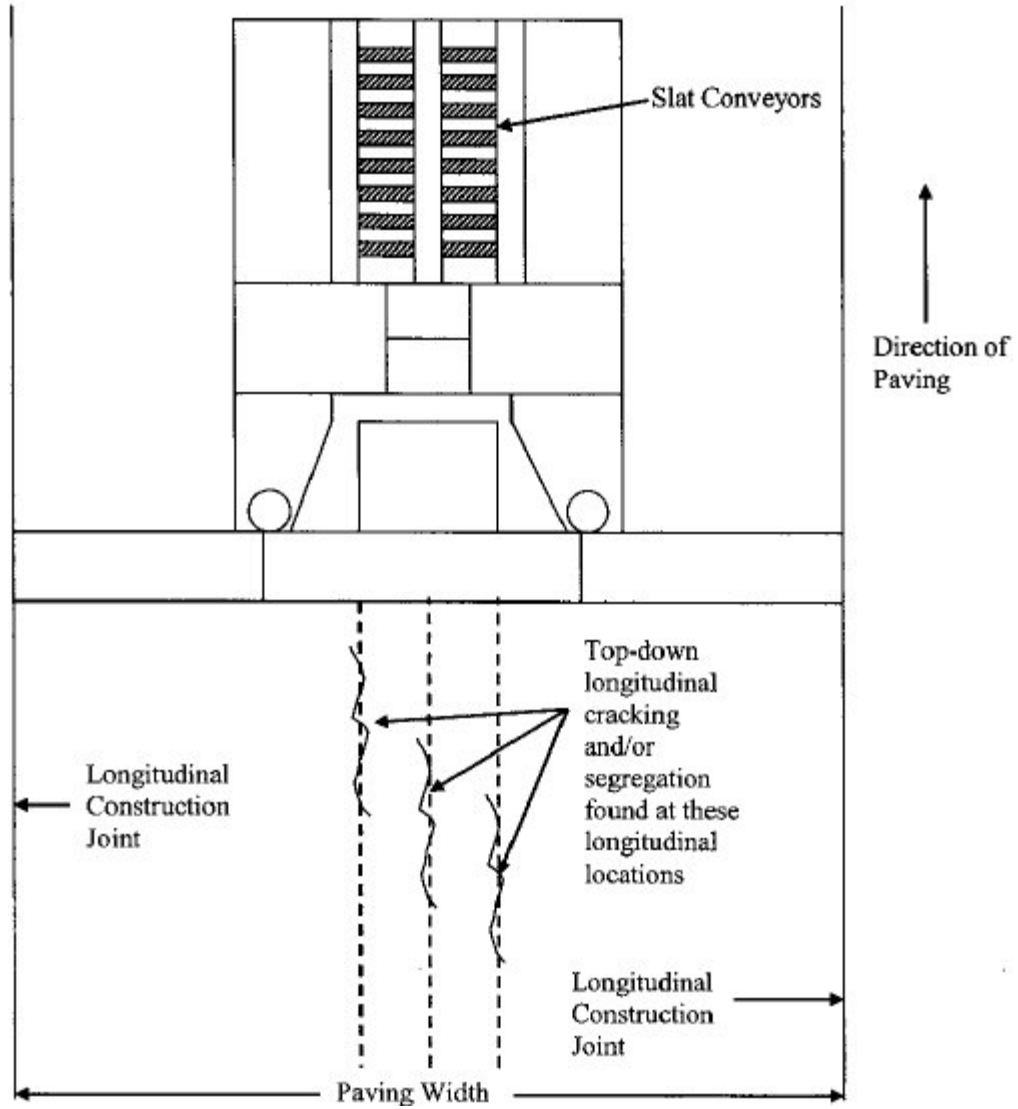


Figure 2.4: Segregation at the Bottom of Pavement lift (*Harmelink et al. 2008*)

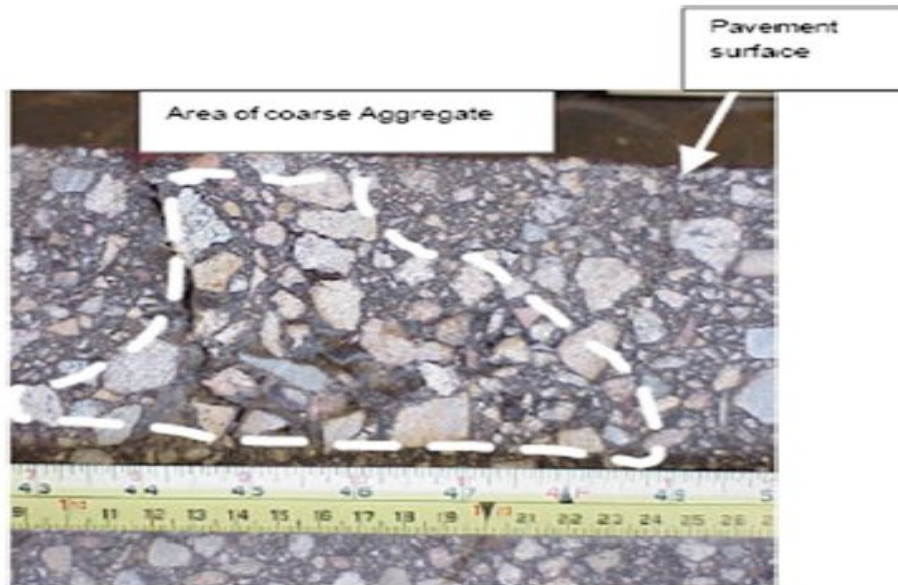


Figure 2.5: Paver Top View and Associated top-Down Longitudinal cracks (*Harmelink et al. 2008*)

A study conducted by the Illinois Department of Transportation (*Lippert 1993*) in 1993 detailed the history and investigation of longitudinal cracks in asphalt pavements. The study indicated that there is a high degree of correlation between the outside edges of the conveyors on the paver and the longitudinal cracking in the pavement. Two pavers were identified in the study that demonstrated the correlation between the longitudinal cracking in the pavement and the outside edges of the conveyor slats.

A micromechanics study on top-down cracking based on the material's microstructure by Wang et al. (*Wang et al. 2003*) indicated that top-down cracking may not necessarily initiate only at the pavement surface. It may also initiate at some distance down from the pavement surface. They concluded that both tensile-type and shear-type cracking could initiate top-down cracking. They also concluded that when the mastic is weaker or the pavement surface temperature is higher, top-down cracking most likely initiate. Therefore, a mix sensitive to rutting may also be sensitive to top-down cracking.

Myers et al. (*Myers et al. 2001*) concluded that top-down cracking can be initiated by traffic induced stresses, temperature changes, or due to their combined effect. Temperature and modulus gradients are assumed to be critical to the top-down cracking initiation and propagation.

Baladi et al. (*Baladi et al. 2003*) concluded that a segregated area in pavement due to poor construction is more prone to top-down cracking along with raveling. They also mentioned that differential stiffness between HMA courses cause a significant increase in load-induced surface tensile stresses. Nighttime temperatures produce the highest magnitude of surface tensile stress.

A study by Freitas et al. (Freitas et al. 2005) concluded that air voids, segregation and binder content have a significant effect on the top-down cracking for all temperatures. They also found that higher temperature and rutted surface contributes significantly to top-down cracking initiation. El-Basyouny and Witzak (El-Basyouny and Witzak 2005) stated that top-down cracking is caused by extremely large contact pressures at the tire edge-pavement interface in combination with highly aged thin surface layer that have become oxidized.

A study by Sridhar et al. (Sridhar et al. 2008) on the Indian Highways indicated that temperature, especially in combination with heavy axle loading, was a critical parameter influencing the top-down cracking susceptibility of the HMA layer. H. Wang and I.L. Al-Qadi (Wang and Al-Qadi 2010) concluded that at high temperatures, shear-induced top-down cracking could initiate from some distance below the pavement surface in conjunction with the distortional deformation. They also indicated that negative temperature gradient in the HMA layer and debonding under the surface layer could lead to premature top-down cracking. Ozer et al. (Ozer et al. 2011) stated that several factors contribute to the top-down cracking such as, heavy traffic and thermal loads, stiffness gradients due to binder aging, variation in bituminous characteristics between lifts, and bituminous material segregation.

There are various opinions related to mechanisms that causes top-down cracking, but there are no conclusive data to suggest that one is more applicable than the other one is (Von Quintus and Moulthrop, 2007). Based on the literature review aforementioned, the following factors are considered to be contributing to top-down cracking initiation and propagation:

- high tire and contact pressures and/or heavy wheel loads
- severe aging of the binder near the surface resulting in large modulus gradients
- combination of thermal stresses with those induced from heavy wheel loads
- mixture properties, including binder type and content, air voids, and aggregate gradation
- construction quality, including segregation and compaction procedures
- climatic conditions as well as structural conditions, including layer thickness

2.4 TOP-DOWN CRACKING MODEL USED IN MEPDG

Over the last 3 to 4 decades of pavement technology, fatigue cracking has been assumed to normally initiate at the bottom of the asphalt layer and propagate to the surface (bottom-up cracking). However, numerous recent worldwide studies have also concluded that fatigue cracking may also initiate from the top of the surface and propagate downward which is known as top-down cracking. This type of cracking is not as well defined from a mechanistic viewpoint as the more classical bottom-up cracking. However, it is a reasonable engineering assumption, with the current state of knowledge, that this distress may be due to critical tensile and/or shear stresses developed at the pavement surface and, perhaps, caused by extremely large contact pressures at the tire edge-pavement interface; coupled with highly aged (stiff) thin surface layer that have become oxidized. In this initial mechanistic attempt to model top-down cracking in the

Design Guide; the failure mechanism for this distress is hypothesized to be a result of tensile surface strains leading to fatigue cracking at the pavement surface.

The MEPDG predicts both bottom-up and top-down fatigue cracks using an incremental damage index approach. Alligator cracks are assumed to initiate at the bottom of HMA layers, while longitudinal cracks are assumed to initiate at the surface of the pavement. For both load related cracking models, the approach to calculate the allowable number of axle-load applications needed for the incremental damage index is shown using Equation 2.1.

$$N_{f-HMA} = k_{f1}(C)(C_H)\beta_{f1}(\epsilon_t)^{k_{f2}}\beta_{f2}(E_{HMA})^{k_{f3}}\beta_{f3} \quad (2.1)$$

Where:

N_{f-HMA} = Allowable number of axle-load applications for a flexible pavement and HMA overlayers

ϵ_t = Tensile strain at critical locations and calculated by the structural response model, in./in.

E_{HMA} = Dynamic modulus of the HMA measured in compression, psi

k_{f1}, k_{f2}, k_{f3} = Global field calibration parameters (from the NCHRP 1-40D re-calibration; $k_{f1}=0.007566$, $k_{f2}=-3.9492$, and $k_{f3}=-1.281$), and

$\beta_{f1}, \beta_{f2}, \beta_{f3}$ = Local or mixture specific field calibration constants; for the global calibration effort, these constants were set to 1.0

C = Correction factor, 10^M , when:

$$M = 4.84 \left(\frac{V_{be}}{V_a + V_{be}} - 0.69 \right)$$

V_a = Percent air voids in the HMA mixture (in situ only, not mixture design)

V_{be} = Effective asphalt content by volume, percent

C_H = Thickness correction term, depending on type of cracking:

For bottom-up or alligator cracking:

$$C_H = \frac{1}{0.000398 + \frac{0.003602}{1 + e^{(11.02 - 3.49H_{HMA})}}}$$

H_{HMA} = Total HMA thickness, in.

For top-down or longitudinal cracking:

$$C_H = \frac{1}{0.01 + \frac{12.00}{1 + e^{(15.676 - 2.8186H_{HMA})}}}$$

H_{HMA} = Total HMA thickness, in.

Using the calculation for allowable number of axle-load applications shown above, the MEPDG calculates an incremental damage index (ΔDI) to predict the load related cracking. The incremental damage index (DI) is calculated for each axle load interval for each axle type and truck type that is applied within a month that is subdivided into five average temperatures.

The cumulative damage index is determined by summing the incremental damage indices (refer to Equation 2.2).

$$DI = \sum (\Delta DI)_{j,m,l,p,T} = \sum \left(\frac{n}{N_{f-HMA}} \right)_{j,m,l,p,T} \quad (2.2)$$

Where:

- n = Actual number of axle load applications within a specific time period
- N_{f-HMA} = Allowable number of axle load applications for a flexible pavement and HMA overlays to fatigue cracking
- j = Axle-load interval
- m = Axle-load type (single, tandem, tridem, quad, or special axle configuration)
- l = Truck type using the truck classification groups included in the MEPDG
- p = Month
- T = Median temperature for the five temperature intervals used to subdivide Each month

The MEPDG calculates the amount of alligator area cracking and the length on LCWP based on the incremental damage index that are summed with time and different truck loadings (Equation 2.2). Different relationships were developed between the amounts of cracking and damage indices. Equation 2.3 is the relationship to predict area alligator cracking based on total lane area, while Equation 2.4 is the relationship to predict length of longitudinal cracking in the wheel paths.

Bottom initiated fatigue cracks:

$$FC_{Bottom} = \left(\frac{1}{60} \right) \left(\frac{C_4}{1 + e^{(C_1 C_1^* + C_2 C_2^* \text{Log}(DI_{Bottom} * 100))}} \right) \quad (2.3)$$

Where:

- FC_{Bottom} = Bottom initiated fatigue cracks, percent of total lane area
- C_4 = Calibration coefficients of 6,000
- C_1 = Calibration coefficients of 1.00
- C_2 = Calibration coefficients of 1.00
- C_1^* = $-2C_2^*$
- C_2^* = $-2.40874 - 39.748 (1 + H_{HMA})^{-2.856}$
 H_{HMA} = Total HMA thickness, in.
- DI_{Bottom} = Bottom incremental damage index

Surface initiated fatigue cracks:

$$FC_{Top} = 10.56 \left(\frac{C_4}{1 + e^{(C_1 - C_2 \text{Log} DI_{Top})}} \right) \quad (2.4)$$

Where:

- FC_{Top} = Surface initiated longitudinal cracks, ft/mile
- C_4 = Calibration coefficients of 1,000
- C_1 = Calibration coefficients of 7.00
- C_2 = Calibration coefficients of 3.5
- DI_{Top} = Surface incremental damage index

2.5 ENERGY RATIO CONCEPT

Energy ratio is used to evaluate the asphalt mixture's resistance to cracking. Roque et al. (Roque et al. 2006) performed an extensive study on 27 pavement sections collected from cracked and uncracked sections throughout the state of Florida to evaluate the top down cracking in flexible pavements, as shown in Figure 2.6.

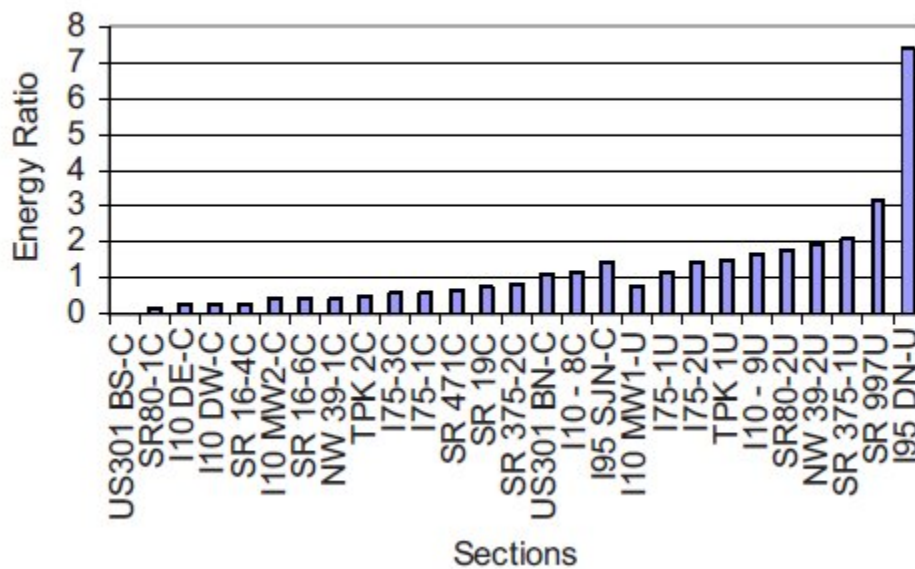


Figure 2.6: Energy Ratio for 27 Field Test Sections in Florida (Kim et al. 2009)

All the cracked sections, as represented by “C” in Figure 2.6, showed top down cracking. All the uncracked sections in Figure 2.6 are represented by “U”. Based on a parameter called energy ratio, Roque et al. (Roque et al. 2004) suggested a simple form of a crack model through the evaluation of known top-down cracking performance data. The higher the value of energy ratio, the better the top down cracking performance of the pavement. The energy ratio (ER) is given by the following equation:

$$ER = \frac{DCSE_f \cdot [7.294 \cdot 10^{-5} \cdot \sigma^{-3.1} (6.36 - S_t) + 2.46 \cdot 10^{-8}]}{m^{2.98} \cdot D_1} \quad (2.5)$$

Where $DCSE_f$ is dissipated creep strain energy at failure, σ is the tensile stress obtained at the bottom of the asphalt layer using elastic layer analysis, m and D_1 are power function parameters.

The parameters required for the top down cracking model can be obtained from resilient modulus, creep compliance and tensile strength tests. The resilient modulus, M_r is determined from the stress-strain curve obtained in resilient modulus test. The power function parameters are obtained by fitting the creep compliance curve performed using a constant load control load. The tensile strength and dissipated creep strain energy at failure are determined from the stress-strain curve of a given mixture from the strength test. Figure 2.7 shows the description of parameters determined for top down cracking model.

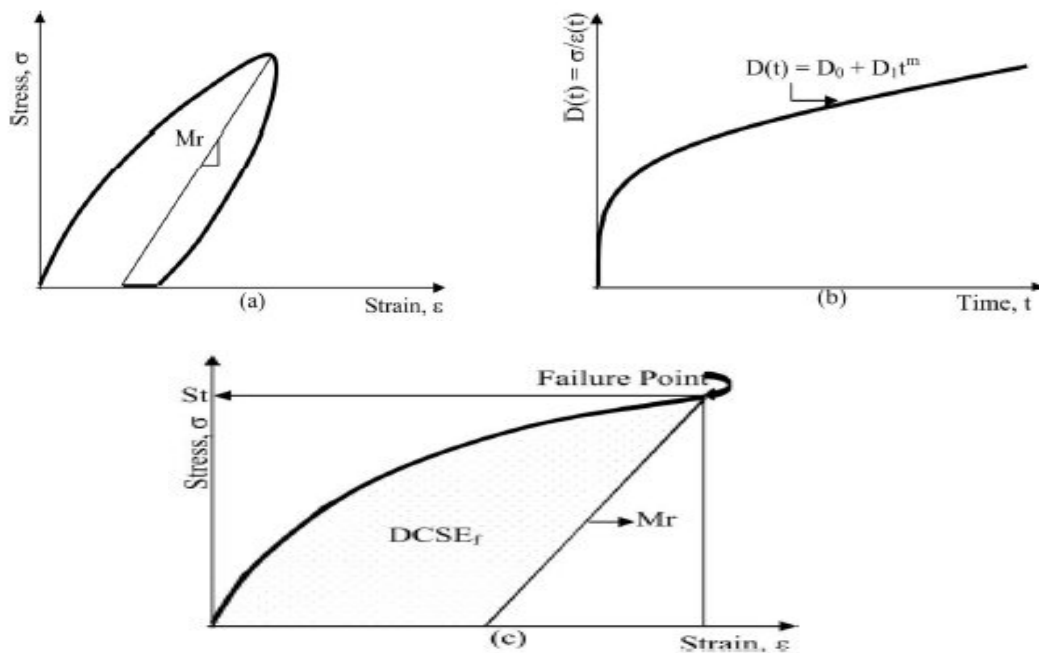


Figure 2.7: Description of Parameters Obtained from (a) Resilient Modulus, (b) Creep Compliance, and (c) Strength Tests (Kim et al. 2009)

Kim et al. (Kim et al. 2009) found that tensile strain obtained at the top is inversely related to energy ratio, if the identified tensile strain at top is a primary cause of top down cracking. Figure 2.8 shows the linear relationship between energy ratio and inverse tensile strain at top at the 50-loading cycle. The study indicated that the tensile strain at the top of asphalt layer is a primary factor affecting the top down cracking performance.

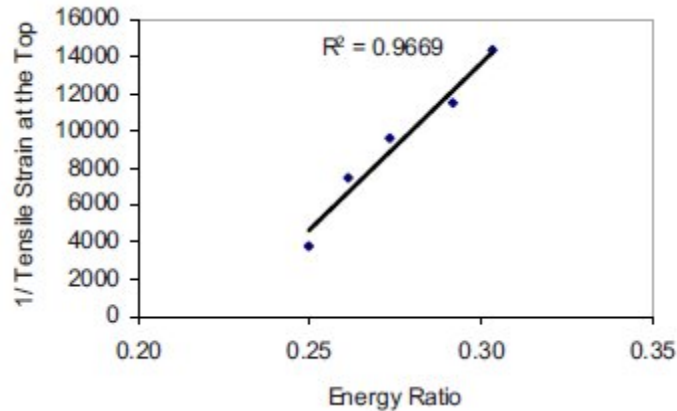


Figure 2.8: Inverse Tensile Strain at Top of the Asphalt Layer versus Energy Ratio (*Kim et al. 2009*)

2.6 PREVENTION AND REHABILITATION OF TOP-DOWN CRACKING

Pellinen et al. (*Pellinen et al. 2004*) reported recommendations related to the prevention of top-down cracking in terms of material selection, material properties and construction practices:

- In-situ air voids content should be reduced below or equal to 7% by requiring tougher density specification.
- The amount of fines in the asphalt mixture is recommended to limit to 5% to 6%.
- No changes for binder grade at this point
- Non-uniformities in the material properties should be prevented by enhancing construction practices and QC/QA work including prevention of segregation during paving.

Emery (*Emery 2006*) reported the two major potential solutions for top-down cracking focus on the most controllable factors:

- “improved heavy vehicle loadings control (weigh-in motion scales for instance - difficult but imperative for developing countries) and appropriate mechanical, axle and tire technology implementation (suspension systems and tires properly matched, inflated and kept in good operating condition - very difficult, but again imperative for developing countries); and
- improved renewable, specialized asphalt surface courses (open graded friction course, stone mastic asphalt and Superpave, for instance) with good permanent deformation (rutting) resistance, and enhanced tensile and shear stress endurance”.

Before rehabilitation strategy, top-down cracking should be distinguished from bottom-up cracking based on the knowledge of the thickness of the pavement structure and the pattern of cracking. Top-down cracking manifests itself as a longitudinal cracking in the wheelpath area or

in the center of the lane. If layer thickness is above 200 mm it is unlikely that cracks will penetrate deeper than through the surface layer in the pavement. Coring from a few locations in the pavement and examining cracks can be used to verify the top-down cracking. A structural analysis based on falling weight deflectometer (FWD) testing must be performed to confirm that the cracking has not weakened the pavement structure. If the pavement structural capacity is good, then the pavement can be rehabilitated by milling and replacing the surface mix. The selection of the materials for rehabilitation strategy should be based on the structural capacity of the pavement. The material selection for rehabilitation should follow the recommendations given to prevent top-down cracking (*Pellinen et al. 2004*).

Segregation was apparent around the top down cracking studied by Harmelink et al. (*Harmelink et al. 2008*). As moisture infiltrates these cracks, progressive deterioration of the pavement around the cracks will occur. Therefore, sealing the cracks should reduce the moisture infiltration if the crack has not widened significantly. Other forms of rehabilitation discussed include milling the affected area surrounding the crack and replacing with hot mix asphalt. However, this repair method has not been successful in the past (*Shuler 2007*) and is discouraged due to the creation of two longitudinal cracks adjacent to the crack being repaired.

Harmelink et al. (*Harmelink et al. 2008*) concluded that the occurrence of top down cracking reduced through the changes to the Superpave mix design process during 2003. The changes included an increase in the asphalt binder content in the mix; which appeared to reduce the potential for segregation. This increase in binder content was accomplished by reducing the number of design gyrations as a function of traffic volume.

Uhlmeier et al. (*Uhlmeier et al. 2000*) studied top-down cracking in the State of Washington and reported that rehabilitation strategy for top-down cracking should be based on the severity of cracking. If the pavement surface is cracking within the top lift, possibly caused by stripping, rotomilling the top lift of asphalt and inlaying would be the preferred rehabilitation option. For some longitudinal cracking, pavement repair prior to overlaying or just overlaying the roadway may be the best choice depending upon the severity of the cracks. Rehabilitation for full depth cracked areas, depending upon the severity of distress, may require removal and replacement of fatigued pavement.

3.0 RESEARCH PLAN DEVELOPMENT

3.1 EXPERIMENTAL PLAN AND SITE SELECTION

The proposed experimental plan summarized in Table 3.1 below represents sampling 10 pavements, 6 with top-down cracking and 4 without top-down cracking. ODOT pavement management databases have been explored to identify top performers and early failures. Database investigation also included reviewing pavement designs, mix designs and construction history. This represents a factorial plan based upon the main effects- with and without top-down cracking, and ESAL level (low vs. high trafficking levels). Each of the pavements with top-down cracking would need 10 cores of 6-inch diameter, 5 next to a crack and 5 away from the crack. Prior to removing the 10 cores, the top-down cracking would need to be verified by coring on a crack. Overall, this would allow for determination of what led to the crack initiation and propagation at a particular location and thus identify potential differences within the same pavement section. Sampling pavements that have not undergone top-down cracking, 5 6-inch diameter cores, will allow for comparison of good performing pavements as compared to ones that are experiencing inadequate performance. These comparisons will allow for determining the mechanisms leading to good performing pavements and those experiencing top down cracking. Table 3.2 illustrates the designation of the pavement sections that will be used in this study.

Figure 3.1: Proposed Experimental Plan

Pavement Performance	Location	ESAL Level							
		Low Volume Traffic				High Volume Traffic			
		Proposed Candidates				Proposed Candidates			
		Name	Highway Number	Begin MP	End MP	Name	Highway Number	Begin MP	End MP
Pavements with Top-Down Cracking	Next To Crack	OR221	150	17.3	20.15	OR99EB	072	0.47	3.41
		OR238	272	38.09	38.75	OR99W	091	21.8	23.76
		OR140	270	53.6	53.79	OR99	091	108.82	109.65
	Away From Crack	OR221	150	17.3	20.15	OR99EB	072	0.47	3.41
		OR238	272	38.09	38.75	OR99W	091	21.8	23.76
		OR140	270	53.6	53.79	OR99*	091	108.82	109.65
Pavements without Top-Down Cracking	N/A	OR22	162	12.11	13.8	US20	007	1.11	2.29
						US97	004	114.25	115.2
						OR99	091	108.82	109.65

*Denotes bad (cracked) performing section of OR99

Figure 3.2: Designation of the Test Sections in the Study

Test Section	Route	Cracking	Designation Used in this Study
OR22:Sublimity Intchg Sect (RW2-WB)	OR22	NO	OR22-U
OR238: Beg. Div Hwy-Jct Hwy 063	OR238	YES	OR238-C
OR 99W:Brutscher St-Jct Hwy 151	OR99W	YES	OR99W-C
OR 221: N. Salem-Orchard Heights Rd	OR221	YES	OR221-C
OR 99EB: Jct Hwy 001-Comm. St.	OR99EB	YES	OR99EB-C
US97: NW Wimp Way-Terrebonne	US97	NO	US97-U
US20: NE 11th St-Purcell Blvd	US20	NO	US20-U
OR 140: Aspen Lake Rd-Boat Landing	OR140	YES	OR140-C
OR99: Junction City 1 (Cracked)	OR99	YES	OR99*-C
OR99: Junction City 1 (Uncracked)	OR99	NO	OR99-U

3.2 FIELD WORK PLAN

This phase included field work including identification of pavements with and without top-down cracking, and field sampling. It is difficult to identify pavements with top-down cracking through examining pavement performance records and only through forensic field study that includes coring, can identify top-down cracking. Thus candidate pavements for top-down cracking evaluation would likely need to be identified through a combination of paper records review, discussion with ODOT personnel, as well as utilizing information gathered from the recently completed M-E Pavement Design Guide calibration project. Once pavements that have been identified as top-down cracking candidates, field sampling via coring will be done for subsequent assessment. It is important to verify top-down cracking via sampling on top of cracks as well as sampling next to the crack and well away for the cracks. Before coring is done, field condition survey and falling weight deflectometer (FWD) testing will be conducted. Also, dynamic cone penetrometer (DCP) testing on base/subbase as well as geoprobe samples up to 4 feet deep at core locations after coring. This field testing information will subsequently be used to assess the adequacy of the pavement structure. Visible assessment of drainage conditions will also done on site. In this phase the following tasks are to be completed:

- Field condition survey compatible with MEPDG
- FWD testing to assess the adequacy of the pavement structure
- Field sampling-10 cores from each pavement with top-down cracking and 5 cores from each pavement without top-down cracking
- DCP testing and geoprobe samples at core locations after coring

3.3 LABORATORY TESTING PLAN

Laboratory testing on the extracted asphalt mixture cores will include dynamic modulus and indirect tensile strength testing in a diametrical test configuration over a range of temperatures

and at multiple frequencies. The binder will then be extracted and recovered from the cores for subsequent rheological testing for binder grade determination. The binder grading will include dynamic shear rheometer and bending beam rheometer testing for grade determination. Further, the recovered aggregate will be tested for gradation, and coarse and fine aggregate angularity. Table 3.3 lists all the tests that will be performed on the asphalt cores, and extracted asphalt binder and aggregate.

Figure 3.3: Tests on Asphalt Mix Cores and Asphalt Binder

Test Name	Standard Be Used
Bulk Specific Gravity & Density of Asphalt Mix Cores	AASHTO T 166-93
Dynamic Modulus (E*)	AASHTO T342-11
Indirect Tensile Strength (ITS)	AASHTO T322-07
Theoretical Maximum Specific gravity of Asphalt Mix	AASHTO T 209-94
Binder Recover & Extraction	AASHTO T319-08
Dynamic Shear Rheometer (DSR)	AASHTO T315
Bending Beam Rheometer (BBR)	AASHTO T313
Aggregate Gradation	AASHTO T 27-93

Upon completion of the tests on asphalt mix cores and asphalt binder, gradation analysis on removed unbound base materials will be performed for subsequent comparison to construction records and material design specifications in place at the time of construction. This will allow for determination whether or not fines have migrated into the unbound base materials and adversely affecting their performance.

4.0 FIELD AND LABORATORY INVESTIGATION

4.1 FIELD INVESTIGATION

Six pavement sections with top-down cracking and four sections without top-down cracking were selected for field and laboratory investigations. Field investigation included conducting a distress survey, taking cores, conducting falling weight deflectometer (FWD) and dynamic cone penetrometer (DCP) testing. The various activities of the field investigation are detailed in the following subsections.

4.1.1 Distress Survey

The field condition distress surveys were conducted according to the FHWA Long Term Pavement Performance (LTPP) publication, “Data Collection Guide for Long Term Pavement Performance,” (*Data Collection Guide for Long Term Pavement Performance 2003*). The summary of the field condition surveys are provided in Table 4.1. It is important to point out that the cores were taken to differentiate top-down cracking from bottom-up cracking. Longitudinal (top-down) cracking and transverse (thermal) cracking are reported in linear feet per mile. The low, medium, and high severity cracking are summed up without adjustment for both alligator cracking and longitudinal cracking. For thermal (transverse) cracking, low, medium, and high severity cracking are summed up using the same weighting function in the national calibration that is shown in the following equation (*ARA, 2004*):

$$\begin{aligned} & \text{Transver Cracking (TC)} \\ = & (\text{Low severity TC} + 3 * \text{Medium severity TC} + 5 * \text{High severity TC})/9 \end{aligned} \quad (4.1)$$

Figures 4.1 through 4.4 show the development of top-down cracking on some of the sections included in this study.

Table 4.1: Summary of Field Condition Distress Surveys

Section	Rut (in)			Longitudinal Cracking (ft/mile)				Transverse Cracking (ft/mile)			
	RW P	LWP	Avg.	Low	Medium	High	Total	Low	Medium	High	Total
OR22-U	0.13	0.25	0.19	0	0	0	0	0	0	0	0
US97-U	0.29	0.29	0.29	0	0	0	0	0	0	0	0
US20-U	0.58	0.38	0.48	0	0	0	0	0	0	0	0
OR99-U	0.53	0.44	0.48	0	0	0	0	0	0	0	0
OR238-C	0.38	0.29	0.33	1784	2676	2460	6920	386	1351	193	600
OR99W-C	0.50	0.38	0.44	1160	4700	3440	9300	190	285	0	116
OR221-C	0.38	0.38	0.38	6135	4910	4005	15050	870	1160	870	967
OR99EB-C	0.25	0.25	0.25	6300	6060	3060	15420	275	960	135	426
OR140-C	0.22	0.16	0.19	1600	6790	1130	9520	0	0	0	0
OR99*-C	0.25	0.25	0.25	1580	5900	2320	9800	360	240	0	120



Figure 4.1: Top-Down and Transverse Cracking on Section OR238-C



Figure 4.2: Top-Down Cracking on Section OR221-C



Figure 4.3: Tow-Down Cracking on Section OR99*-C



Figure 4.4: Top-Down and Transverse Cracking on Section OR99EB-C

4.1.2 Falling Weight Deflectometer Testing

Falling weight deflectometer (FWD) testing has been widely adopted to obtain surface deflection data in order to evaluate existing pavement conditions since the 1980s (*NCHRP 2008*). The Oregon Department of Transportation (ODOT) has been using FWD testing as a non-destructive evaluation method of pavement structure, as shown in Figure 4.5. The FWD test imparts an impulse load on the road surface and the resulting surface deflections are recorded at different locations using deflection measuring sensors known as geophones, as illustrated in Figure 4.6. Then the stiffness moduli of the pavement layers are estimated by measuring the deflection basin under the applied load.



Figure 4.5: FWD Testing Used by ODOT

The response of the pavement to impulse loading was measured with a set of seven deflection measuring sensors (geophones) placed on different radial distances from the center of the loaded area. The spacing of the seven FWD deflection measuring sensors (geophones) are shown in Table 4.2. The diameter of the loading plate was 5.91 inches and the testing used stress levels of approximately 55, 82, and 110 psi. All deflection data were recorded by an on-board computer to within 0.01 mils (0.00001 in). At each FWD test location, the pavement and air temperatures were also recorded.

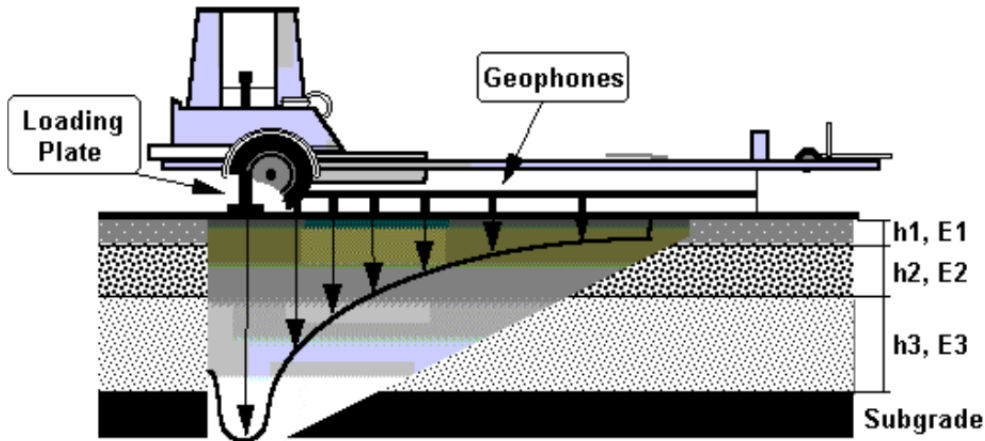


Figure 4.6: Schematic of standard loading configuration and deflection basin (Pellinen et al. 2004)

Table 4.2: Geophone Spacing Used in FWD Testing

Geophones	Radial Distance (mm)	Radial Distance (in)
d1	0	0
d2	203	8
d3	305	12
d4	457	18
d5	610	24
d6	914	36
d7	1524	60

4.1.2.1 Temperature Correction for HMA Modulus

Asphalt concrete (AC) mixture stiffness varies with temperature. All deflection measurements or backcalculated HMA stiffness (modulus) must be corrected to a particular type of loading system and a standard reference temperature (*Chen et al. 2000*). The temperature correction procedure for FWD deflections and back calculated AC layer moduli involves two steps (*Ceylan et al. 2013*): (1) HMA pavement temperature estimation and (2) temperature correction algorithm for HMA modulus.

4.1.2.2 HMA Pavement Temperature Prediction

Before correction of the backcalculated HMA moduli to a standard reference temperature, mid-depth HMA pavement temperature at which FWD deflections were obtained should be estimated. The temperature can be measured directly by installing a temperature probe into pavement, but the process is very time-consuming. Temperature estimates based on correlations with externally measurable variables are preferable. This temperature may be measured from approximate methods based on air and surface temperatures taken at the time of FWD testing. Several equations to estimate pavement temperature have been proposed. By using measured pavement-depth temperatures from SHRP's long term pavement performance (LTPP) database, Lukanen et al. (*Lukanen et al. 2000*) developed a set of equations called the BELLS models for predicting in-depth pavement temperatures. Among these equations, the BELLS3 model accounts for shaded conditions of pavement surfaces under routine testing conducted by most highway agencies. The BELLS3 model employed in this study to predict mid-depth pavement temperature is expressed as follows:

$$T_d = 0.95 + 0.892T_s + \{\log(d) - 1.25\}\{-0.448T_s + 0.621T_{avg} + 1.83 \sin(hr_{18} - 15.5)\} + 0.042T_s \sin(hr_{18} - 13.5) \quad (4.2)$$

where:

T_d = Pavement temperature at mid-depth d in ($^{\circ}\text{C}$);

T_s = Infrared surface temperature measured at the time of FWD testing ($^{\circ}\text{C}$);

Log = Base 10 logarithm;

d = Layer mid-depth at which temperature is to be predicted (mm);

T_{avg} = Average air temperature the day before testing ($^{\circ}\text{C}$);

\sin = Sine function on an 18-hr clock system, with 2 radians equal to one 18-hr cycle; and hr_{18} = Time of day, in 24-hr clock system, but calculated using an 18-hr asphalt concrete (AC) temperature rise and fall time cycle.

4.1.2.3 Temperature Correction for HMA Modulus

As HMA stiffness (modulus) is temperature sensitive, backcalculated HMA moduli must be corrected to a standard reference temperature. In recognition of the urgent need to develop a realistic temperature correction procedure, many researchers (*Kim et al. 1995, Ali and Lopez 1996, Park and Kim 1997, Lukanen et al. 2000, Chen et al. 2000*) have proposed equations relating the HMA modulus to a standard reference temperature. Among them, the temperature correction equation developed by Chen et al. (*Chen et al. 2000*) is the only available model which provides the flexibility to normalize to any reference temperature with good accuracy. Considering this advantage, it was employed in this study and is expressed as follows:

$$E_{T_w} = E_{T_c} / [(1.8T_w + 32)^{2.4462} * (1.8T_c + 32)^{-2.4462}] \quad (4.3)$$

. where:

- E_{T_w} = The adjusted modulus of elasticity at T_w (MPa);
- E_{T_c} = The adjusted modulus of elasticity at T_c (MPa);
- T_w = The temperature to which the modulus of elasticity is adjusted ($^{\circ}\text{C}$); and
- T_c = The mid-depth temperature at the time of FWD testing ($^{\circ}\text{C}$).

$$W_{T_w} = W_{T_c} \left\{ \frac{1.0823^{-0.098t}}{0.8631} \right\} * T_w^{0.8316} * T_d^{-0.8419} \quad (4.4)$$

where:

- W_{T_w} = Deflection adjusted to temperature T_w (mm);
- W_{T_c} = The adjusted modulus of elasticity at T_c (MPa);
- t = Thickness of the pavement (mm);
- T_d = Mid-depth pavement temperature at the time of FWD data collection ($^{\circ}\text{C}$); and
- T_w = Temperature to which deflection is adjusted ($^{\circ}\text{C}$).

4.1.2.4 Structural Capacity

FWD testing is currently the most widely used method for non-destructive evaluation of the structural capacity of a pavement. Pavement deflection measurements are important inputs to calculate pavement structural capacity and the remaining service life of pavements (*Gedafa et al. 2010*). Many different approaches have been proposed to estimate the structural number (SN) of an existing pavement directly from FWD

deflections. A mechanistic procedure developed by Jameson (*Jameson 1992*) to estimate the SN from FWD deflections is expressed by Equation 4.5.

$$SN = 13.47 - 6.47 * \log(DEF_0) + 3.697 * \log(V_{900}) \quad (4.5)$$

where:

SN = Structural number of the existing pavement;

DEF₀ = Temperature-corrected central deflection (microns); and

V₉₀₀ = Normalized deflection at 900-mm (36 inch) offset (microns).

AASHTO (*AASHTO 1993*) has also developed equations to calculate SN from non-destructive deflection test results. The AASHTO method suggests that at a sufficiently large distance from the load center, deflections measured at the pavement surfaces are due to subgrade deformation only, and are also independent of the size of the loading plate (*Gedafa et al. 2010*). The equation used to estimate subgrade resilient modulus (M_r) is expressed in Equation 4.6. In order to estimate M_r of the subgrade, the deflection must be measured far enough away from the load so that it provides a good estimate of the subgrade modulus, independent of the effects of any layer above, but also close enough so that it is not too small to be measured accurately. Equation 4.7 provides the distance requirement be determined based on the radius of the stress bulb at the subgrade-pavement interface. The average values of the M_r back calculated from deflections at 36 and 60 inches were used as the determined subgrade resilient moduli.

$$M_r = \frac{0.24P}{d_r r} \quad (4.6)$$

where:

M_r = Backcalculated subgrade resilient modulus (psi);

P = Applied load (lb);

r = Radial distance (in); and

d_r = Deflection at a distance r (in) from the center of the load (in)

$$r \geq 0.7 \sqrt{[a^2 + (D \sqrt[3]{\frac{E_p}{M_r}})^2]} \quad (4.7)$$

where:

a = FWD loading plate radius (in);

D = Total thickness of pavement layers above the subgrade (in); and

E_p = Effective modulus of all pavement layers above the subgrade (psi).

When the subgrade resilient modulus and total thickness of all layers above the subgrade are known, the effective modulus (E_p) of the entire pavement structure above the subgrade is determined from the deflection measured at the center of the load through Equation 4.8. and Equation 4.9 is used to compute the effective structural number (SN_{eff}).

$$d_0 = 1.5 pa \left\{ \frac{1}{M_R \sqrt{1 + \left(\frac{D}{a}\right)^3 \frac{E_p}{M_R}}} + \frac{1 + \frac{1}{\sqrt{a + \left(\frac{D}{a}\right)^2}}}{E_p} \right\} \quad (4.8)$$

where:

- E_p = Effective modulus of all pavement layers above the subgrade (psi);
- d_0 = Deflection measured at the center of the load plate (adjusted to a standard reference temperature of 68 °F) (in);
- p = FWD loading plate pressure (psi);
- a = FWD loading plate radius (in);
- M_R = Subgrade resilient modulus (psi); and
- D = Total thickness of pavement layers above the subgrade (in).

$$SN_{eff} = 0.0045 D \sqrt[3]{E_p} \quad (4.9)$$

where:

- SN_{eff} = Effective structural number;
- D = Total thickness of pavement layers above the subgrade (in); and
- E_p = Effective modulus of all pavement layers above the subgrade (psi).

4.1.3 Dynamic Cone Penetrometer Test

The Oregon Department of Transportation has been using dynamic cone penetrometer (DCP) test to verify the quality of unbound base materials during construction because variations in density can have relatively large effects on the properties that determine pavement performance. The DCP penetration distance per drop is known as the DCP penetration index (DCPI) or penetration resistance (PR). The DPI can be used to estimate the shear strength and modulus of unbound materials using empirical relationships.

DCP consists of two vertical shafts connected to each other at the anvil. The upper shaft has a handle and hammer. Along with providing a way to easily hold the DCP vertical, the handle is used to provide a standard drop height of 22.6 in (575 mm). The hammer is 17.6 lb (8 kg) and provides a constant impact force. The lower shaft contains an anvil at the top and a pointed cone on the bottom. The anvil is fixed and stops the hammer from falling any farther than the standard drop height. When the hammer is dropped and hits the anvil, the cone is driven into the base

materials. Figure 4.7 shows the typical configuration of DCP with Figure 4.8 demonstrating the use of a DCP.

Several correlation equations have been proposed to convert the DCP penetration index (DCPI) into the California Bearing Ratio (CBR). The most common conversion is expressed in the form of equations for CBR as a function of DPI (mm/blow). The North Carolina Department of Transportation (NCDOT) developed the following DCP and CBR relationship, based on the field CBR and the average of three DCP readings taken within an area with a radius of less 1 ft around the CBR test sections:

$$\mathbf{Log (CBR) = 2.64 - 1.08 Log (DCPI) \quad or \quad CBR = \frac{435}{DCPI^{1.08}} \quad (4.10)}$$

Ese et al. (*Ese et al. 1995*) also developed the following correlation equation between CBR and DPI for aggregate base course:

$$\mathbf{Log (CBR) = 2.44 - 1.07 Log (DCPI) \quad (4.11)}$$

The U.S. Army Corps of Engineers (*Webster et al. 1992*) developed another equation, used by many state departments of transportation and federal agencies:

$$\mathbf{Log (CBR) = 2.465 - 1.12 Log (DCPI) \quad or \quad CBR = \frac{292}{DCPI^{1.12}} \quad (4.12)}$$

Modulus is one of the most common parameters used in pavement design. The American Association of State Highway and Transportation Officials (AASHTO) Design guide recommends the use of the following equation to convert a CBR value to a Young's modulus (E) value:

$$\mathbf{E(psi) = 1,500 * CBR \quad or \quad E(MPa) = 10.34 * CBR \quad (4.13)}$$

The U.S. Army Corps of Engineers Research and Development Centers Waterways Experiment Station proposed the following equation:

$$\mathbf{E(psi) = 5409 * CBR^{0.711} \quad or \quad E(MPa) = 37.3 * CBR \quad (4.14)}$$

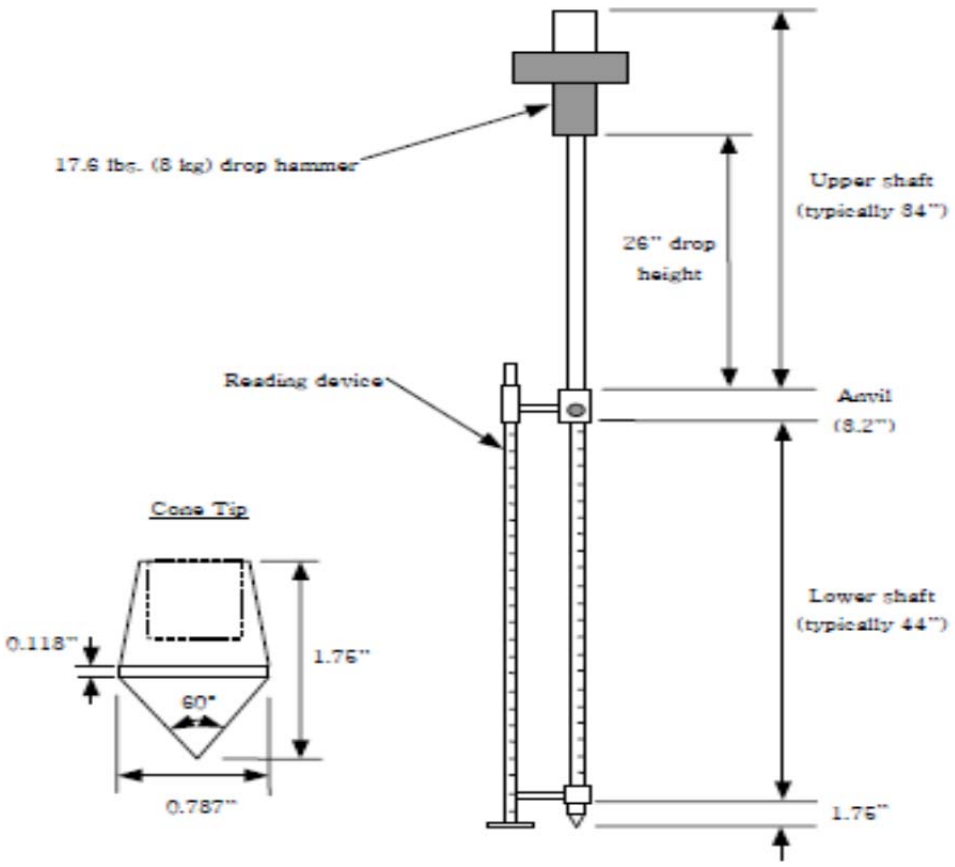


Figure 4.7: Schematic of Dynamic Cone Penetrometer (*Deepika and Chakravarthi 2012*)



Figure 4.8: Photos of Dynamic Cone Penetrometer Testing

4.2 LABORATORY TESTING

After all non-destructive tests had been completed, cores were extracted at the designated locations using a power rotary drill. Five cores from each of good performing (no cracks) pavements and 10 cores from each of cracked pavements were brought to the laboratory for testing and evaluation. For cracked pavements, approximately five cores were taken near the cracked sections while the remaining cores were taken away from the cracks.

4.2.1 Dynamic Modulus Testing

4.2.1.1 Dynamic Modulus

Dynamic modulus, E^* , is a complex number that relates stress to strain of linear viscoelastic materials under a continuous sinusoidal loading. The absolute value of the complex modulus, is commonly referred to as the dynamic modulus (*Witczak et al. 2002b*). HMA mixtures can be considered as a viscoelastic material under small strain levels, typically less than 100 micro-strain ($\mu\epsilon$) (*Schwartz 2005*). Thus, the HMA stress-strain relationship in the linear viscoelastic region under continuous sinusoidal loading can be defined by the complex dynamic modulus as illustrated in Figure 4.9.

The complex dynamic modulus is defined as the ratio of amplitude of the sinusoidal stress and sinusoidal strain, as mathematically expressed by the following equation:

$$E^* = \frac{\sigma}{\epsilon} = \frac{\sigma_o e^{i\omega t}}{\epsilon_o e^{i(\omega t - \delta)}} = \frac{\sigma_o \sin(\omega t)}{\epsilon_o \sin(\omega t - \delta)} \quad (4.15)$$

where:

- E^* = Complex dynamic modulus;
- σ_o = Maximum (peak) stress;
- ϵ_o = Maximum (peak) strain;
- δ = Phase angle, degrees;
- ω = Angular velocity;
- t = time, seconds; and
- i = imaginary component of the complex modulus.

Thus, the dynamic modulus is defined as:

$$|E^*| = \sigma_o / \epsilon_o \quad (4.16)$$

For pure elastic materials, $\delta = 0$ and for pure viscous materials, $\delta = 90^\circ$.

The dynamic modulus, $|E^*|$, is an overall measure of relative stiffness for asphalt mixtures. Asphalt mixtures of higher dynamic moduli tend to deform less under a traffic loading compared to mixtures with lower dynamic modulus. At high temperatures, less deformation indicates better resistance to rutting while high dynamic modulus at low temperatures could result in greater susceptibility to low-temperature cracking.

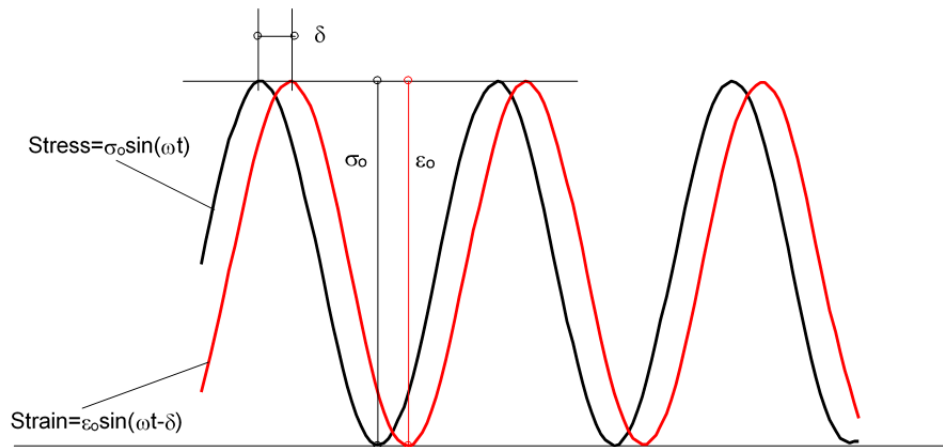


Figure 4.9: Stress and Strain of Typical Viscoelastic Materials under Sinusoidal Loading (*Garcia and Thompson 2007*)

4.2.1.2 Dynamic Modulus Testing

Coffman and Pagen at Ohio State University developed the first dynamic modulus protocol in the 1960's. It was accepted as an ASTM standard in 1979. The designation is D3496 in ASTM standards and TP62 in AASHTO specifications. Dynamic modulus testing is generally conducted in axial compression mode on laboratory fabricated asphalt concrete specimens of 4-inch (100-mm) diameter and 6-inch (150-mm) tall. It is sometimes impossible to obtain this size of specimen (e.g., height) from actual pavements. Thus, the indirect tension (IDT) testing of cores becomes more appropriate for the evaluation of existing pavements. However, there are two major differences between uniaxial compression dynamic modulus testing and IDT dynamic modulus testing. The uniaxial compression testing creates a uniaxial state of stress while the stress state in the IDT test is biaxial. The other difference is the relationship between compaction direction and direction in which the stress-strain analysis is performed. In axial compression these two directions are the same, whereas in IDT they are perpendicular (*Kim et al. 2004*). Kim et al. (*Kim et al. 2004*) developed the linear viscoelastic solution for the dynamic modulus of HMA under the IDT mode and the results were verified by conducting both axial compression and IDT test methods on 12 asphalt mixtures commonly used in North Carolina.

IDT dynamic modulus testing was performed following AASHTO method “*Determining the Dynamic Modulus for Hot-mix Asphalt (HMA) Using the Indirect Tension Testing Method*”. Unlike axial compression test, both vertical and horizontal linear variable differential transformers (LVDTs) are needed in the IDT dynamic modulus testing as shown in Figure 4.10. Testing was done with a closed-loop servo-hydraulic testing machine to apply the sinusoidal loading and is shown in Figure 4.11. Cores were sawed to 6-inch (150-mm) diameter and 2.5-inch (62-mm) height. A temperature chamber was used to control the test temperature. A dummy specimen with a thermocouple embedded in the middle of the specimen is used to control the temperature of the testing specimens.

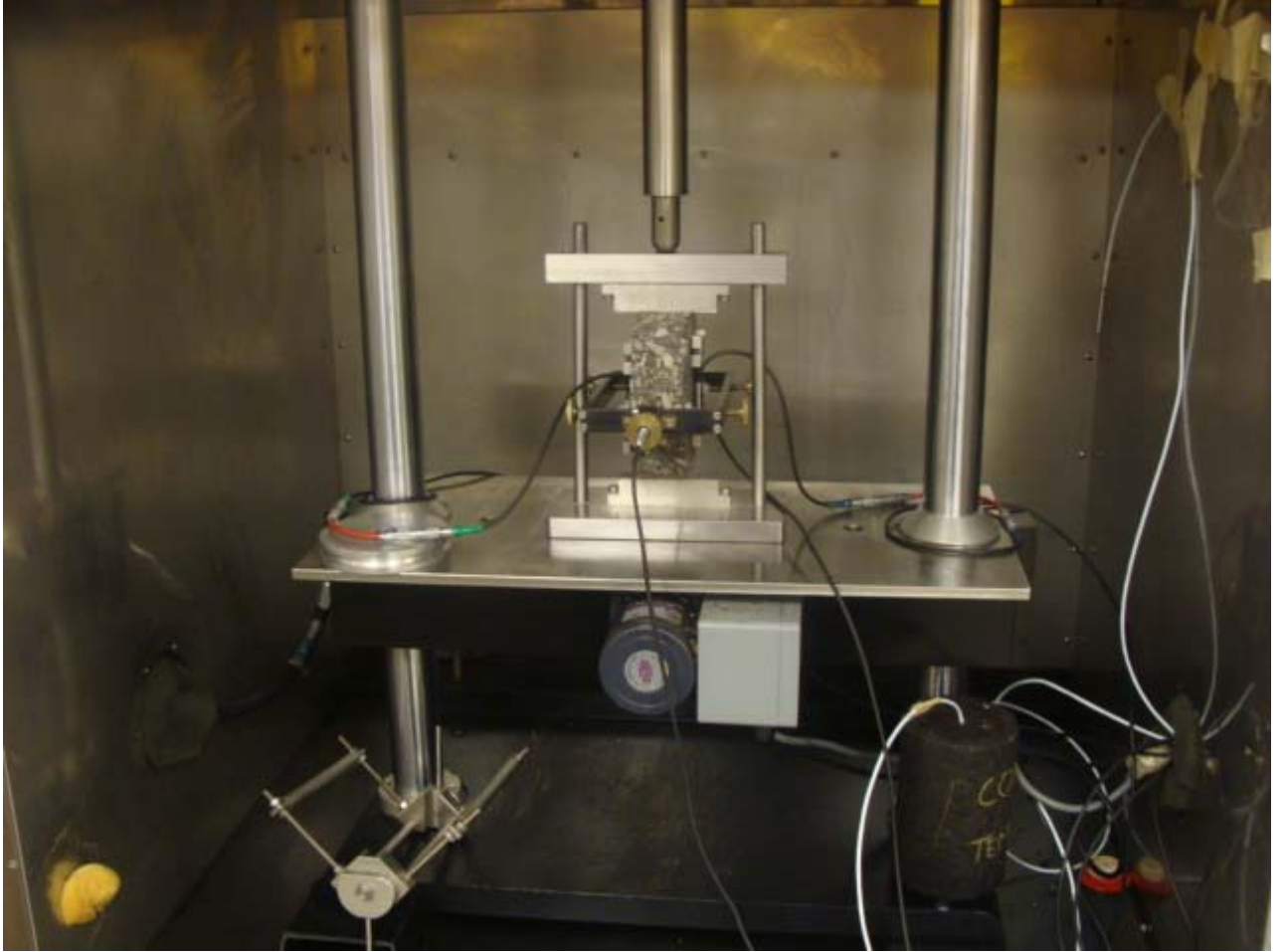


Figure 4.10: Specimen Set-Up for Dynamic Modulus Testing in IDT Mode



Figure 4.11: UTM-25 Machine for Dynamic Modulus Testing

4.2.1.3 Dynamic Modulus Master Curve

Asphalt mixture dynamic modulus varies with temperature and rate of loading. To account for the influence of temperature and rate of loading, asphalt mixture dynamic modulus can be determined from a master curve developed at an arbitrarily selected reference temperature, generally taken as 70°F (21.1°C). A master curve represents the response of an asphalt mix at a selected reference temperature over a wide range of frequency or time (*Christensen and Anderson 1992*). It allows comparisons of linear viscoelastic materials when testing are done using different test temperatures and loading frequencies.

Master curves are constructed at a reference temperature or frequency based on the time-temperature superposition principle. Asphalt mixtures exhibit higher modulus (E^*) values at low temperatures or high loading frequencies. Therefore, an E^* value tested at a lower temperature and higher frequency could be equal to an E^* value tested at a higher temperature and lower frequency. Therefore, E^* values tested at different temperatures and frequencies can be transferred to a single reference temperature or frequency. The

shift needed at each temperature is called the shift factor, $a(T)$, which is a constant for a given temperature. The actual frequency must be divided by this shift factor to obtain a reduced frequency, f_r , for the master curve. The following equations show the mathematical definition of this shift factor:

$$f_r = \frac{f}{a(T)} \rightarrow \log(f_r) = \log(f) - \log(a(T)) \quad (4-17)$$

where:

f_r = Reduced frequency (loading frequency at the reference temperature);

f = Loading frequency; and

$a(T)$ = Shift factor.

And, in terms of time of loading:

$$t_r = \frac{t}{a(T)} \rightarrow \log(t_r) = \log(t) - \log(a(T)) \quad (4-18)$$

where:

t_r = Reduced time (loading time at the reference temperature);

t = Loading time; and

$a(T)$ = Shift factor.

The shift factor is 1 at reference temperature and the $\log(a(T))$ is therefore 0. According to the “2002 Guide for the Design of New and Rehabilitated Pavement Structures”, the master modulus curve can be mathematically modeled by a sigmoidal function described as:

$$\log(|E^*|) = \delta + \frac{\alpha}{1 + e^{\beta + \gamma \log(t_r)}} \quad (4-19)$$

where:

$|E^*|$ = Dynamic modulus;

t_r = Reduced time of loading at reference temperature;

δ = Minimum modulus value;

$\delta + \alpha$ = Maximum modulus value; and

β, γ = Parameters describing the shape of the sigmoidal function.

The parameters that are used to represent the master modulus curve including α, β, γ , and $a(T)$ can be solved by using the Excel Solver function to match the calculated $|E^*|$ values from the sigmoidal function with the laboratory tested $|E^*|$ values. Figure 4.12 shows the results of a dynamic modulus test and how the data at each temperature can be shifted to

form a smooth curve. Figure 4.13 illustrates the resultant master curve at a reference temperature of 70°F (21°C).

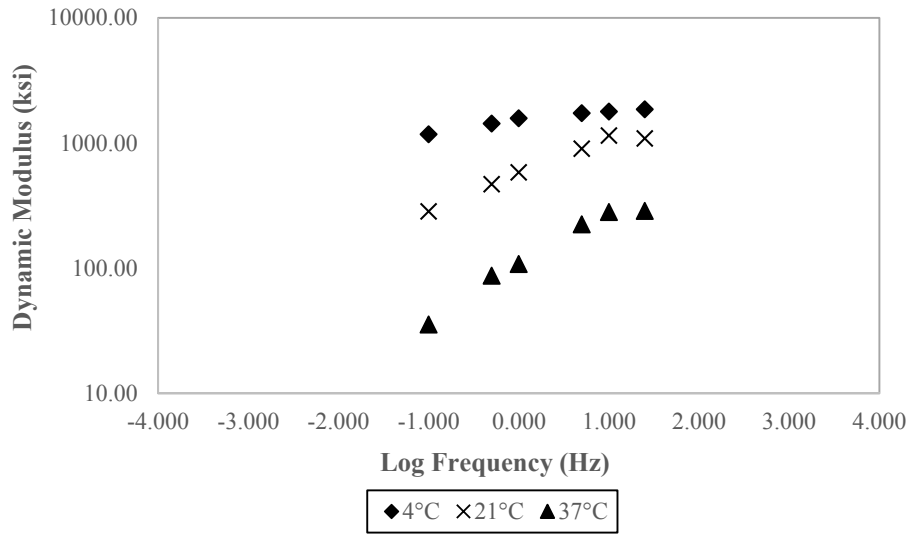


Figure 4.12: Results of Dynamic Modulus Test and Data Shifting

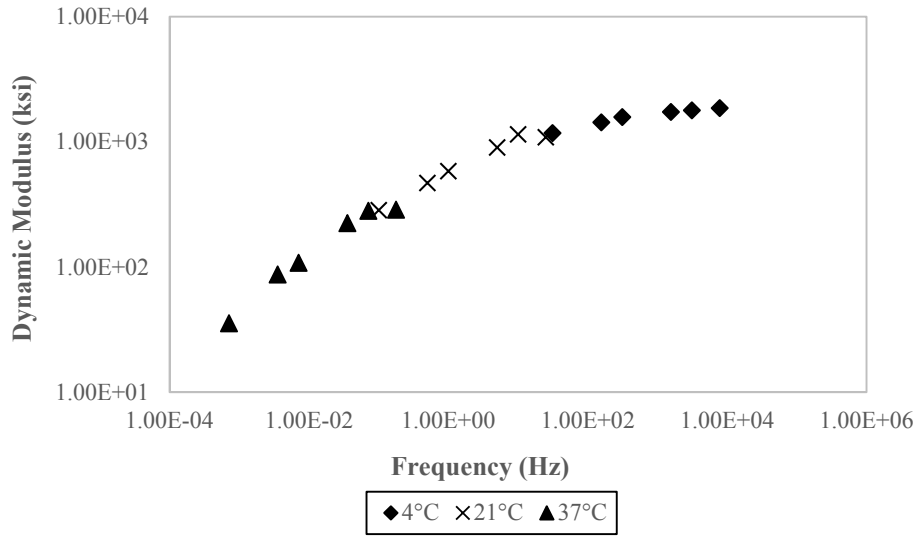


Figure 4.13: Test Data Shifted to Form Master Curve

4.2.2 Indirect Tensile Strength

The indirect tensile strength (IDT) test is one of the most popular tests used for HMA mixtures to determine the tensile strength of asphalt mixes. The IDT test is conducted by loading a cylindrical specimen with a compressive load which acts parallel to and along the vertical

diametral plane (shown in Figure 4.14). The IDT test is a destructive test because the specimen is loaded until tensile failure occurs (shown in Figure 4.15).

The IDT test was performed following ASTM D6931-12 “*Standard Test Method for Indirect Tensile (IDT) Strength of Bituminous Mixtures*” where specimens were loaded at a rate of 50 mm of ram (vertical) movement per minute. Once specimens’ dimensions (thickness and height) and the peak load at failure are known, the IDT strength is calculated as follows:

$$S_t = \frac{2 \times P}{\pi \times b \times D} \quad (4-20)$$

where:

- S_t = Tensile strength of specimen;
- P = Failure load for specimen;
- b = Thickness of the specimen; and
- D = Diameter of the specimen.

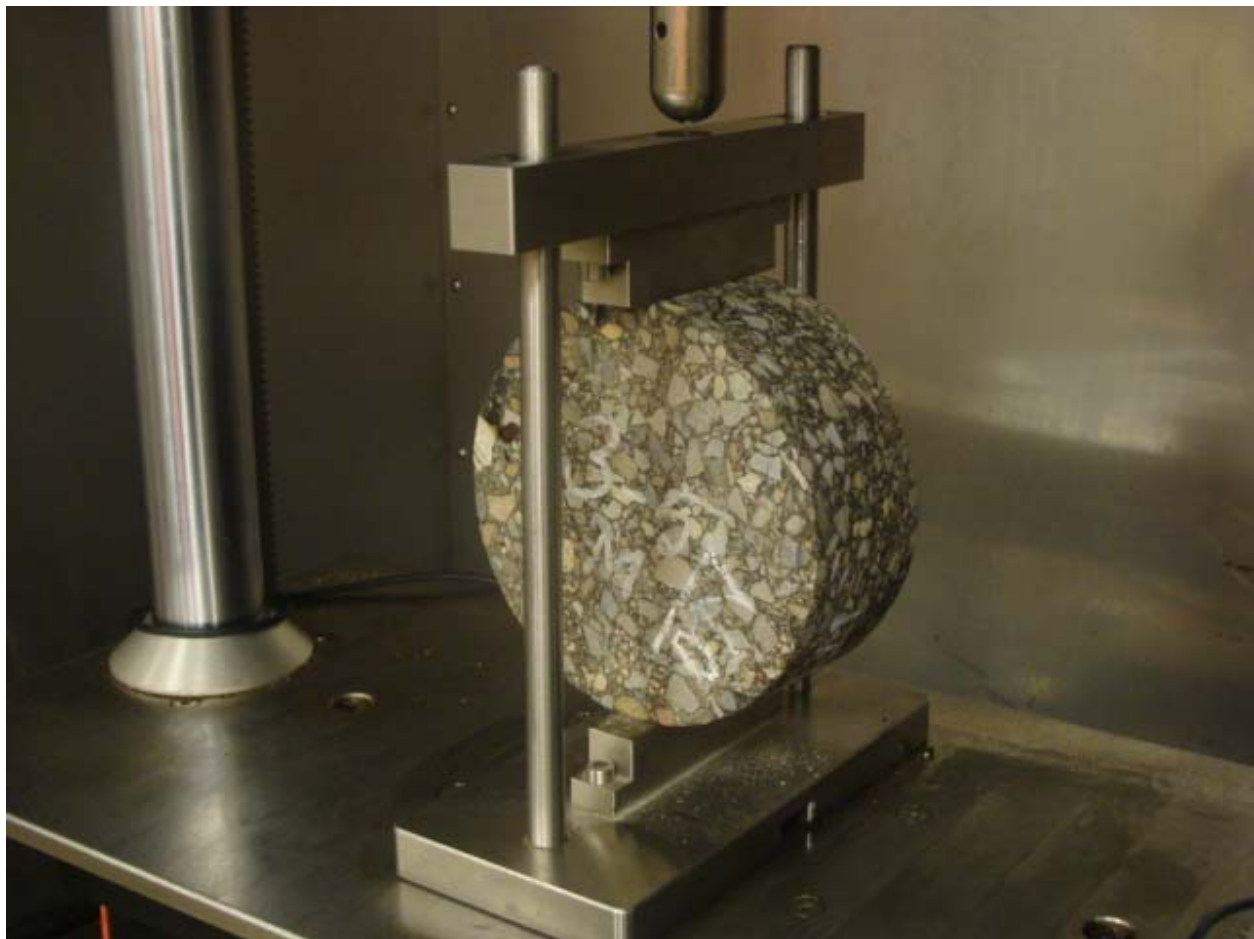


Figure 4.14: Specimen Set-Up for IDT Strength Test

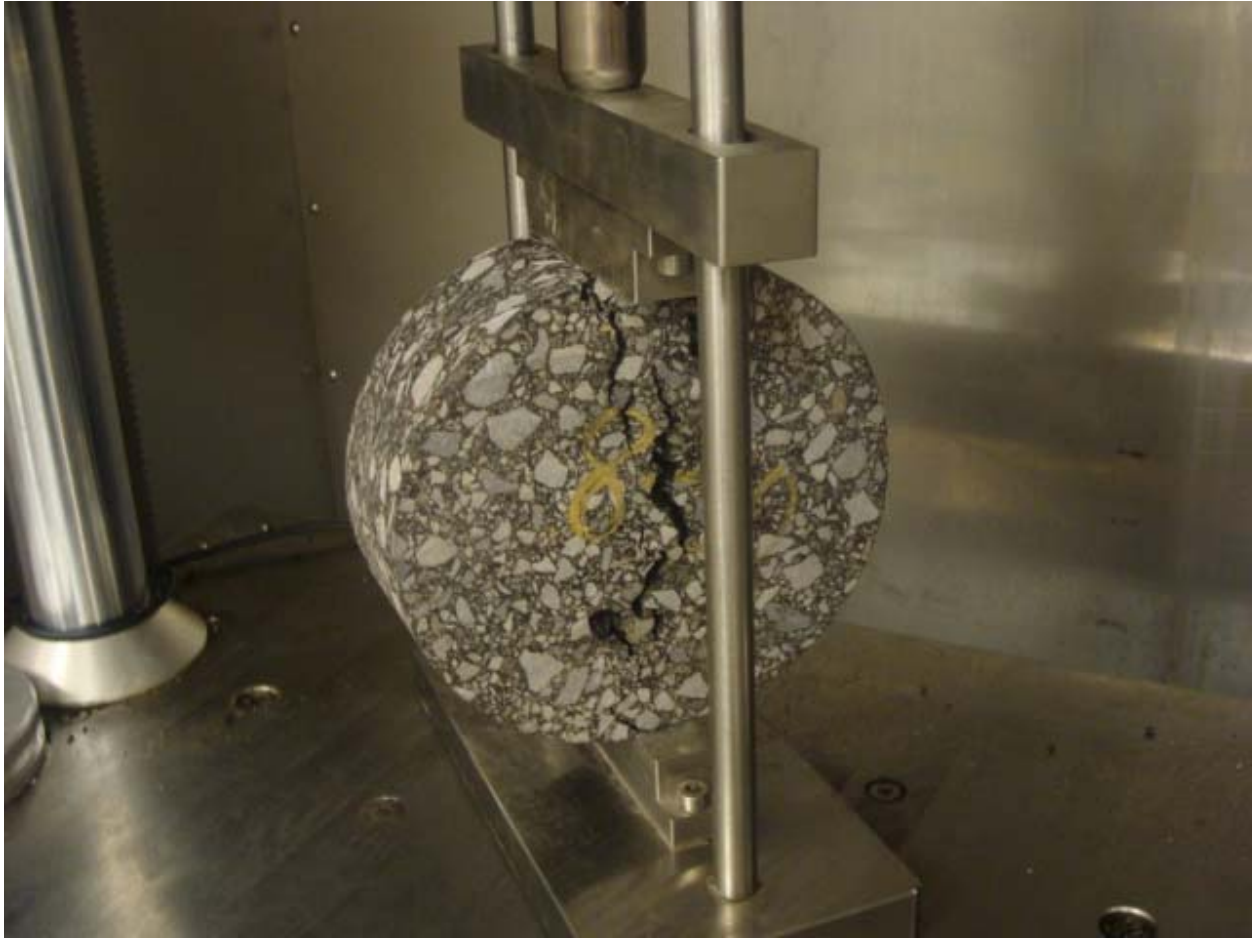


Figure 4.15: Failure Mode in IDT Strength Test

4.2.3 Specific Gravity Tests

Bulk specific gravity tests were conducted on the extracted cores following AASHTO T 166-93 “*Bulk Specific Gravity of Compacted Asphalt Mixtures Using Saturated Surface Dry Specimens*”. The following equation was used to determine the bulk specific gravity of the cores:

$$G_{mb} = \frac{A}{B - C} \quad (4-20)$$

Where:

- G_{mb} = Bulk specific gravity;
- A = Mass of the dry specimen in air (g);
- B = Mass of the saturated surface-dry specimen in air (g); and
- C = Mass of the specimen in water (g).

Theoretical maximum specific gravity tests were also conducted for every project once IDT strength tests were completed following Iowa Test Method 510 and AASHTO T209-90 “*Method of Test for Determining the Maximum Specific Gravity of Hot Mix Asphalt (HMA) Mixtures*”. The test results were used to determine the theoretical maximum specific gravity of the mixture using the following equation:

$$G_{mm} = \frac{A}{B + A - C} \quad (4-21)$$

where:

G_{mm} = Theoretical maximum specific gravity;

A = Weight of dry sample in air (g);

B = Weight of calibrated pycnometer filled with water (g); and

C = Weight of pycnometer containing sample and filled with water to the calibrated level (g).

4.2.4 Binder Rheological Properties Test

4.2.4.1 Dynamic Shear Rheometer Test

Dynamic shear rheometer (DSR) tests are conducted to characterize the elastic and viscous behavior of asphalt binders at medium to high temperature. In the DSR test operation, a thin asphalt binder is sandwiched between two parallel plates, one of which is fixed and the other one oscillates. The DSR test measures the complex shear modulus (G^*) and phase angle (δ). The complex shear modulus is a measure of the total resistance to deform when subjected to repeated pulses of shear stress. The phase angle is an indicator of the relative amounts of the recoverable and non-recoverable deformations. G^* and δ are used to predict rutting and fatigue cracking in pavement analysis. In order to resist rutting, the elastic portion of the complex shear modulus, $G^*/\sin\delta$, should be large. Therefore, a minimum value of $G^*/\sin\delta$ is specified. On the other hand, the viscous portion of the complex shear modulus, $G^*\sin\delta$, should be minimum to resist fatigue cracking and therefore, maximum value of $G^*\sin\delta$ is specified.

Asphalt binders were extracted from field cores following AASHTO TP2-94, “*Standard Test Method for the Quantitative Extraction and Recovery of Asphalt Binder from Hot Mix Asphalt (HMA)*”. The extraction method uses solvents blended with ethanol to separate the asphalt binder from aggregates. The commonly used asphalt solvents are n-Propyl Bromide, Trichloroethylene, and Toluene. Asphalt binder is recovered through a centrifuge. The standard method for DSR testing is ASTM D7175, “*Standard Test Method for Determining the Rheological Properties of Asphalt Binder using a Dynamic Shear Rheometer*”. DSR tests were conducted to determine both asphalt binder high temperature grade and intermediate temperature properties following the Superpave test specifications.

DSR frequency sweep tests were performed to construct master curves of asphalt binder complex shear modulus (G^*) and phase angle (δ). The master curves characterizes binder

rheological properties over a wide range of temperature or frequency. The frequency sweep procedure was performed at different temperature ranging from 20 to 82° C at frequencies ranging between 0.1 to 100 Hz, using 25 mm parallel plates with a 1 mm gap. Table 4.3 shows the temperatures and frequencies used in the frequency sweep procedure. The dynamic rheological properties were estimated by measuring the required shear stress to achieve a required strain level. The strain level should be large enough so that it is measureable and also small enough so that the required stress does not exceed the capacity of the testing device or damage the sample. The controlled strain level for the 25 mm sample is 10%. DSR tests were carried out with an AR1500 dynamic shear rheometer shown in Figure 4.16.

Table 4.3: Temperatures and Frequencies used in Frequency Sweep Procedure

Frequency Sweep Temperatures and Frequencies	
Temperature (°C)	20 30 40 46 52 58 64 70 76 82
Frequency (Hz)	0.1 0.126 0.159 0.2 0.251 0.316 0.398 0.501 0.631 0.794 1 1.259 1.585 1.995 2.512 3.162 3.981 5.012 6.310 7.943 10 12.59 15.85 19.95 25.12 31.62 39.81 50.12 63.1 79.43 100



Figure 4.16: AR1500 Dynamic Shear Rheometer

4.2.4.2 Bending Beam Rheometer

A bending beam rheometer (BBR) test is used to accurately characterize asphalt binder properties at low temperatures. Coupled with DSR test results, BBR tests provide

rheological properties of asphalt binder over a wide range of in-service temperatures in cold to warm climatic regions. The BBR test measures creep stiffness, $S(t)$, at the lowest in-service temperatures and change in stiffness (m-value). The creep stiffness is indicative of the susceptibility of the asphalt binder to low-temperature cracking while m-value represents the rate of change of binder stiffness with time. m-value is estimated from the slope of the log stiffness versus log time curve from the BBR test results. The higher the value of the creep stiffness the more susceptible to cracking while the reverse is true for the m-value. Therefore, the PG binder specification recommends a maximum value of 300 MPa for creep stiffness and a minimum value of 0.3 for the m-value.

The standard method for BBR testing is AASHTO T 313, “*Determining the Flexural Creep Stiffness of Asphalt Binder Using the Bending Beam Rheometer (BBR)*”, which was followed to test the asphalt binders at low temperatures. The BBR is a simple device that measures the creep stiffness and creep rate (m-value) by loading the asphalt beam four minutes with a constant load and measuring the deflection at the center of the beam continuously throughout the four minutes (McGennis et al. 1994).

Classic beam analysis theory is used to obtain creep stiffness of the asphalt used in the BBR test as follows:

$$S(t) = \frac{PL^3}{4bh^3\delta(t)} \quad (4-22)$$

where:

- S(t) = Creep stiffness at time, t = 60 seconds;
- P = Applied constant load, 100 gm (980 mN);
- L = Distance between beam supports, 102 mm;
- b = Beam width, 12.5 mm;
- h = Beam thickness, 6.25 mm; and
- $\delta(t)$ = Deflection at time, t = 60 seconds.

Computer-generated output for the BBR test automatically reports the creep stiffness and m-value including plots of deflection and load versus time, actual load and deflection values at various times, test parameters, and operator information for a specific test temperature.

5.0 RESULTS AND DISCUSSION

5.1 FIELD INVESTIGATION RESULTS

5.1.1 Falling Weight Deflectometer Test Results

Each pavement section included in this study was tested using ODOT Dynatest falling weight deflectometer (FWD) as described in Chapter 4 in an effort to evaluate the variations in the pavement deflections along the pavement sections and also backcalculate the layer moduli. This section discusses the variations of the deflection data, backcalculation of layer moduli, and estimation of structural capacity of the existing pavement included in this study.

5.1.1.1 Deflection Data

Deflection is the response of the pavement to the applied load. Deflection is an index which expresses the structural capacity of the pavement. Therefore, variations in the measured deflections reflect variations in the structural capacity of the pavement. Figures 5.1 through 5.10 illustrate deflection profiles for all the pavement sections included in this study while Table 5.1 provides a summary of the coefficient of variation (CV) in D1 through D7 deflections. Several of the sections, such as OR22-U, US97-U, US20-U, OR238-C, and OR140-C, showed relatively lower variations in the D1 sensor compared to the variations in the D7 sensor. The reverse is true for pavement sections OR99W-C, OR221-C, OREB-C, and OR99*-C. Only pavement section OR99-U exhibited similar variations both in the D1 and the D7 sensors. As can be seen, all the non-cracked pavement sections except OR99-U exhibited higher variations in the D7 sensor compared to variations in the D1 sensor. The reverse trend was observed for most of the top-down cracked pavement sections except OR238-C and OR 140-C.

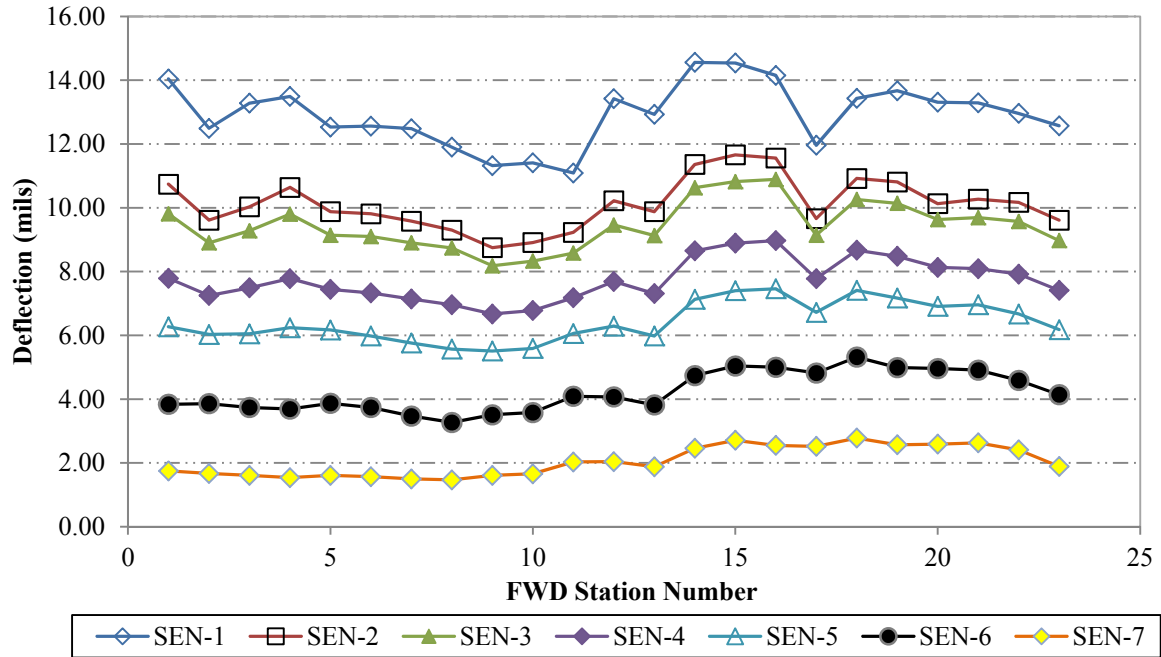


Figure 5.1: Deflection Profiles, OR22-U

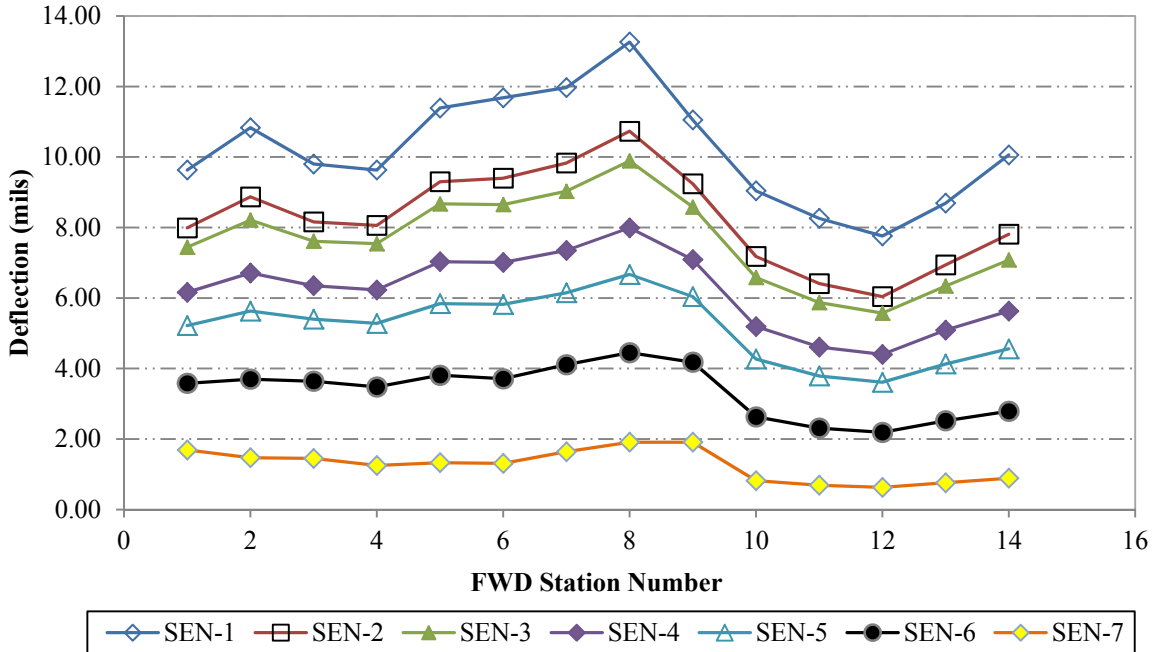


Figure 5.2: Deflection Profiles, US97-U

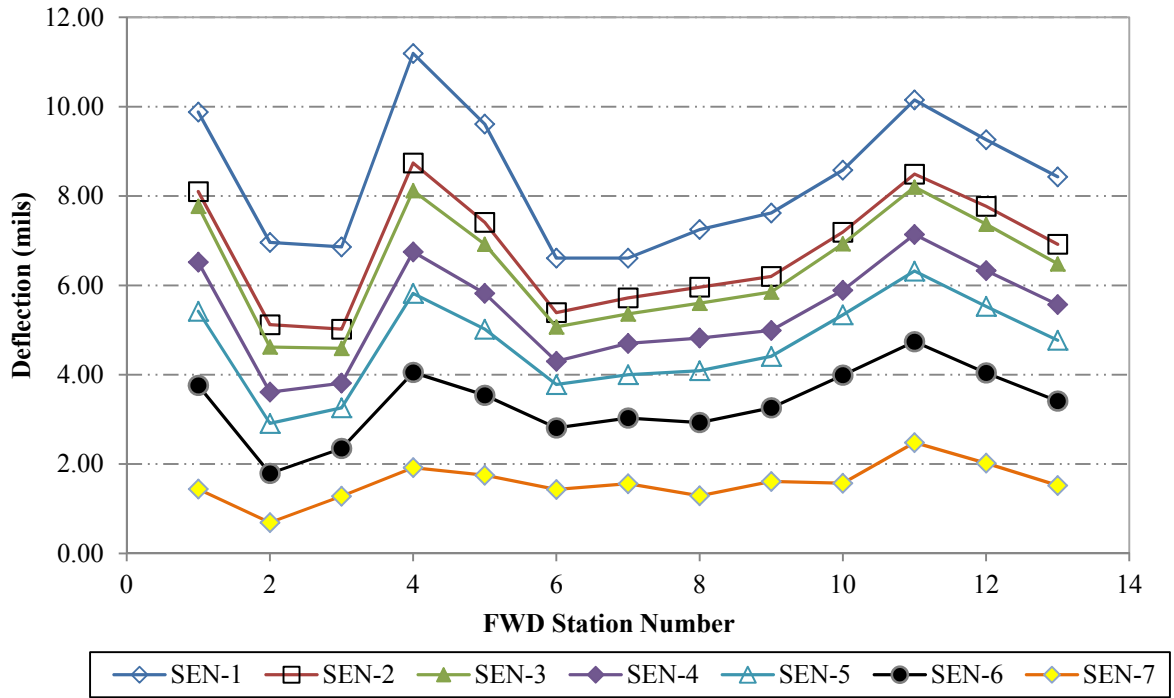


Figure 5.3: Deflection Profiles, US20-U

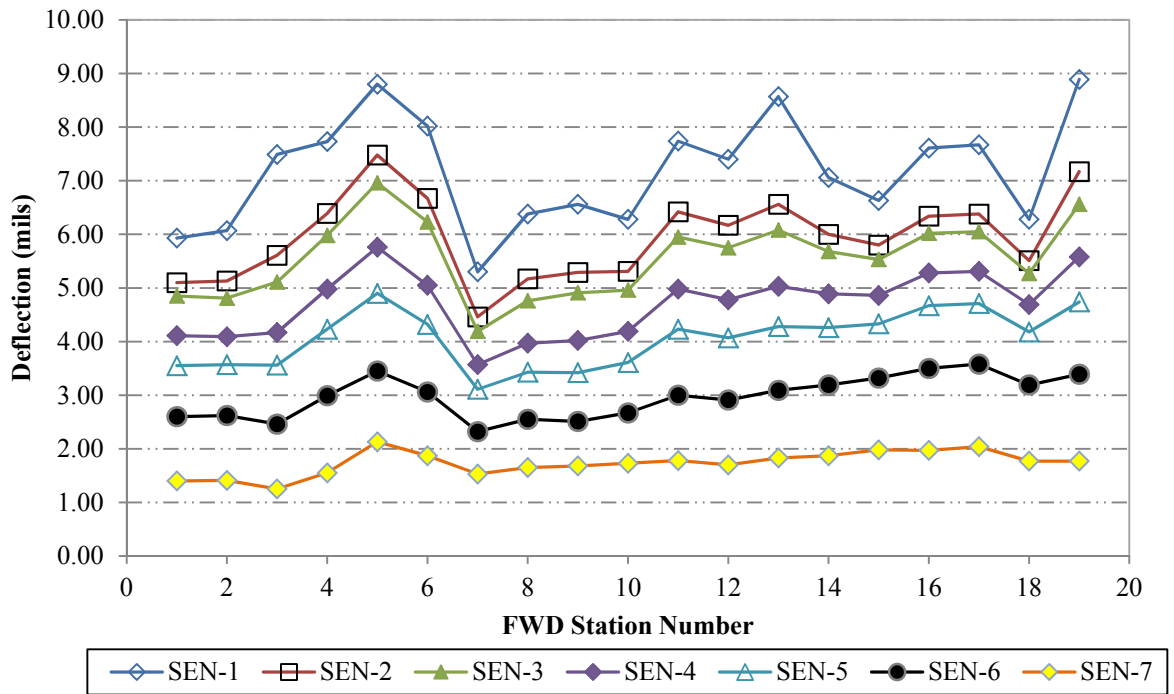


Figure 5.4: Deflection Profiles, OR99-U

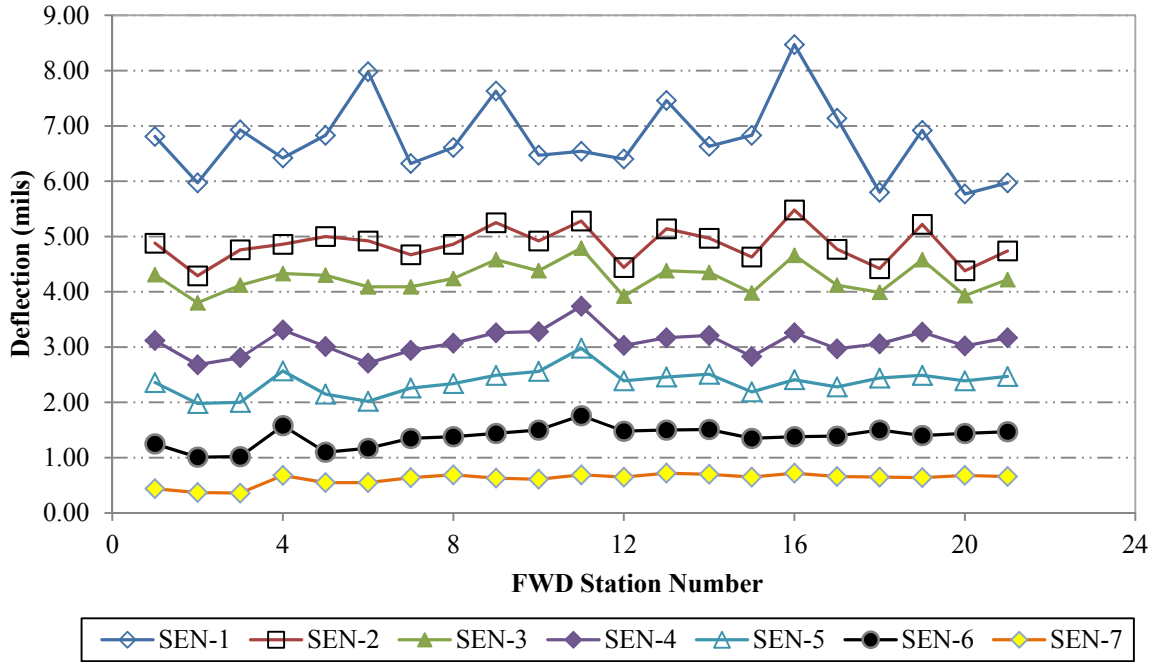


Figure 5.5: Deflection Profiles, OR238-C

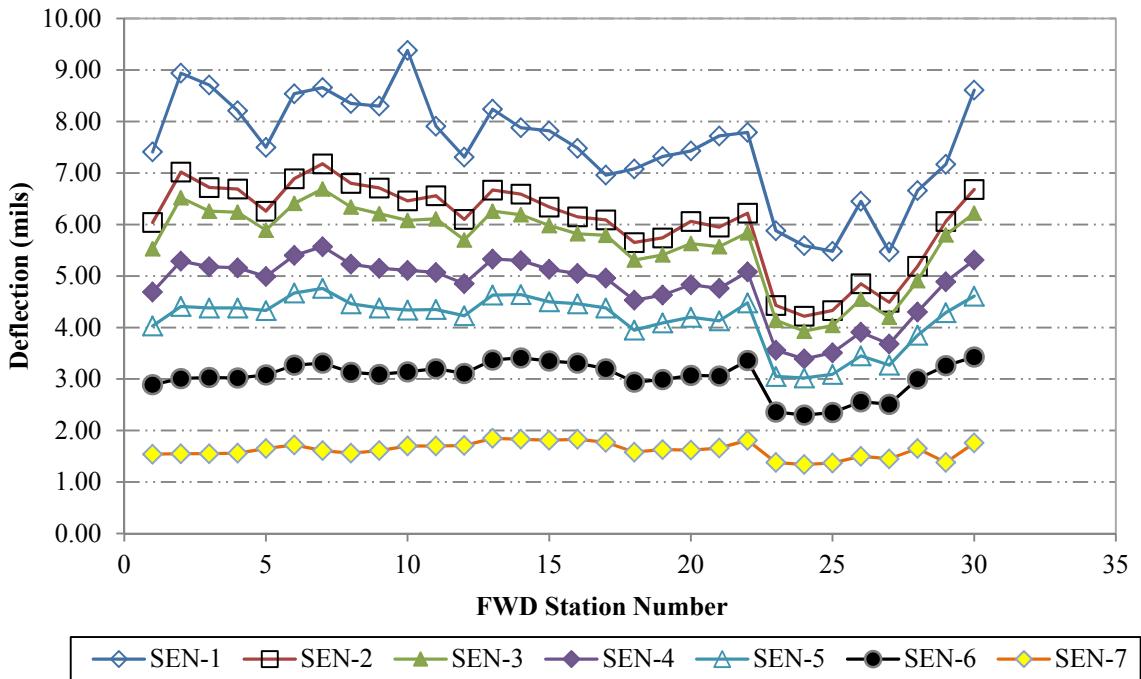


Figure 5.6: Deflection Profiles, OR99W-C

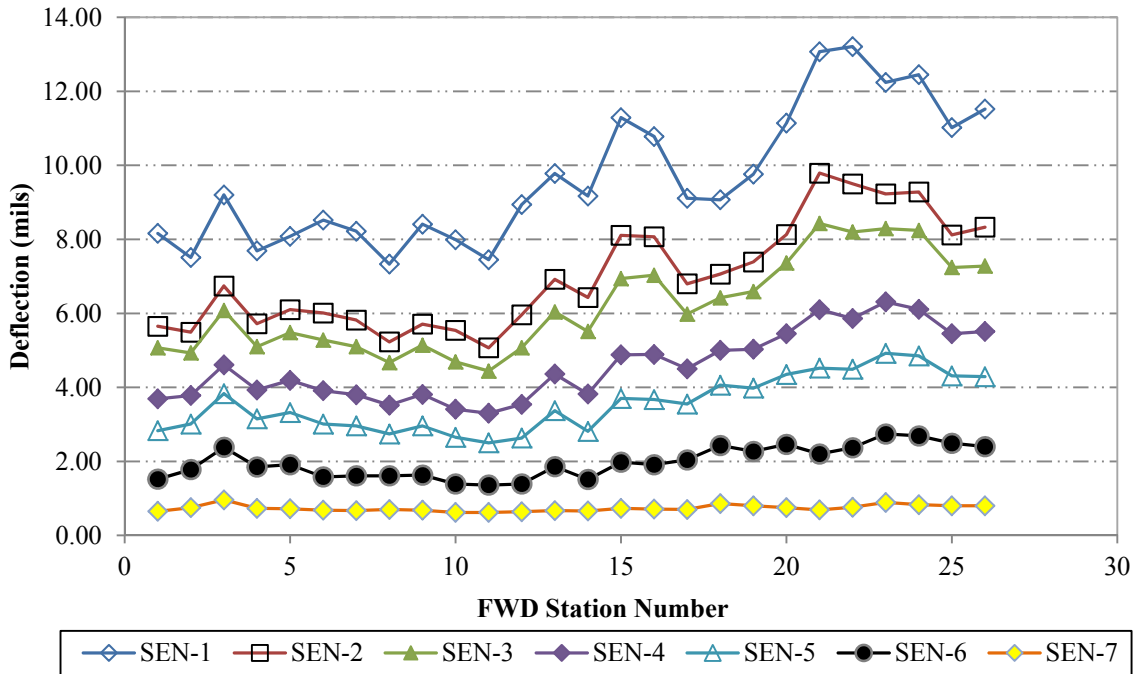


Figure 5.7: Deflection Profiles, OR221-C

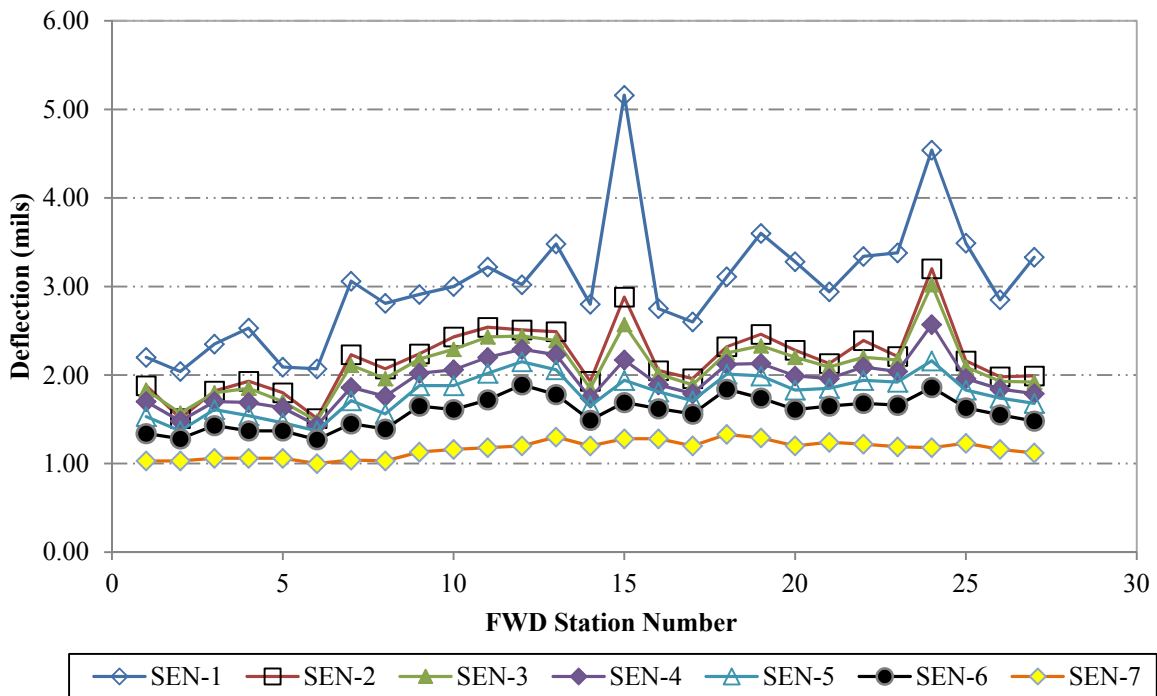


Figure 5.8: Deflection Profiles, OR99EB-C

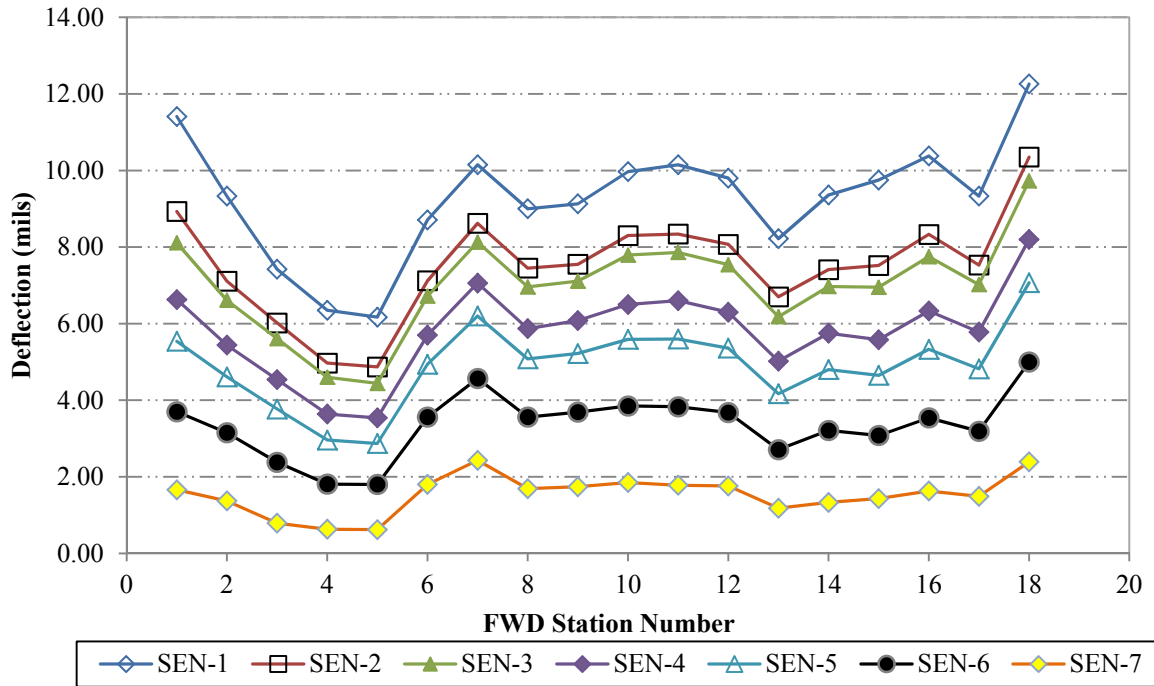


Figure 5.9: Deflection Profiles, OR140-C

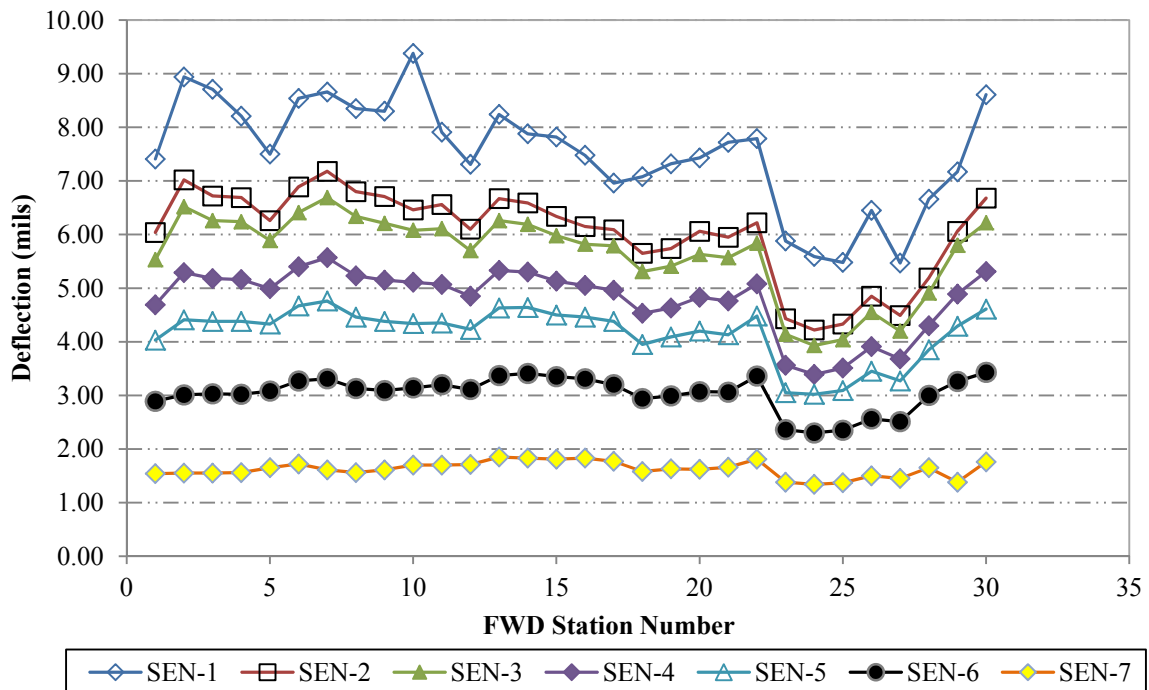


Figure 5.10: Deflection Profiles, OR99*-C

Table 5.1: Coefficient of Variation of the Measured Deflection Data

Test Site	Coefficient of Variation of the Measured Deflections (%)						
	D1	D2	D3	D4	D5	D6	D7
OR22-U	8	8	8	9	10	15	23
US97-U	15	16	17	17	18	22	35
US20-U	18	19	20	21	22	24	27
OR99-U	14	13	13	13	13	13	13
OR238-C	10	7	6	8	10	13	17
OR99W-C	14	14	14	13	12	11	9
OR221-C	19	21	20	20	21	22	12
OR99EB-C	23	17	16	13	12	11	8
OR140-C	17	18	18	20	21	24	33
OR99*-C	14	14	14	13	12	11	9

Figure 5.11 shows the center deflection normalized to a 9000-lb load and temperature of 68 °F as described in Chapter 4. Figure 5.12 illustrates the variations of the center deflection across the pavement sections. As can be seen, all the non-cracked sections except OR99-U exhibited higher center deflections (larger than 6 mils). US97-U (good performing section) displayed the highest amount of center deflection with the greatest variation (average 10.5 mils and a standard deviation of 2.225 mils) while section OR99EB-C (cracked section) exhibited the lowest amount of center deflection of 2.2 mils. It is important to point out that OR99EB-C was built with cement treated base (CTB) of 11 inches. Among top-down cracked pavements, pavement sections OR238-C, OR99W-C, and OR99*-C showed center deflection values between 4.0-5.0 mils. The other two cracked sections, OR221-C and OR140-C, exhibited center deflection greater than 7.5 mils.

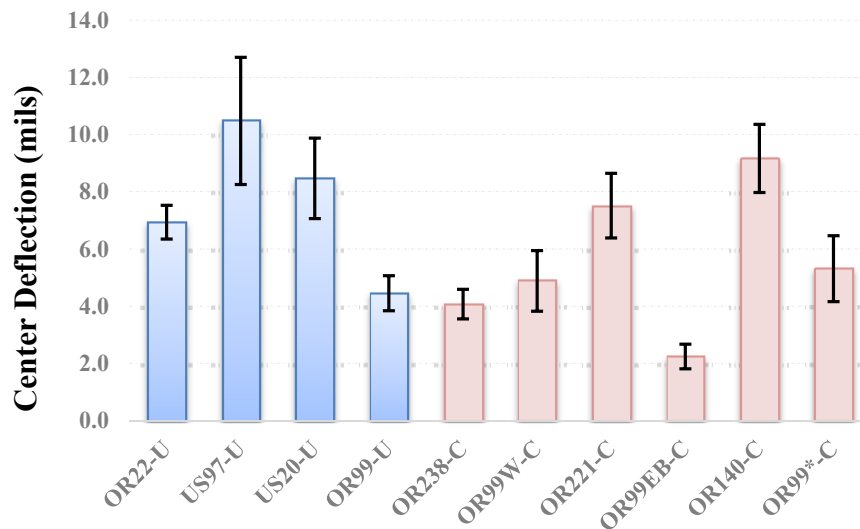


Figure 5.11: Normalized Center Deflection

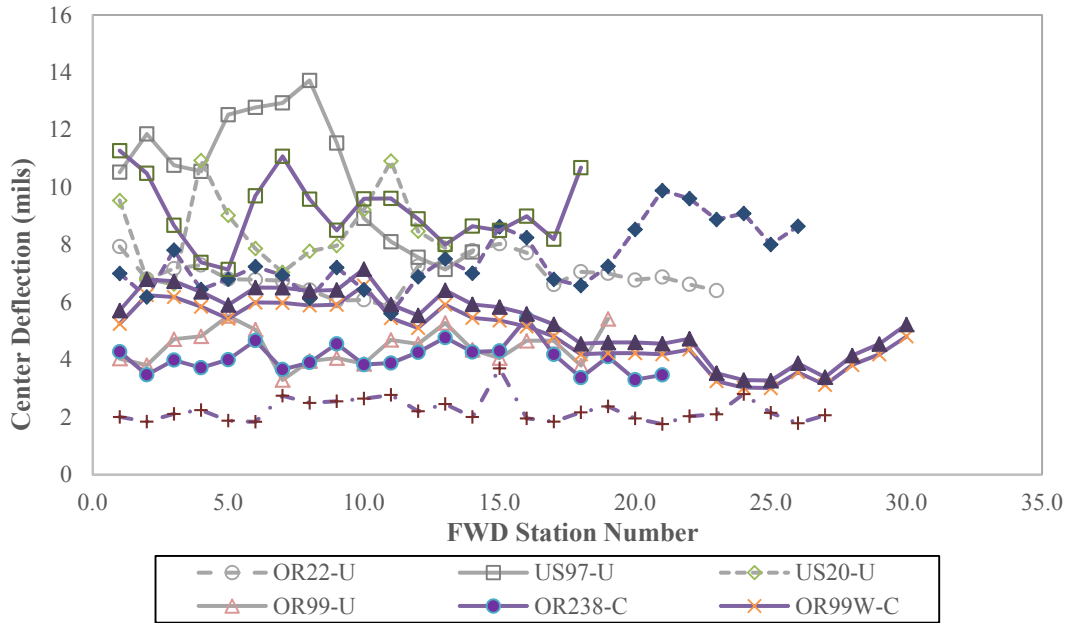


Figure 5.12: Variations of Normalized Center Deflection across the Pavement Sections
5.1.1.2 Backcalculated Layer Moduli

The stiffness moduli of the pavement layers were determined from the FWD deflection data using backcalculation software Elmod 6.0 (Evaluation of Layer Moduli and Overlay Design) and BAKFAA (FAA backcalculation analysis). The use of backcalculation procedures is an iterative adaptation of elastic layer theory. In a backcalculation procedure, deflection values are calculated for assumed elastic moduli values, compared with the observed deflection values and then accordingly the assumed moduli values are further adjusted for the next iteration. The iteration process continues until calculated and observed deflection values match closely. Both software, Elmod 6.0 and BAKFAA, require information on pavement layers (layer thickness and type of materials), pavement condition (pavement temperature and time of the day) at FWD test site, and the FWD measured deflection data to obtain backcalculated layer moduli (shown in Table 5.2).

Table 5.2: Input Used in the Backcalculation Process

Test Section	Surface Temp. (F)	Air Temp. (F)	Pavement Temp. (F)	Thickness (in)	
				AC	Base
OR22-U	107.5	76.8	99.7	9.6	11
US97-U	68.1	59.4	62.8	8.4	14
US20-U	65.2	57.2	60.7	9.9	9
OR99-U	92.0	84.5	87.1	10.0	8
OR238-C	91.9	79.5	91.2	8.5	10
OR99W-C	82.4	78.3	80.1	12.8	8
OR221-C	77.4	70.0	74.5	8.6	11

OR99EB-C	78.1	71.3	75.1	8.2	11
OR140-C	73.0	52.6	61.2	9.5	8
OR99*-C	82.4	78.3	79.7	8.9	8

Table 5.3 summarizes the normalized (temperature corrected to 68°F) backcalculated moduli for the average, 15-percentile, and 85-percentile properties while Table 5.4 shows the coefficient of variation of the backcalculated layer moduli. Figure 5.13 illustrates comparisons of the backcalculated layer moduli of the projects included in this study. As can be seen, OR22-U and OR99-U exhibited higher AC moduli (E1) values compared to US97-U and US20-U, among non-cracked sections.

Table 5.3: Temperature Corrected Backcalculated Moduli

OR22-U						
Parameter	Backcalculated Moduli (ksi)					
	Elmod			BAKFAA		
	AC	Base	Subgrade	AC	Base	Subgrade
Average	741	21	23	980	15	22
15th Percentile	620	13	19	770	6	15
85th Percentile	830	29	27	1131	31	28
US97-U						
Parameter	Backcalculated Moduli (ksi)					
	Elmod			BAKFAA		
	AC	Base	Subgrade	AC	Base	Subgrade
Average	454	35	19	577	23	36
15th Percentile	337	21	14	315	8	23
85th Percentile	568	49	25	816	73	54
US20-U						
Parameter	Backcalculated Moduli (ksi)					
	Elmod			BAKFAA		
	AC	Base	Subgrade	AC	Base	Subgrade
Average	423	50	27	471	56	30
15th Percentile	332	29	21	316	8	20
85th Percentile	525	93	34	780	81	47
OR99-U						
Parameter	Backcalculated Moduli (ksi)					
	Elmod			BAKFAA		
	AC	Base	Subgrade	AC	Base	Subgrade
Average	1098	64	32	1283	75	27
15th Percentile	670	41	27	810	26	23
85th Percentile	1518	82	37	1682	140	31
OR238-C						
Parameter	Backcalculated Moduli (ksi)					
	Elmod			BAKFAA		
	AC	Base	Subgrade	AC	Base	Subgrade
Average	956	76	36	1050	53	58
15th Percentile	604	58	28	660	21	44
85th Percentile	1426	96	40	1644	104	65

Table 5.3: Temperature Corrected Backcalculated Moduli (Cont.)

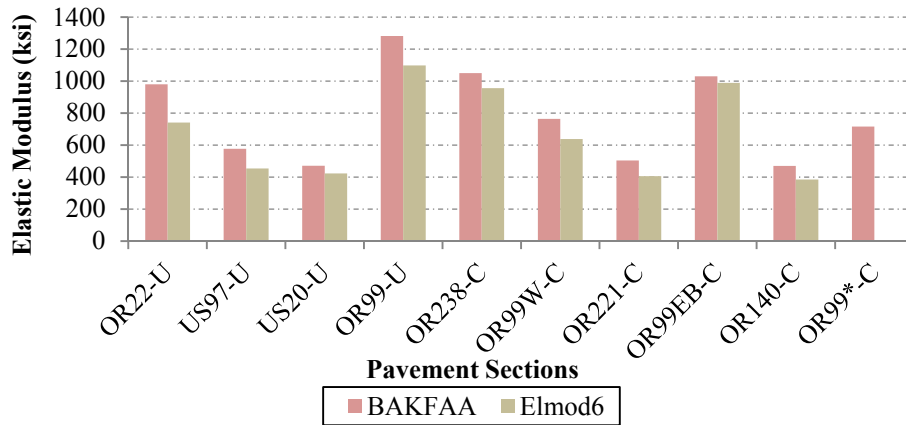
OR99W-C						
Parameter	Backcalculated Moduli (ksi)					
	Elmod			BAKFAA		
	AC	Base	Subgrade	AC	Base	Subgrade
Average	638	35	28	764	35	36
15th Percentile	453	19	19	453	5	22
85th Percentile	896	59	35	1145	68	35
OR221-C						
Parameter	Backcalculated Moduli (ksi)					
	Elmod			BAKFAA		
	AC	Base	Subgrade	AC	Base	Subgrade
Average	407	53	21	504	25	46
15th Percentile	341	31	15	408	10	33
85th Percentile	467	71	27	616	64	56
OR99EB-C						
Parameter	Backcalculated Moduli (ksi)					
	Elmod			BAKFAA		
	AC	Base	Subgrade	AC	Base	Subgrade
Average	989	1673	24	1030	2974	35
15th Percentile	758	767	22	651	684	23
85th Percentile	1207	2687	27	1403	8070	42
OR140-C						
Parameter	Backcalculated Moduli (ksi)					
	Elmod			BAKFAA		
	AC	Base	Subgrade	AC	Base	Subgrade
Average	385	40	26	470	34	31
15th Percentile	329	28	20	321	6	21
85th Percentile	493	52	31	643	75	39
OR99*-C						
Parameter	Backcalculated Moduli (ksi)					
	Elmod			BAKFAA		
	AC	Base	Subgrade	AC	Base	Subgrade
Average				716	89	16
15th Percentile				471	54	15
85th Percentile				943	124	17

Table 5.4: Coefficients of Variation of the Backcalculated Layer Moduli

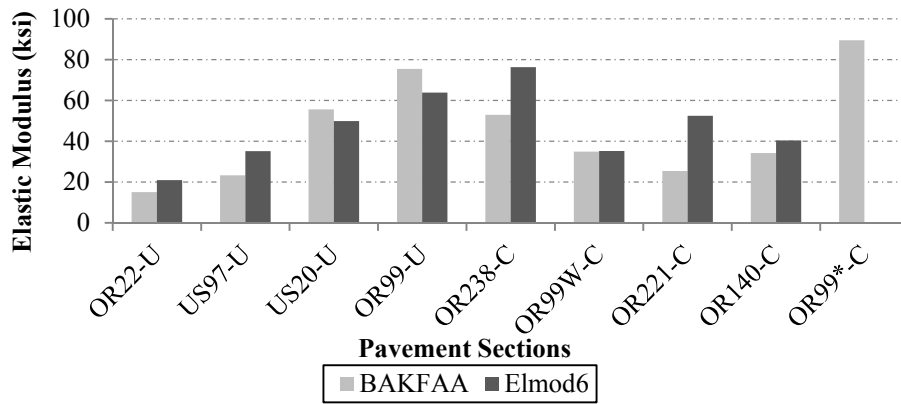
Test Section	Coefficient of Variation of Backcalculated Moduli (%)					
	Elmod			BAKFAA		
	E1	E2	E3	E1	E2	E3
OR22-U	17	39	17	18	86	25
US97-U	22	30	22	35	115	34
US20-U	21	51	26	39	77	40
OR99-U	28	27	15	29	63	13
OR238-C	34	32	26	39	66	25
OR99W-C	36	53	24	45	98	94
OR221-C	16	30	26	19	85	19
OR99EB-C	27	52	9	38	148	21
OR140-C	16	27	16	30	93	54
OR99*-C				31	39	22

Among pavements with top-down cracking, OR238-C, OR99W-C, OR99EB-C, and OR99*-C display higher AC moduli (E1) values compared to values of OR221-C and OR140-C. For base moduli (E2), higher moduli values are observed with US20-U, OR99-U, OR238-C, and OR99*-C than the remaining sections included in this study. For subgrade moduli (E3), similar moduli values are displayed by most of the sections included in this study except OR238-C.

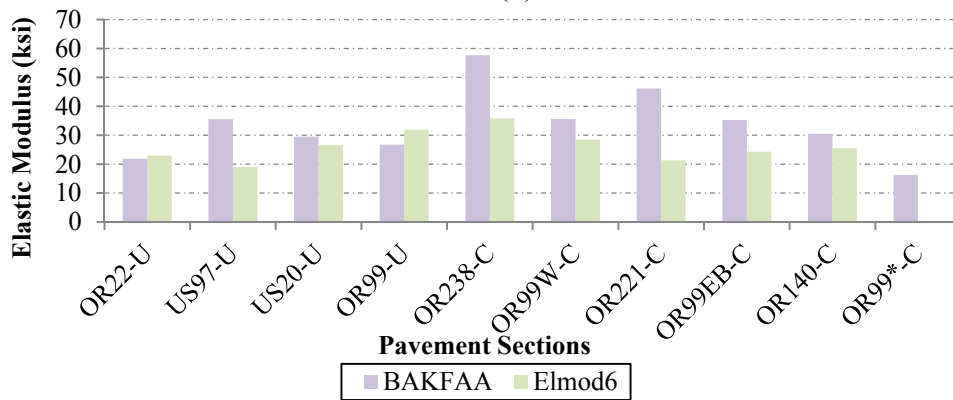
Figure 5.14 describes the comparison (correlation) between the two backcalculation softwares, Elmod and BAKFAA for AC modulus, base modulus, and subgrade modulus. As can be seen, a good correlation for AC modulus was observed while no consistent correlation for base and subgrade moduli was found. AC moduli determined by BAKFAA were higher than the values predicted by Elmod. Figures 5.15 through 5.25 illustrates the variations of backcalculated moduli along the pavement sections.



(a)

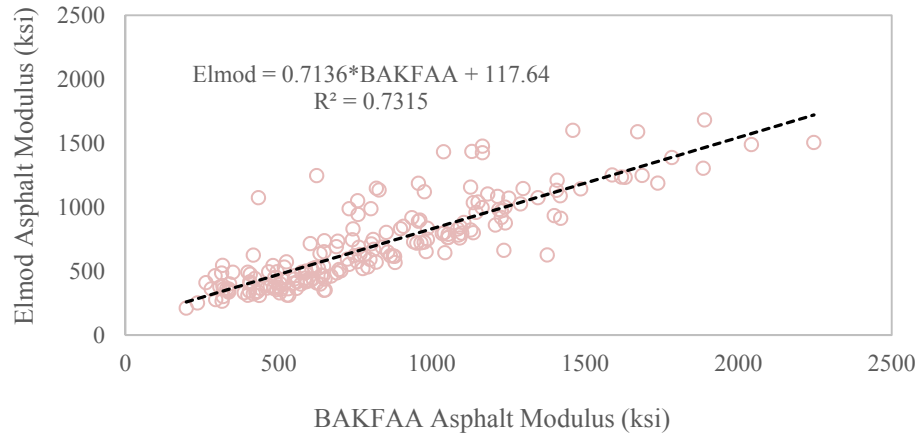


(b)

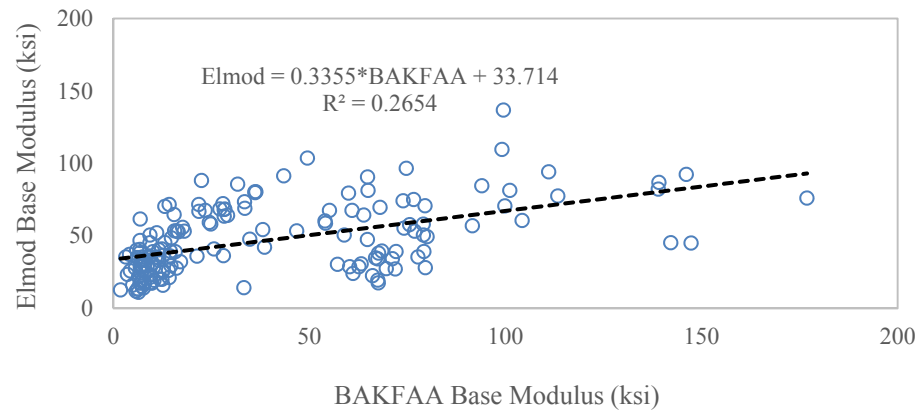


(c)

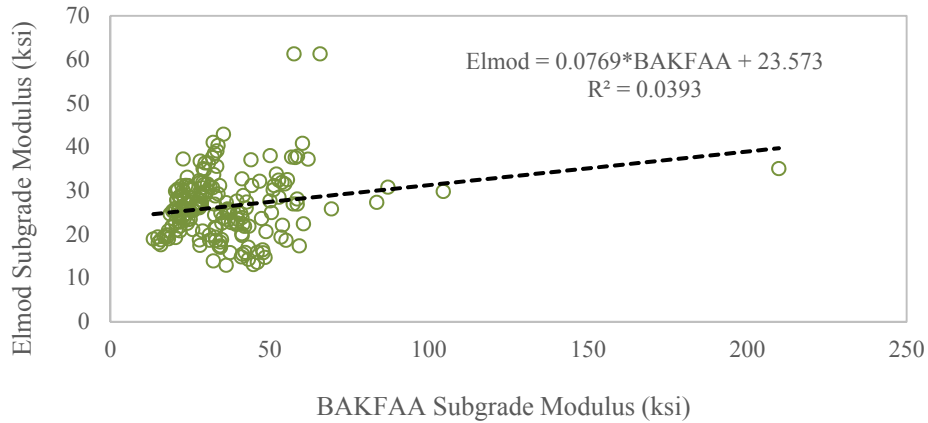
Figure 5.13: Average Backcalculated Moduli (a) AC Moduli, (b) Base Moduli, and (c) Subgrade Moduli



(a)



(b)



(c)

Figure 5.14: Correlation between Elmod and BAKFAA for (a) AC Moduli, (b) Base Moduli, and (c) Subgrade Moduli

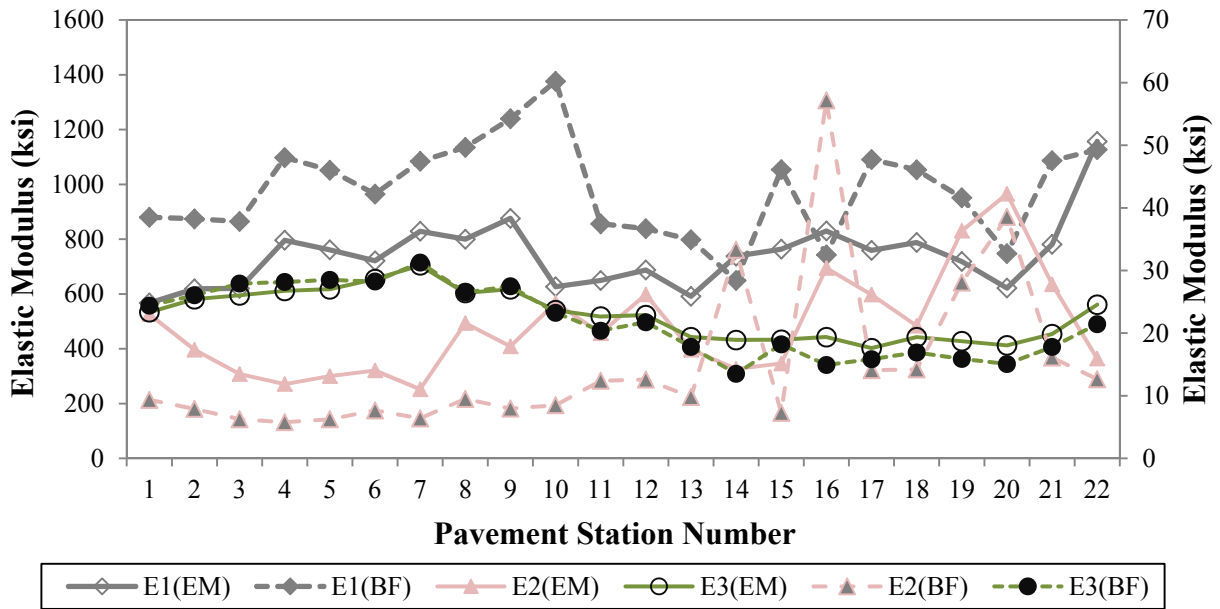


Figure 5.15: Variations of Backcalculated Layer Moduli, OR22-U

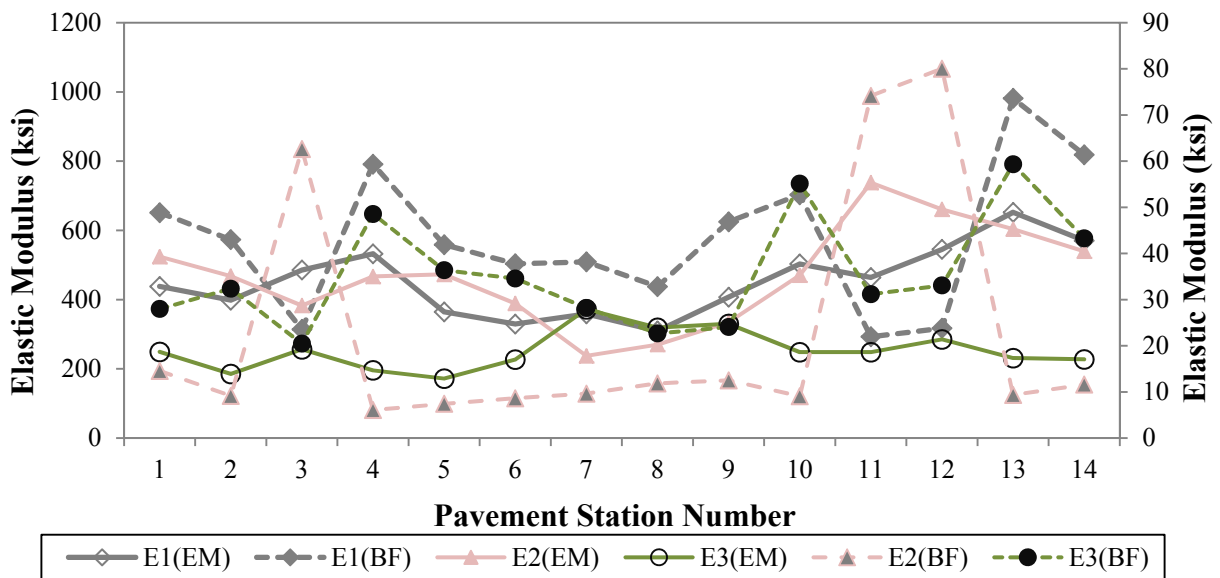


Figure 5.16: Variations of Backcalculated Layer Moduli, US97-U

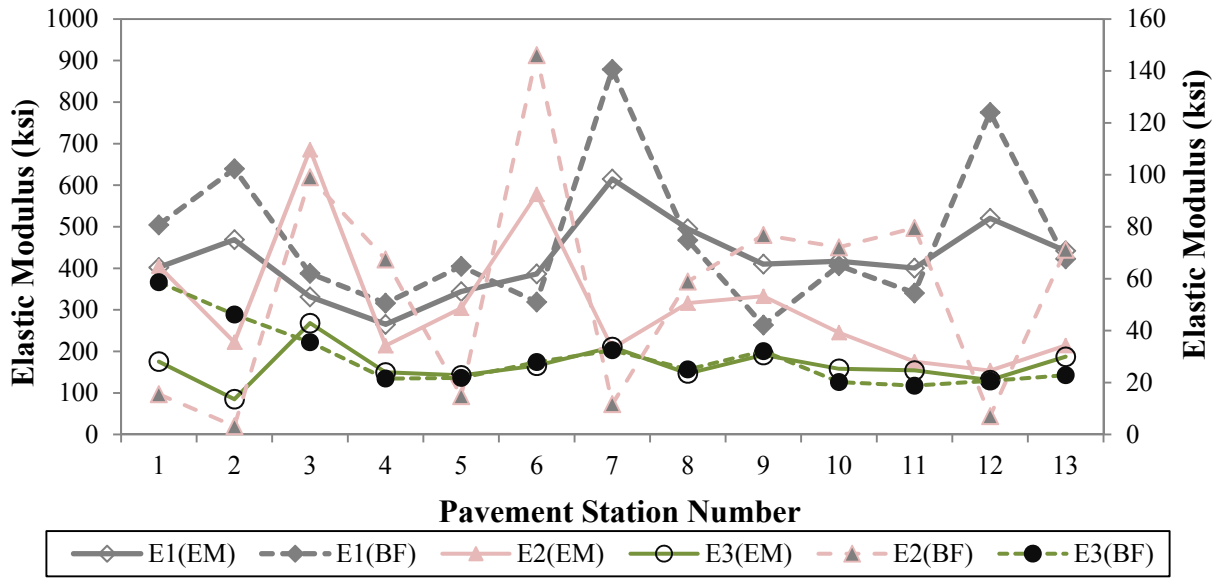


Figure 5.17: Variations of Backcalculated Layer Moduli, US20-U

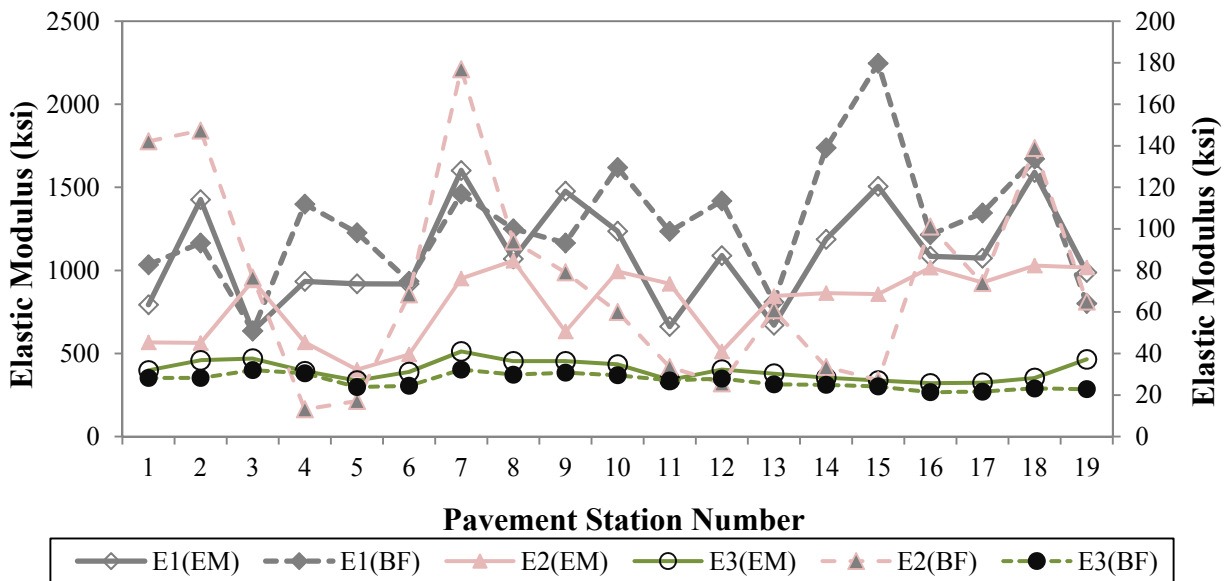


Figure 5.18: Variations of Backcalculated Layer Moduli, OR99-U

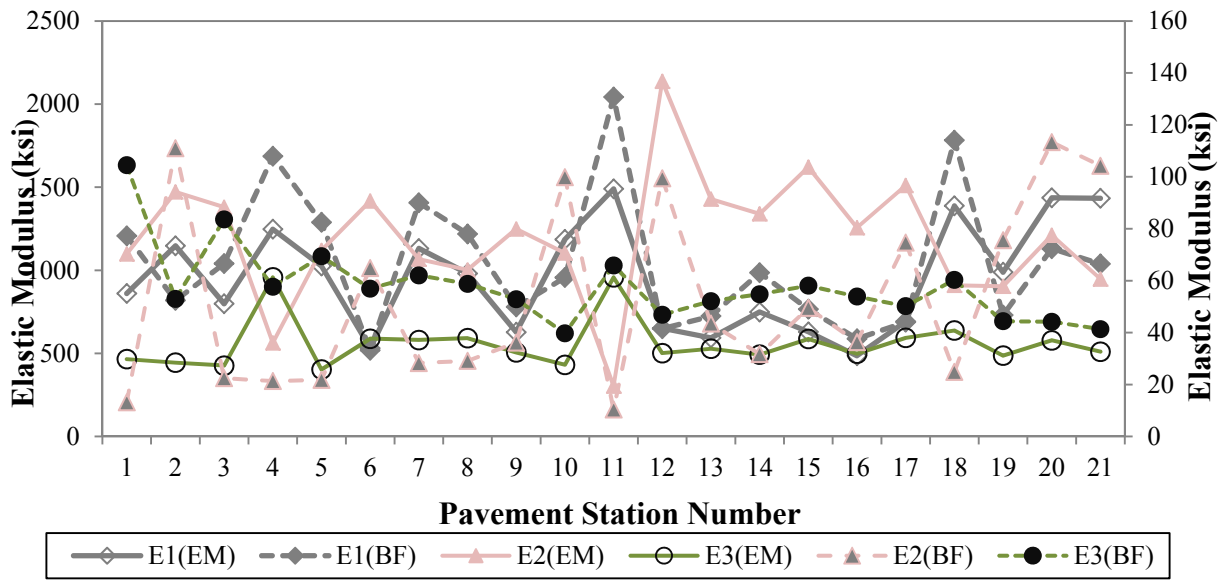


Figure 5.19: Variations of Backcalculated Layer Moduli, OR238-C

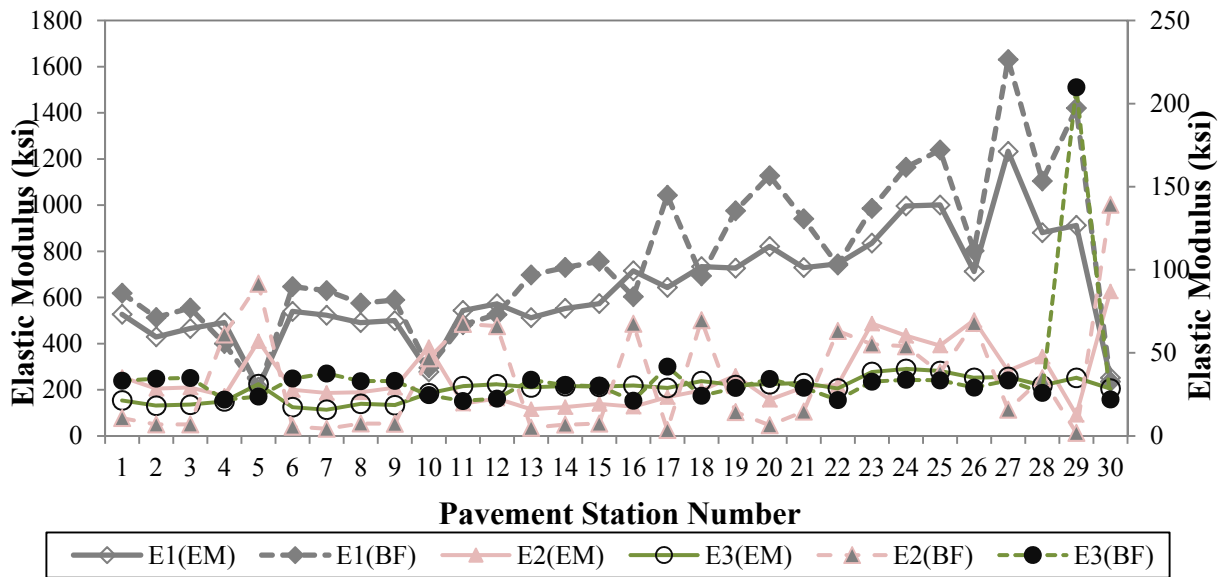


Figure 5.20: Variations of Backcalculated Layer Moduli, OR99W-C

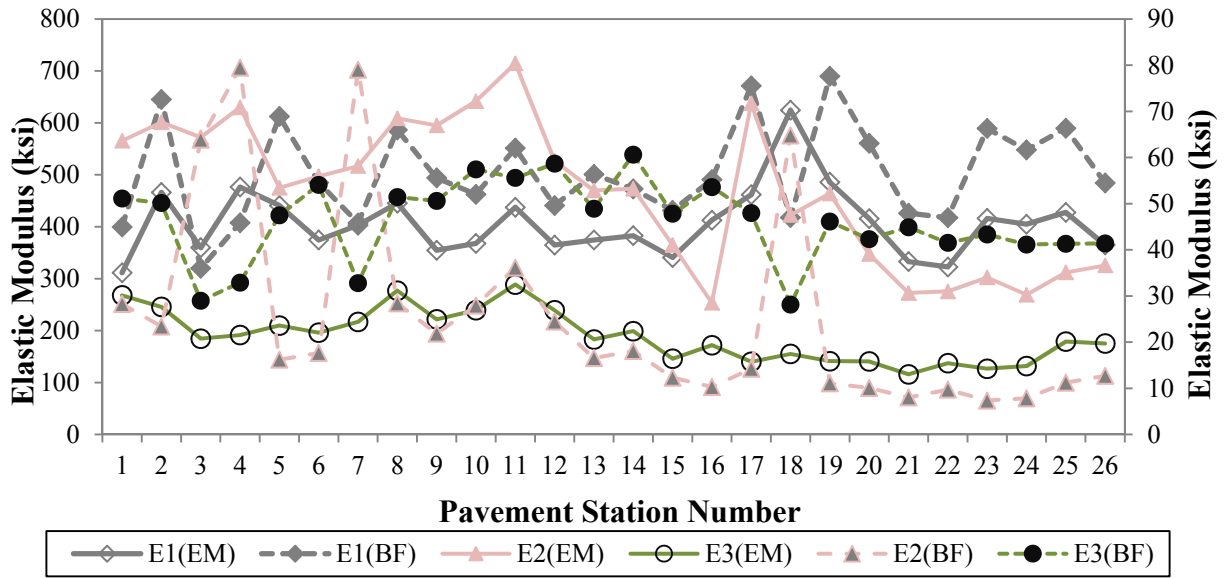


Figure 5.21: Variations of Backcalculated Layer Moduli, OR221-C

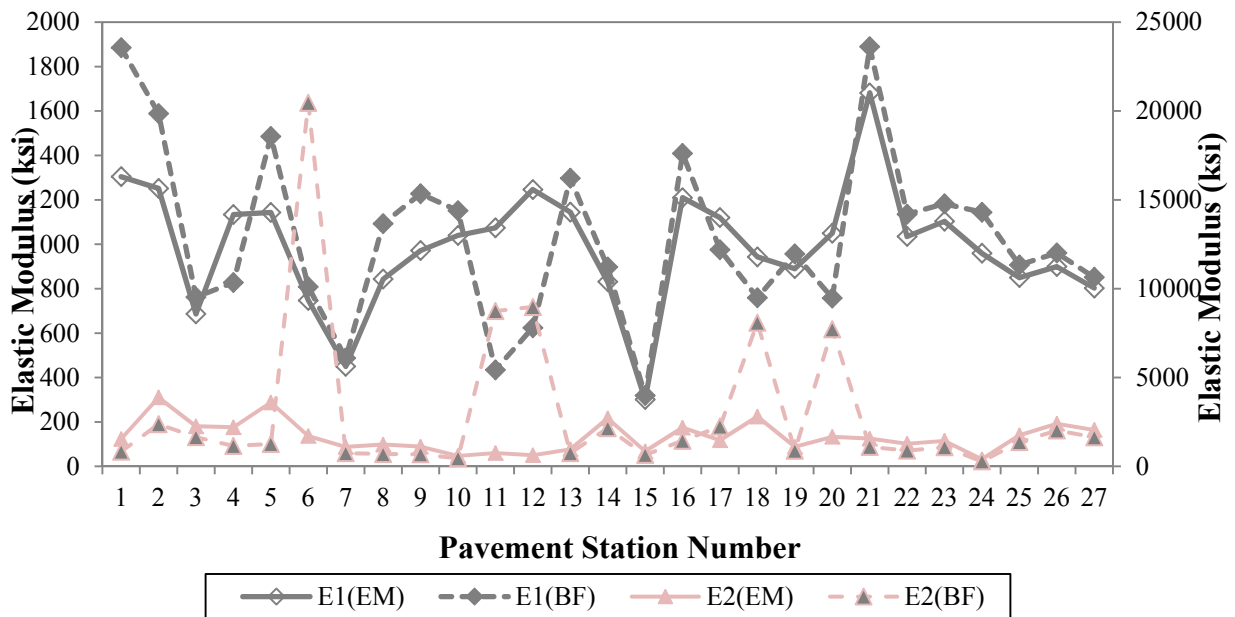


Figure 5.22: Variations of Backcalculated Layer Moduli, OR99EB-C

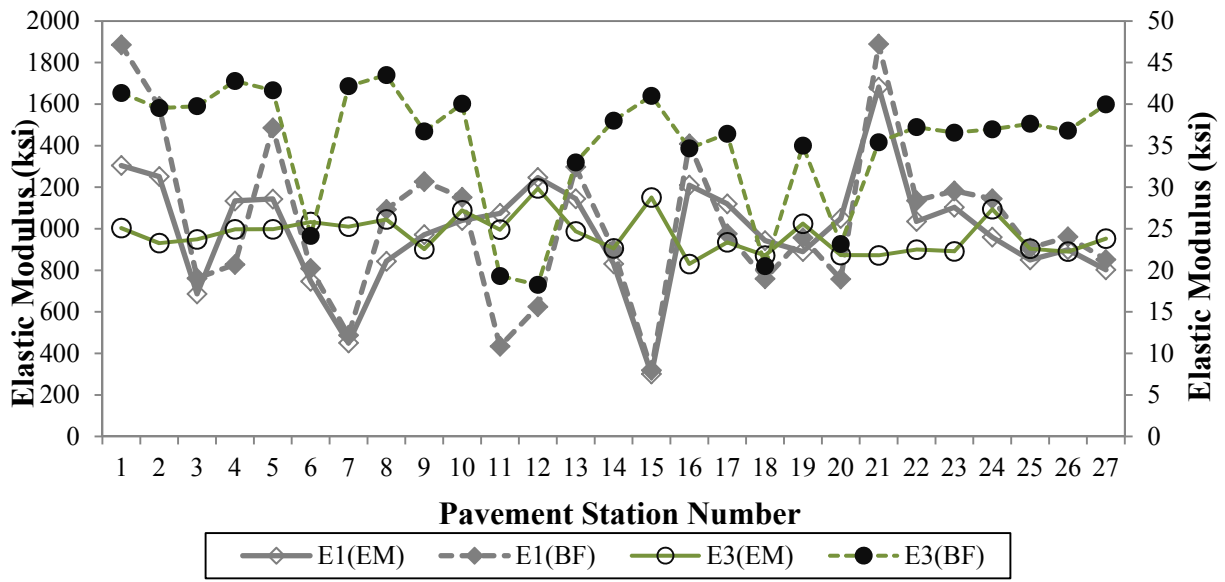


Figure 5.23: Variations of Backcalculated Layer Moduli, OR99EB-C

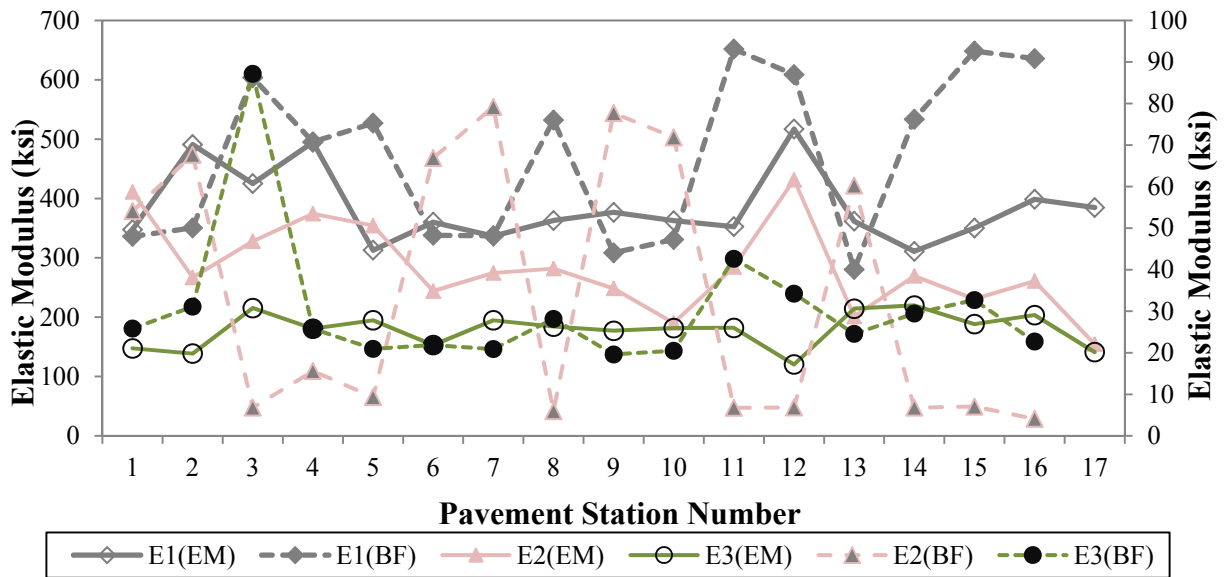


Figure 5.24: Variations of Backcalculated Layer Moduli, OR140-U

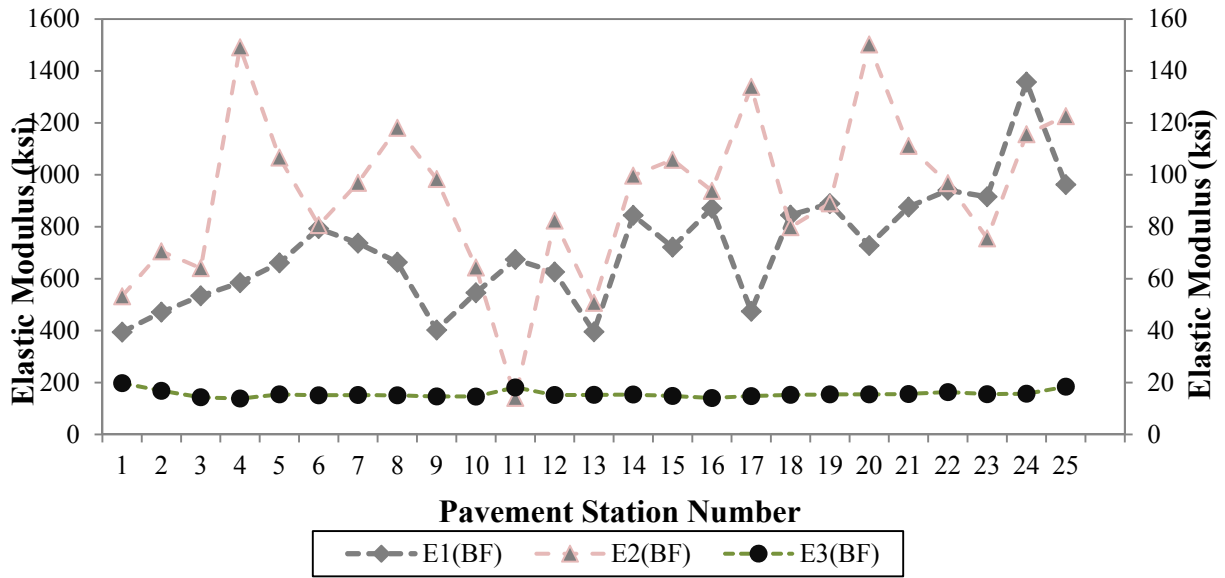


Figure 5.25: Variations of Backcalculated Layer Moduli, OR99*-C

5.1.1.3 Structural Capacity

Table 5.5 summarizes the average subgrade resilient modulus, effective pavement elastic modulus, and effective structural number of each test section included in this study. The average values of the M_r back calculated from deflections at 48 and 60 inches were used as the determined subgrade resilient moduli. The effective pavement modulus above subgrade (E_p) and effective structural number (S_{Neff}) were computed following the AASHTO (1993) procedure described in Chapter 4. Among non-cracked sections, the highest S_{Neff} value of 7.1 was estimated with OR99-U while US97-U had the lowest S_{Neff} value of 4.8. The highest S_{Neff} value of 7.9 and the lowest S_{Neff} value of 4.9 were estimated for OR99EB-C and OR221-C, respectively, among top-down cracked pavement sections.

Table 5.5: Subgrade Resilient Modulus, Effective Modulus and Effective Structural Number Backcalculated from FWD Test Results

Section	Mr (psi)	Ep (psi)	S _{Neff}
OR22-U	18485	333217	6.4
US97-U	28627	108665	4.8
US20-U	25029	254963	5.4
OR99-U	25512	663015	7.1
OR238-C	61048	388291	6.1
OR99W-C	25512	291348	6.8
OR221-C	48269	172638	4.9
OR99EB-C	42426	758348	7.9
OR140-C	26140	276269	5.1
OR99*-C	24020	636189	6.6

5.1.2 Dynamic Cone Penetrometer Test Results

Dynamic cone penetrometer (DCP) tests were conducted on each of the pavement sections except OR99W-C and OR140-C to evaluate the variations in density. The DCP penetration distance per drop is known as the DCP penetration index (DCPI) or penetration resistance (PR). The DPI can be used to estimate the shear strength and modulus of unbound materials using empirical relationships. Figure 5.26 illustrates average penetration resistance (PR) of the test sections included in this study. Both sections OR238-C and OR221-C had three locations along the longitudinal direction where DCP tests were conducted. Only one location on OR99-U while the remaining sections had two locations for DCP tests. As can be seen from Figure 5.26, OR99EB-C exhibited the highest variability in PR while sections US20-U, OR238-C, and OR99*-C showed consistent PR values at different locations. Similar variability in PR values at different locations was observed on the sections OR22-U and US97-U. For section OR221-C, two locations had identical PR (around 3 mm/blow) values but the third location had a PR value of over 5 mm/blow.

Figures 5.27 through 5.34 show the DCP penetration resistance of the test sections along the depth. Table 5.6 shows the CBR and modulus values estimated from empirical correlations described in Chapter 4. Table 5.6 illustrates that modulus values of base and subgrade estimated from DCP testing are significantly higher than that of backcalculation process from FWD testing.

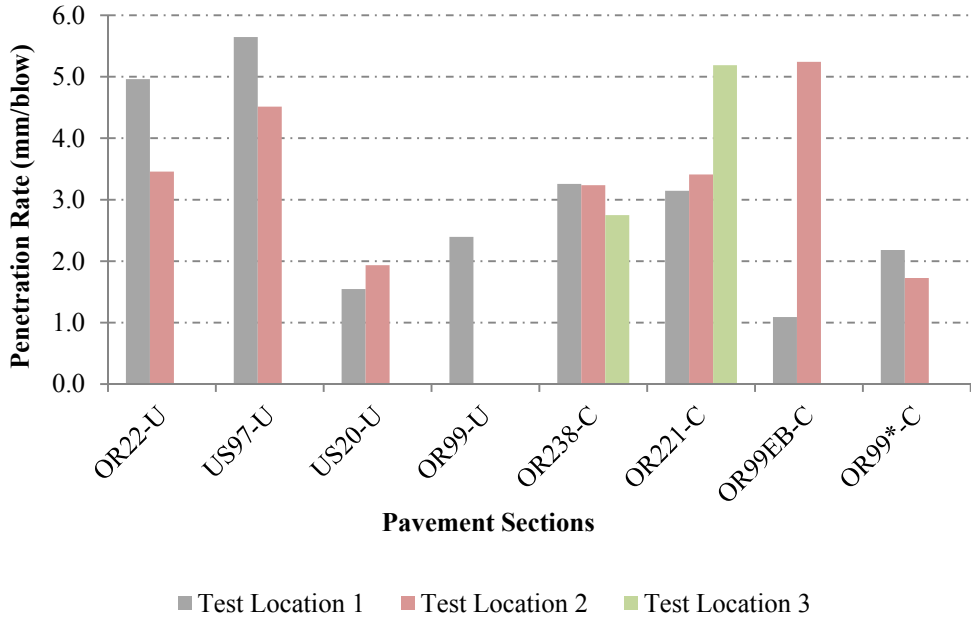


Figure 5.26: Average Penetration Resistance (PR) of the Test Sections

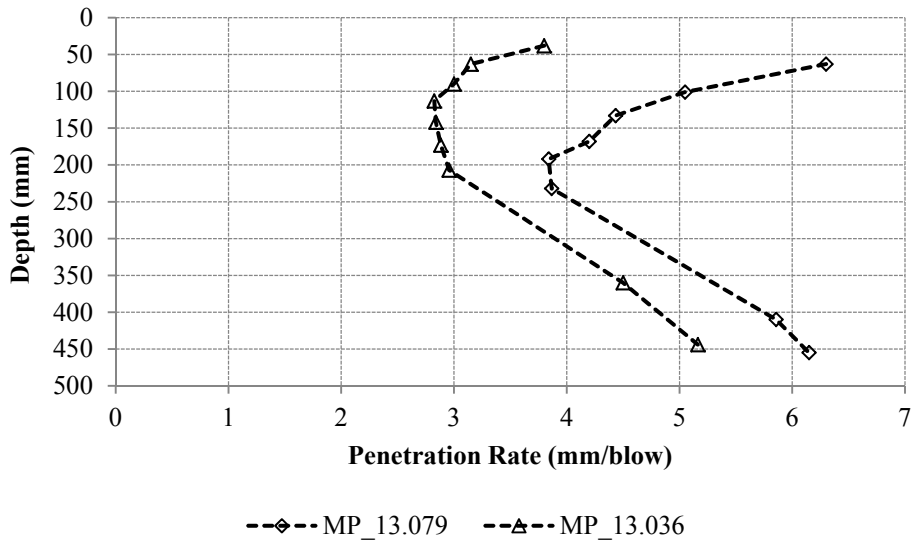


Figure 5.27: DCP Penetration Resistance, OR22-U

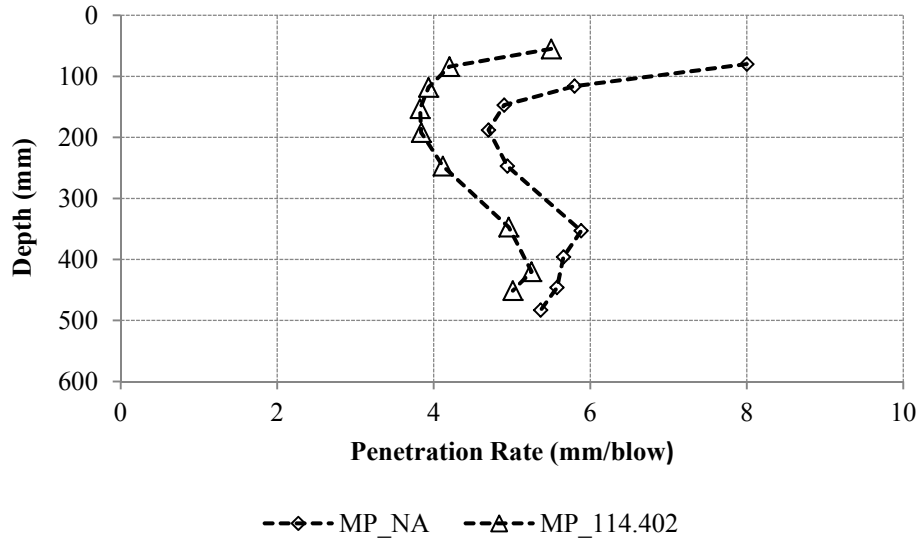


Figure 5.28: DCP Penetration Resistance, US97-U

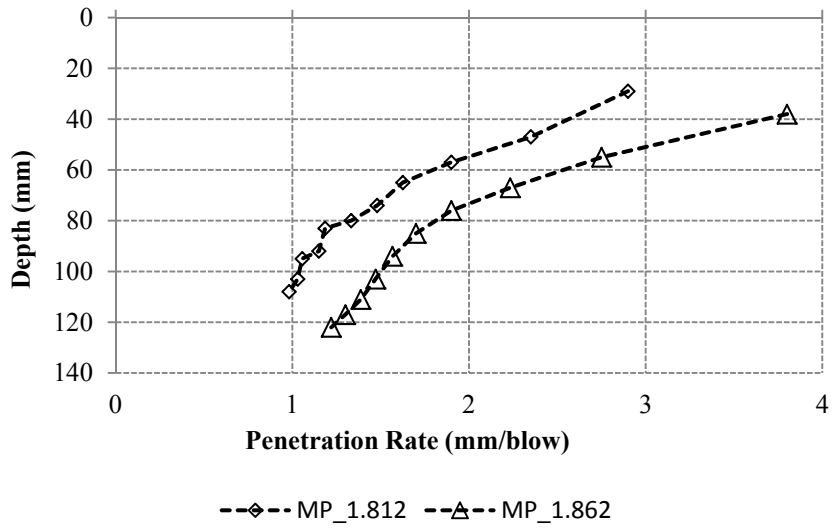


Figure 5.29: DCP Penetration Resistance, US20-U

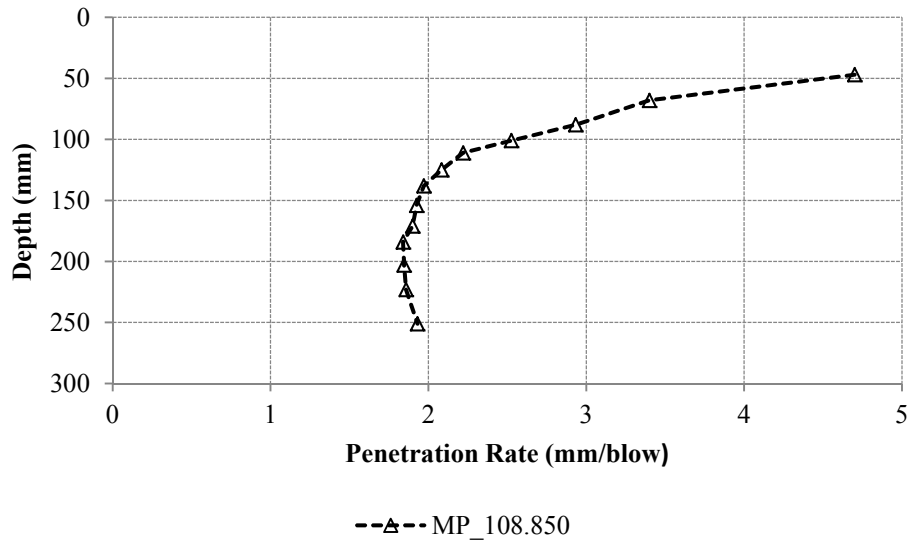


Figure 5.30: DCP Penetration Resistance, OR99-U

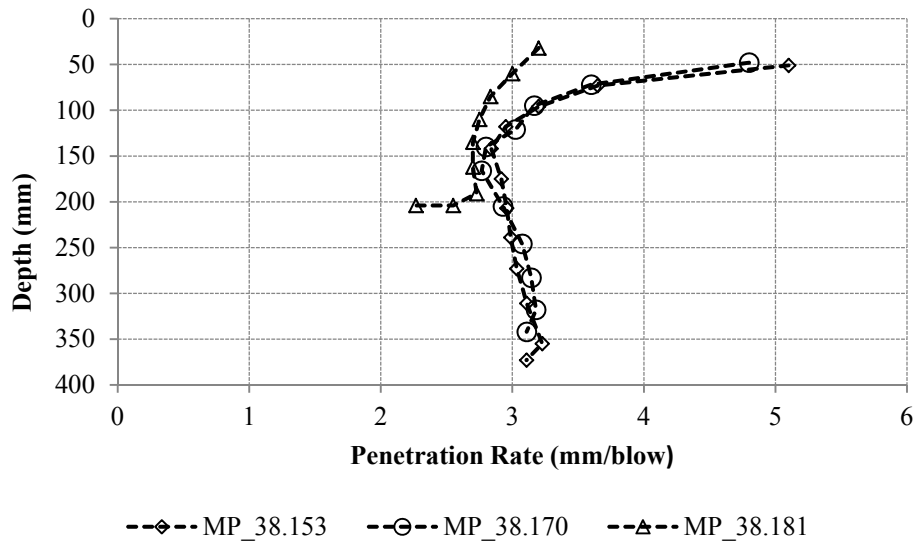


Figure 5.31: DCP Penetration Resistance, OR238-C

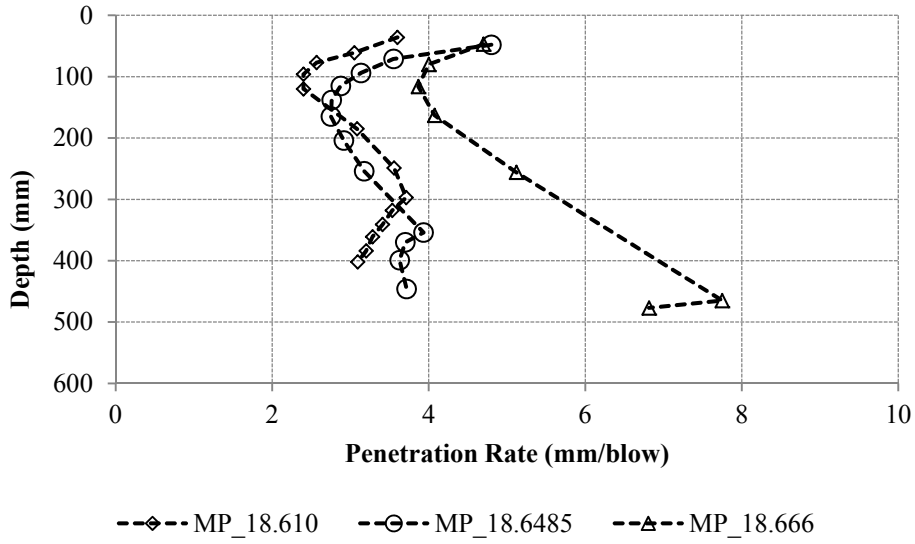


Figure 5.32: DCP Penetration Resistance, OR221-C

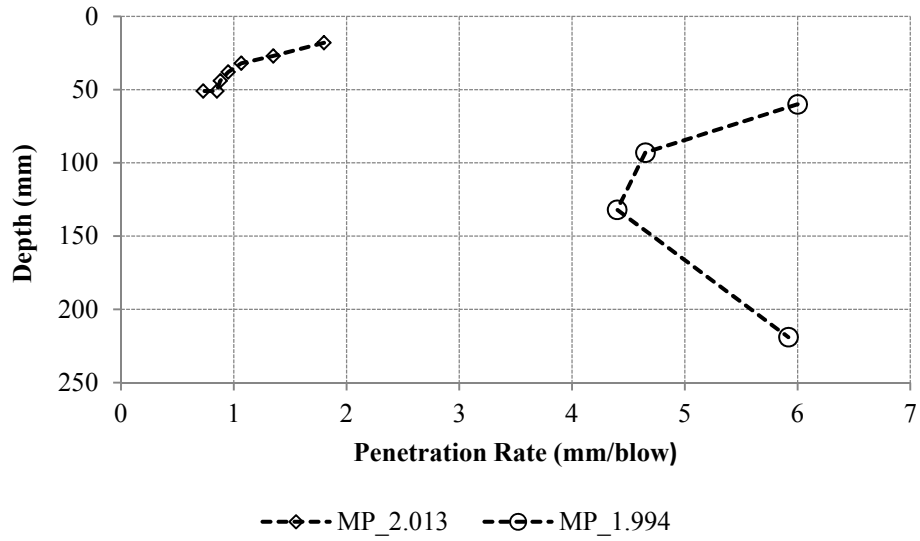


Figure 5.33: DCP Penetration Resistance, OR99EB-C

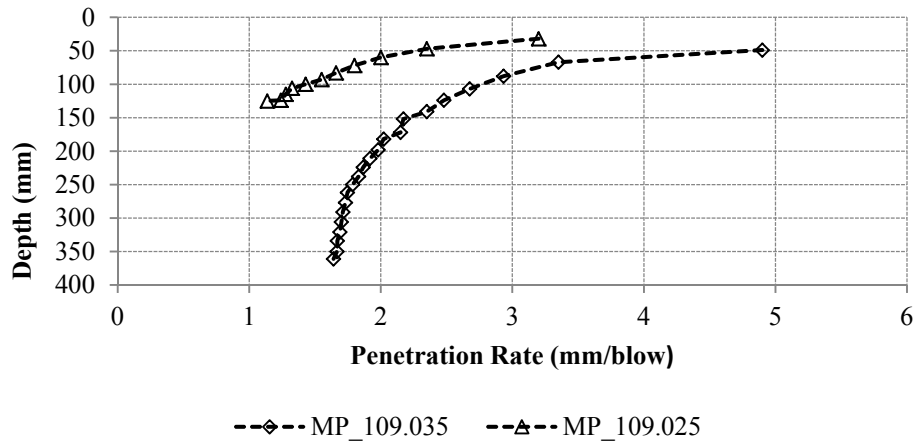


Figure 5.34: DCP Penetration Resistance, OR99*-C

Table 5.6: CBR and Modulus Values Estimated from PR through Empirical Correlations

Test Section	PR (mm/blow)	CBR ¹	CBR ²	Modulus ¹¹ (ksi)	Modulus ²² (ksi)	FWD Modulus (ksi)
OR22-U	3.8	102	65	153	97	21
US97-U	5.0	77	49	116	73	35
US20-U	1.7	239	157	359	236	50
OR99-U	2.4	169	110	254	165	64
OR238-C	3.1	127	82	191	122	76
OR221-C	3.5	114	73	171	109	53
OREB-C	1.1	397	265	595	398	
OR99*-C	2.2	184	120	277	180	65
Base/Subbase						
OR22-U	5.4	70	44	105	66	23
US97-U	5.2	73	46	109	69	19
OR238-C	3.1	127	82	191	122	36
OR221-C	6.6	57	36	86	53	21
OREB-C	5.2	73	46	109	68	21
OR99*-C	1.7	238	156	357	235	20
Subgrade						

¹CBR obtained from NCDOT correlations, ²CBR from U.S. Army Corp of Engineers, ¹¹Modulus from CBR¹ through ASSHTO correlations, ²²Modulus from CBR² using ASSHTO correlations.

5.1.3 Core Thickness Data

After all non-destructive tests were completed, cores were extracted at the designated locations using a power rotary drill. Ten cores were extracted from each of the pavement section with top-down cracking and five cores from each of the non-cracked pavement sections. Table 5.7 shows a lists of the average, maximum, minimum, and standard deviation of the measured thicknesses of pavement cores included in this study. Figures 5.35 illustrates the comparison of core thicknesses among the pavement sections. Among non-cracked sections, an average core thickness of 8.4-in was found with US97-U whereas the remaining sections had identical average core thicknesses of around 10 in. Section OR99-U exhibited largest variability (standard deviation of 1.744 in) in core thicknesses followed by US97-U with standard deviation of 1.0 in. OR99W-C had the largest core thickness of 12.8-in while the remaining sections showed an average core thickness in the range between 8.2 and 9.5-in, among top-down cracked sections.

Table 5.7: Variation in Core Thickness

Test Section	Number of Cores	Core Thickness (in)			
		Average	Maximum	Minimum	STD
OR22-U	5	9.6	10.0	9.3	0.33
US97-U	5	8.4	9.5	7.0	1.00
US20-U	5	9.9	10.0	9.5	0.22
OR99-U	4	10.0	12.5	8.5	1.74
OR238-C	10	8.5	9.3	8.0	0.45
OR99W-C	10	12.8	14.0	12.0	0.64
OR221-C	10	8.6	9.5	7.8	0.64
OR99EB-C	10	8.2	9.5	6.5	0.88
OR140-C	10	9.5	10.0	9.0	0.28
OR99*-C	10	8.9	9.5	8.5	0.36

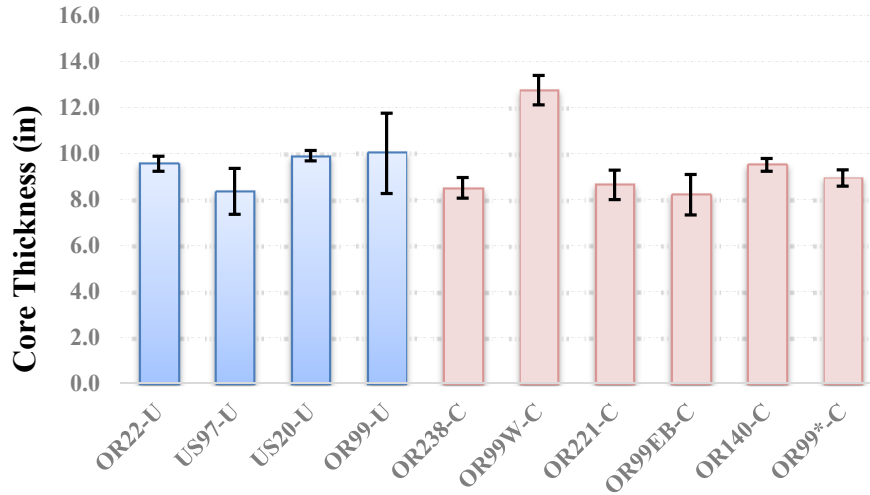


Figure 5.35: Average Core Thickness of the Sections

5.2 LABORATORY TEST RESULTS

5.2.1 Dynamic Modulus Test Results

Dynamic modulus tests were conducted on all the extracted cores under IDT mode described in Chapter 4. Each sample was tested at three different temperatures (4, 21, and 37°C) and six different frequencies (25, 10, 5, 1, 0.5, and 0.1 Hz). Table 5.8 summarizes the average $|E^*|$ results along with their standard deviation and coefficient of variation. The dynamic modulus test data output were used to construct master curves. Figure 5.36 shows the master curves of all the projects. It can be observed that all the top-down cracked sections except OR140-C displayed higher dynamic modulus values compared to the non-cracked sections. Figure 5.37 illustrates the comparisons of average dynamic modulus at different frequencies. It can be seen that at lower frequencies, the difference in dynamic modulus between top-down cracked sections and non-cracked sections was more pronounced.

Table 5.8: Summary of Dynamic Modulus (E^*) Test Results

Project	Temp	E^* -Dynamic Modulus (ksi)																	
		4C						21C						37C					
		Freq (Hz)	25	10	5	1	0.5	0.1	25	10	5	1	0.5	0.1	25	10	5	1	0.5
OR22-U	Avg.	1861	1852	1732	1577	1435	1177	1089	1179	904	584	470	285	288	282	224	108	87	36
	STD	121	140	122	85	112	60	65	67	72	46	44	31	40	52	32	24	19	8
	% CV	7	8	7	5	8	5	6	6	8	8	9	11	14	18	14	22	22	23
US97-U	Avg.	1349	1531	1369	1165	1085	832	780	830	629	362	280	165	214	192	139	70	51	27
	STD	544	60	121	52	74	73	78	85	71	52	49	35	34	20	23	14	10	7
	% CV	40	4	9	4	7	9	10	10	11	14	18	21	16	10	16	20	20	25
US20-U	Avg.	1935	2057	1754	1549	1446	1198	1079	1096	903	589	486	307	330	322	254	130	104	53
	STD	234	132	181	42	52	56	111	44	63	70	62	47	47	36	44	23	16	13
	% CV	12	6	10	3	4	5	10	4	7	12	13	15	14	11	17	18	15	24
OR99-U	Avg.	1933	1983	1868	1717	1583	1290	948	1250	1109	643	476	252	170	139	118	79	55	22
	STD	212	373	314	155	179	135	268	316	108	56	69	101	71	56	56	47	38	21
	% CV	11	19	17	9	11	10	28	25	10	9	14	40	42	40	47	59	69	95
OR238-C	Avg.	1904	2040	1888	1737	1640	1475	1270	1341	1131	856	742	514	519	550	427	245	210	108
	STD	164	290	102	147	123	195	189	179	155	197	217	183	184	199	177	134	116	57
	% CV	9	14	5	8	8	13	15	13	14	23	29	36	35	36	41	55	55	53
OR99W-C	Avg.	1547	1948	1967	1699	1531	1347	1215	1245	1045	787	680	481	466	477	383	223	188	102
	STD	291	344	244	236	251	193	173	150	162	210	212	215	203	207	193	130	126	77
	% CV	19	18	12	14	16	14	14	12	15	27	31	45	44	43	50	58	67	76

Table 5.8: Summary of Dynamic Modulus ($|E^*|$) Test Results (Cont.)

Project	Temp	$ E^* $ -Dynamic Modulus (ksi)																	
		4C						21C						37C					
		Freq (Hz)	25	10	5	1	0.5	0.1	25	10	5	1	0.5	0.1	25	10	5	1	0.5
OR221-C	Avg.	171 3	1856	1676	1544	1450	1239	1067	1102	924	642	534	369	388	397	306	177	155	83
	STD	145	208	163	204	219	248	182	134	207	224	212	206	238	219	185	118	118	70
	% CV	8	11	10	13	15	20	17	12	22	35	40	56	61	55	60	67	76	84
OR99EB-C	Avg.	154 8	2122	1839	1813	1690	1494	1262	1294	1158	877	767	544	588	568	446	273	213	109
	STD	620	320	314	328	210	210	164	148	164	181	174	153	151	124	108	96	87	64
	% CV	106 75	1463 3	1267 6	12501	11652	10298	8699	8925	7984	6045	5286	3749	4053	3913	3074	1885	1466	748
OR140-C	Avg.	163 7	1702	1479	1300	1169	933	929	966	762	481	390	241	265	268	202	110	83	43
	STD	309	292	361	348	351	334	250	91	79	121	108	85	168	173	120	63	53	27
	% CV	19	17	24	27	30	36	27	9	10	25	28	35	63	64	59	57	64	64
OR99*-C	Avg.	158 2	1700	1618	1444	1370	1148	1024	1028	866	641	555	374	422	415	314	189	163	85
	STD	172	243	223	165	143	100	119	104	115	139	142	137	105	108	116	92	89	51
	% CV	11	14	14	11	10	9	12	10	13	22	26	37	25	26	37	48	55	60

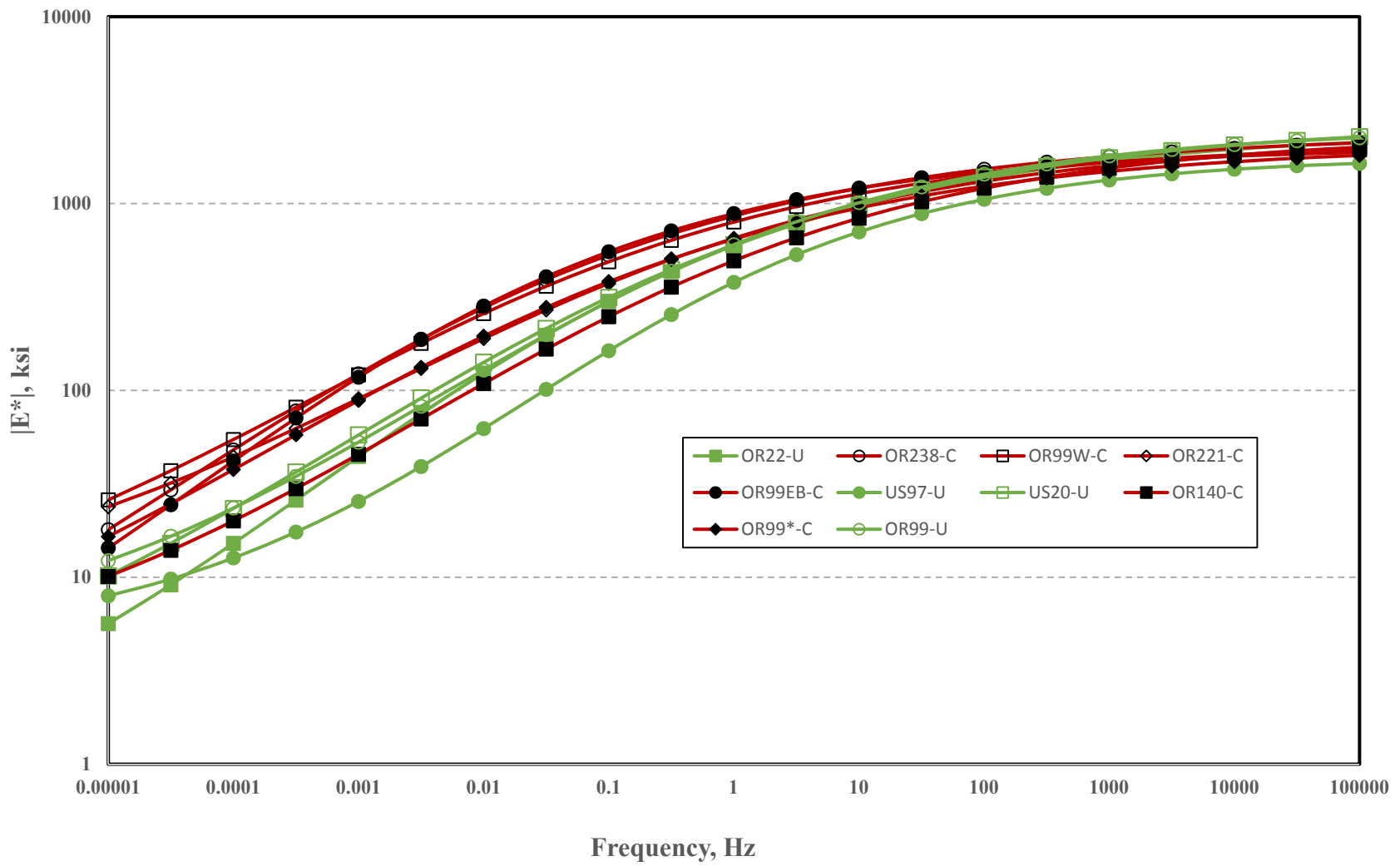
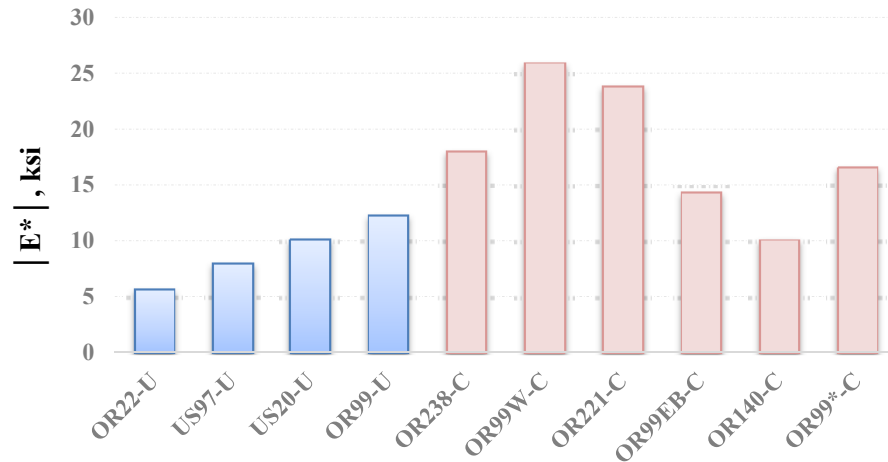
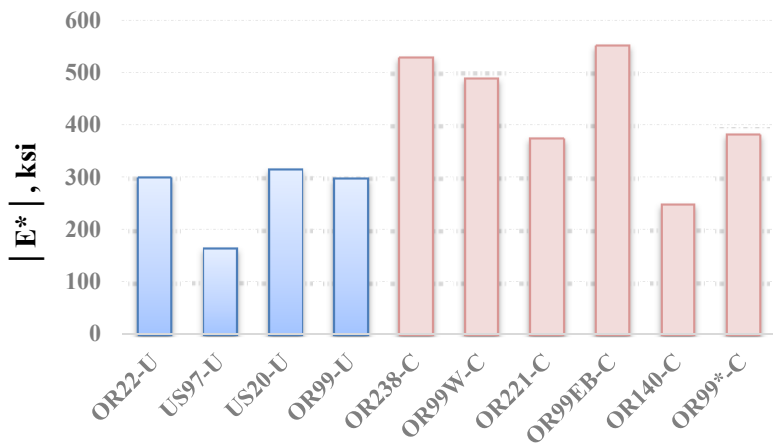


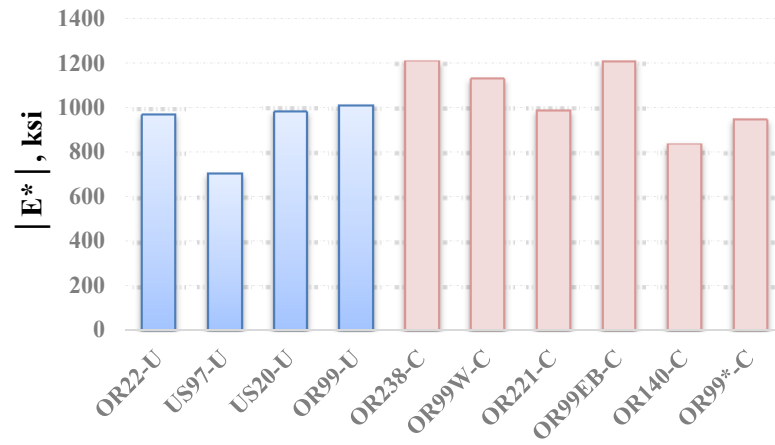
Figure 5.36: Dynamic Modulus Master Curves of All the Projects



(i)



(ii)



(iii)

Figure 5.37: Comparison of Average Dynamic Modulus for (i) Frequency 0.00001 Hz, (ii) Frequency 0.1 Hz, and (iii) Frequency 10 Hz

5.2.2 Indirect Tensile Strength Test Results

Indirect tensile (IDT) strength tests were conducted on specimens obtained from pavement cores to evaluate the tensile strength of the asphalt mix. Tensile strength is also an indicator of fatigue performance of the mixture. The test was performed at 21°C. Table 5.9 summarizes the average IDT strength along with standard deviation and coefficient of variation. Figure 5.38 illustrates the comparison of the IDT strength of the all projects investigated in this study. Among pavement sections with top-down cracking, sections OR221-C, OR140-C, and OR99*-C displayed substantially lower IDT strength values than the values obtained from OR238-C, OR99W-C, and OR99EB-C. All the top-down cracked sections except OR99EB-C exhibited very high variability in IDT strength with standard deviation ranging from 34 psi for OR140-C to 53 psi for OR99*-C. All the non-cracked sections showed fairly low variability (standard deviation ranges from 12 to 18 psi) in IDT strength compared to the top-down cracked sections. Among non-cracked sections, the highest IDT strength value of 226 psi was obtained with OR22-U while section US20-U displayed the lowest IDT strength value of 184 psi.

Table 5.9: Indirect Tensile (IDT) Strength Test Results

Test Section	IDT Strength Results (psi)				
	Average	Max	Min	STD	CV (%)
OR22-U	226	243	211	14	6
US97-U	191	202	177	12	7
US20-U	184	190	158	18	10
OR99-U	211	225	197	14	7
OR238-C	221	260	135	46	21
OR99W-C	209	239	145	36	17
OR221-C	167	235	113	43	26
OR99EB-C	247	266	241	8	3
OR140-C	170	212	145	34	20
OR99*-C	190	277	112	53	28

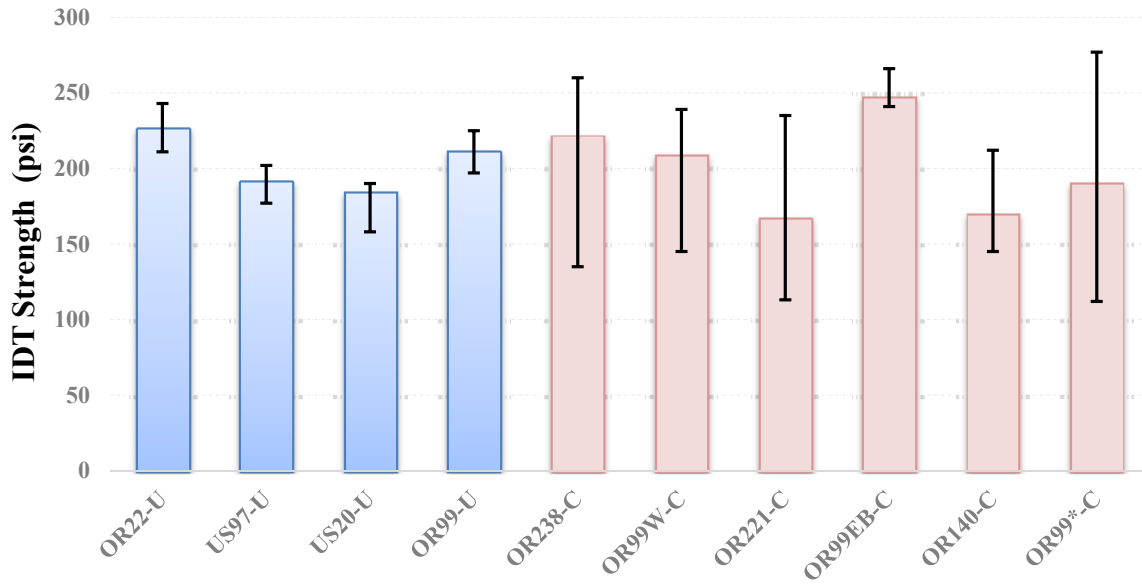


Figure 5.38: Comparison of IDT Strength Test Results

5.2.3 Air Void Analysis Results

Bulk specific gravity (G_{mb}) tests and theoretical maximum specific gravity (G_{mm}) tests were conducted on the extracted cores following appropriate standard test procedures. The air voids (%) were then computed by the following equation:

$$\text{Air Voids (\%)} = \frac{(G_{mm} - G_{mb})}{G_{mm}} \times 100 \quad (5-1)$$

where:

G_{mm} = Theoretical maximum specific gravity of the mixture; and

G_{mb} = Bulk specific gravity of the mixture.

Table 5.10 summarizes average air voids along with standard deviation and coefficient of variation and Figure 5.39 shows the comparison of the air voids of the all projects investigated in this study. Among non-cracked sections, an average air voids of 7.3% was observed with section US97-U followed by 6.0%, 5.3%, and 4.1% with OR99-U, OR22-U, and US20-U, respectively. Section OR99*-C displayed the highest average air voids of 8.3% while the lowest average air voids of 5.4% was observed on the section OR238-C, among top-down cracked pavement sections. It is important to point out that top-down cracked sections exhibited higher variability in air voids than the non-cracked sections.

Table 5.10: Air Voids Analysis Results

Test Section	Air Void Analysis Results (%)				
	Average	Max	Min	STD	CV (%)
OR22-U	5.3	5.9	4.2	0.76	15
US97-U	7.3	7.9	6.9	0.37	5
US20-U	4.1	5.1	3.3	0.67	16
OR99-U	6.0	6.6	5.3	0.56	9
OR238-C	5.4	7.8	3.3	1.64	30
OR99W-C	6.2	7.7	4.4	1.13	18
OR221-C	6.6	8.4	4.8	1.17	18
OR99EB-C	6.2	7.3	4.8	0.79	13
OR140-C	7.4	9.9	5.0	1.70	23
OR99*-C	8.3	10.9	7.5	0.87	11

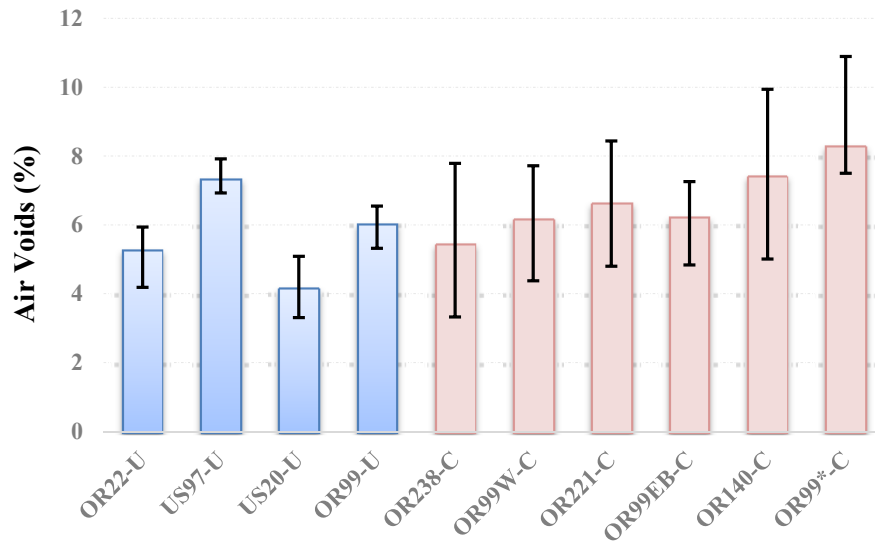


Figure 5.39: Comparison of Air Voids (%) Test Results

5.2.4 Binder Rheological Test Results

Asphalt binders were subjected to rheological tests once the binders were extracted and recovered from field cores following AASHTO TP2-94, “*Standard Test Method for the Quantitative Extraction and Recovery of Asphalt Binder from Hot Mix Asphalt (HMA)*”. Dynamic shear rheometer (DSR) testing was employed to test three replicate samples for each pavement section according to ASTM D7175, “*Standard Test Method for Determining the Rheological Properties of Asphalt Binder using a Dynamic Shear Rheometer*” to characterize the binder rheological properties at high and intermediate temperatures. The complex shear modulus (G^*) and phase angle (δ) determined from the DSR tests were used to evaluate the high and

intermediate critical temperatures and PG ranges. Moreover, DSR frequency sweep tests were performed to construct master curves for the asphalt binder complex shear modulus (G^*) and phase angle (δ). The master curves characterize binder rheological properties over a wide range of temperature or frequency. The frequency sweep procedure was performed at different temperatures ranging from 20 to 82° C at frequencies ranging between 0.1 to 100 Hz. Bending beam rheometer (BBR) tests were also conducted to evaluate the binder rheological properties at low temperatures. The standard method for BBR testing is AASHTO T 313, “*Determining the Flexural Creep Stiffness of Asphalt Binder Using the Bending Beam Rheometer (BBR)*” and was followed to test the asphalt binders at low temperatures. Two key properties, stiffness (S) and change in stiffness (m-slope) were recorded from the computer-generated output of the BBR test. The BBR test was employed to evaluate the low critical temperatures.

5.2.4.1 DSR Test Results at High Temperature

Figure 5.40 shows the variation of binder complex shear modulus with the corresponding DSR test temperatures. As can be seen from Figure 5.40, all top-down cracked sections except OR221-C exhibited higher complex shear modulus than the non-cracked sections across all test temperatures. Among sections with top-down cracking, OR99EB-C, OR238-C, and OR99*-C displayed higher complex shear modulus values than the other sections. OR99-U showed the lowest complex shear modulus while sections US20-U and US-97 exhibited identical behavior, among non-cracked sections. It was mentioned earlier that OR99 the Junction City section, had two sections, one OR99-U (non-cracked section) and the other one OR99*-C with top-down cracking. Rut on OR99-U (rut of 0.48 in) was found to be higher than that of OR99*-C (rut value of 0.25 in) during the distress surveys. Section OR99*-C is more rut resistant than section OR99-U but more susceptible to fatigue cracking as evident from Figure 5.40. Table 5.11 lists the high temperature performance grade for all the sections investigated in this study, determined from the DSR tests.

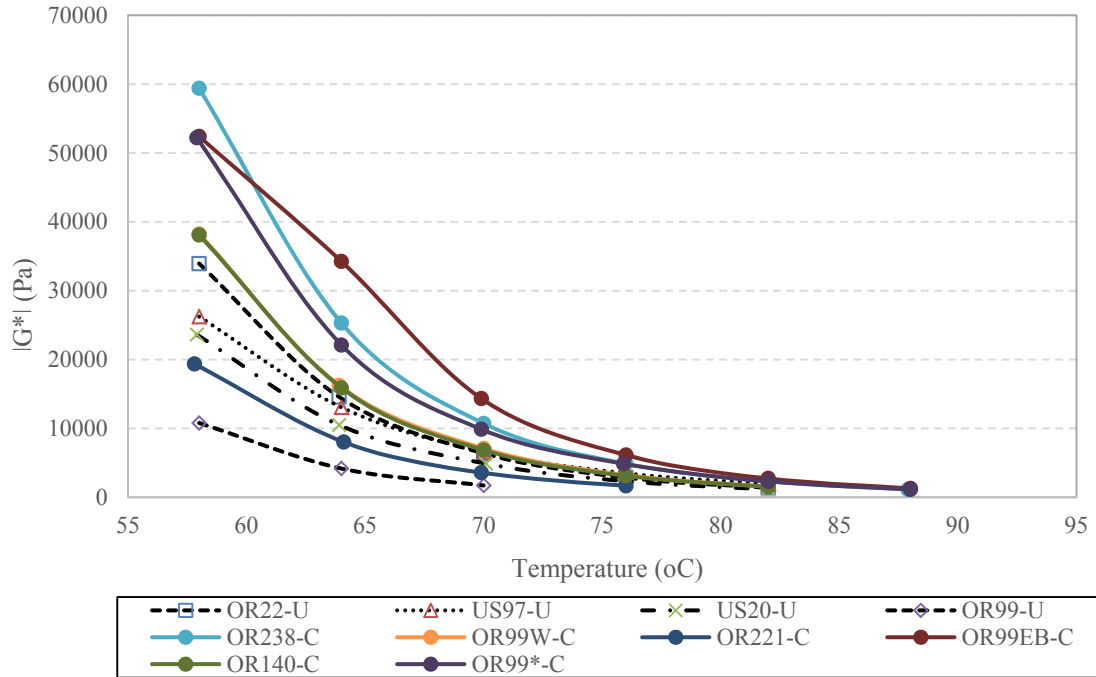


Figure 7062: Variation of Binder Complex Shear Modulus at High Temperatures

Table 7063: High Temperature Performance Grade (PG)

OR22-U	US97-U	US20-U	OR99-U	OR238-C	OR99W-C	OR221-C	OR99EB-C	OR140-C	OR99*-C
76	76	76	64	82	76	70	82	76	82

1.1.1.1 DSR Test Results at Intermediate Temperature

DSR test results at intermediate temperatures are used to evaluate the fatigue cracking susceptibility in asphalt binders. The temperatures at which a maximum value of 5000 kPa for $|G^*|\sin(\delta)$ is recorded determines the limiting temperature related to fatigue cracking. Figure 5.41 illustrates the variation of $|G^*|\sin(\delta)$ with respect to test temperatures. As can be seen, the DSR test results at intermediate temperatures are almost identical to the results discussed in the previous section (DSR test results at high temperatures). Most of the top-down cracked sections except OR221-C were more susceptible to fatigue cracking compared to non-cracked sections. Table 5.12 lists the temperatures at which the asphalt binders investigated in this study met the criteria for fatigue cracking in binders.

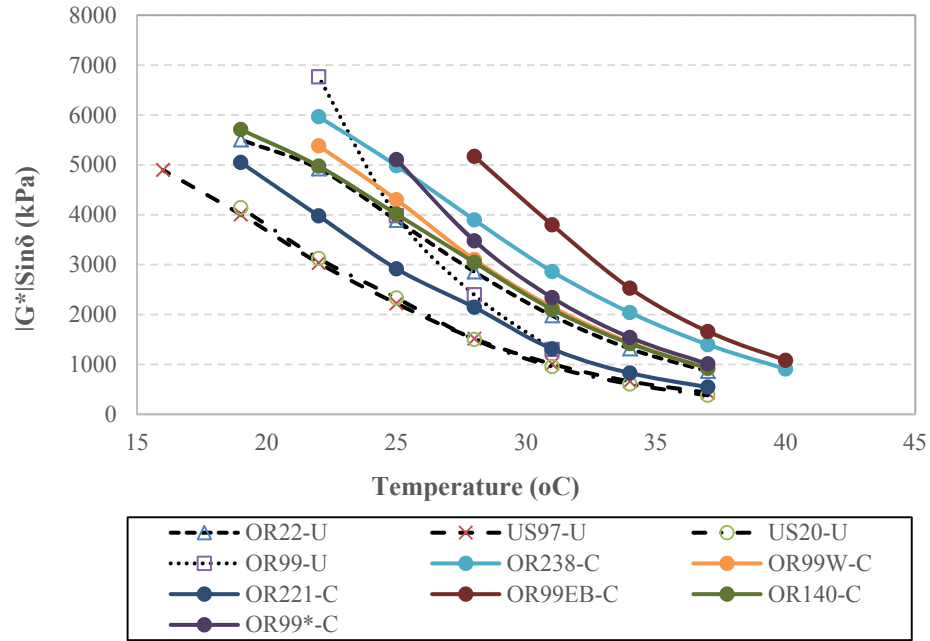


Figure 5.41: Variation of $|G^*|\sin(\delta)$ at Intermediate Temperatures

Table 5.12: Minimum Temperature for Fatigue Cracking in Asphalt Binder

OR22-U	US97-U	US20-U	OR99-U	OR238-C	OR99W-C	OR221-C	OR99EB-C	OR140-C	OR99*-C
21.58	17.14	16.78	23.74	24.87	23.43	20.13	28.6	21.87	25.26

5.2.4.3 Frequency Sweep Tests Results

Frequency sweep tests were conducted at different temperatures ranging from 20 to 82° C at frequencies ranging between 0.1 to 100 Hz to develop master curves for asphalt binders. Figures 5.42 through 5.51 show the frequency dependence of the all the projects at 20°C. Figure 5.52 illustrates the comparison of complex shear modulus ($|G^*|$) of all the sections while comparison of the phase angle is shown in Figure 5.53. As can be seen, all the sections with top-down cracking except OR221-C exhibited higher shear modulus than the non-cracked pavement sections.

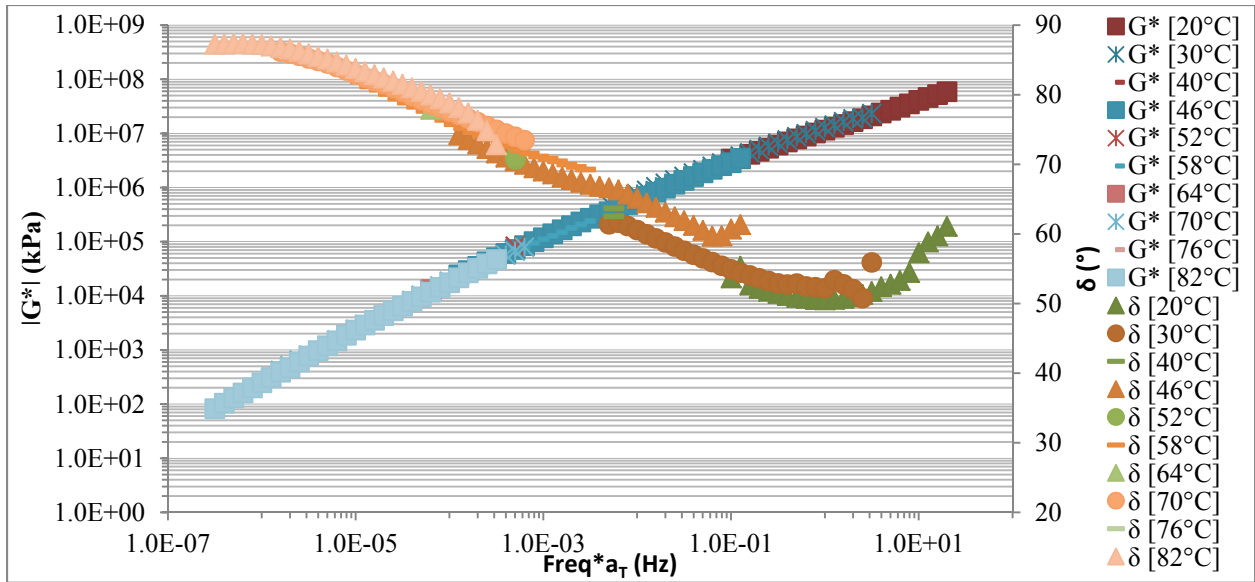


Figure 5.42: Master Curves, OR22-U

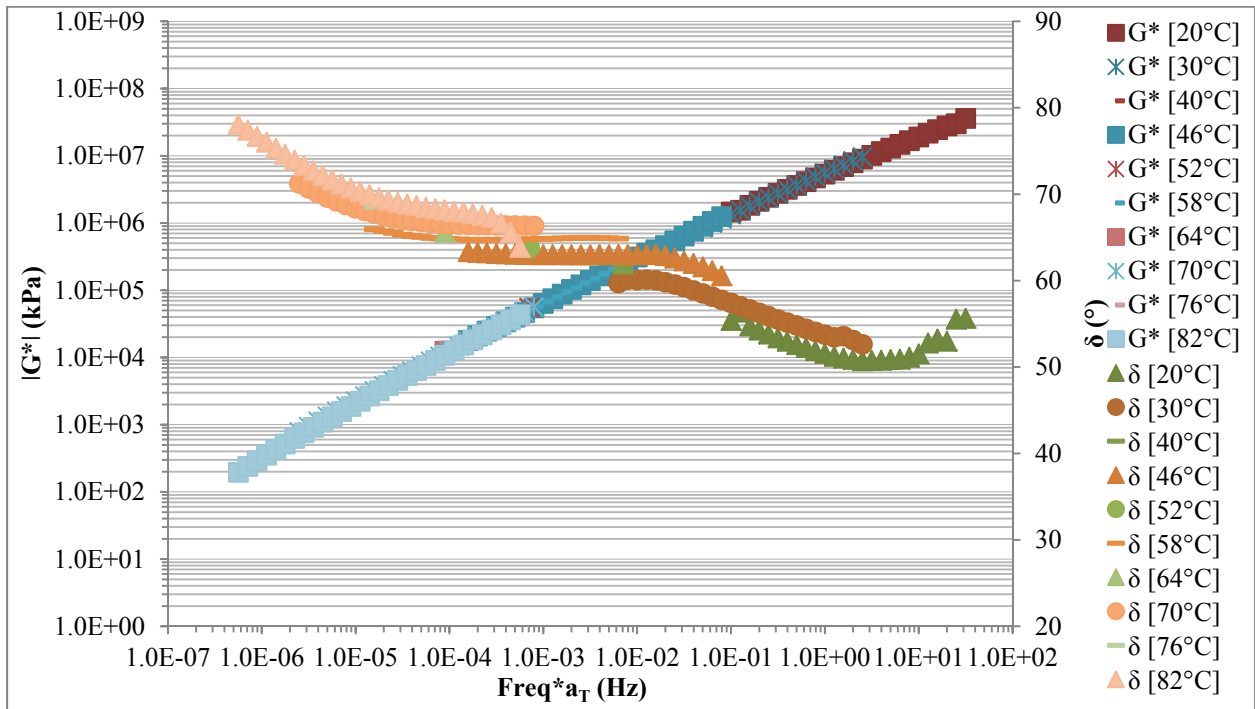


Figure 5.43: Master Curves, US97-U

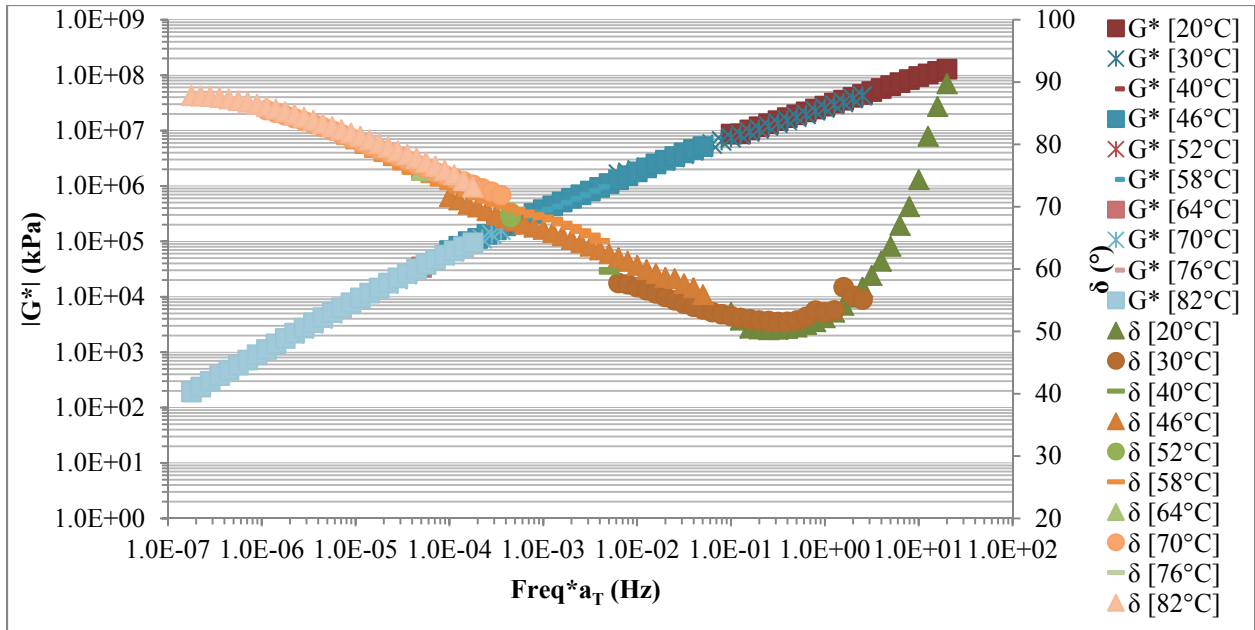


Figure 5.44: Master Curves, US20-U

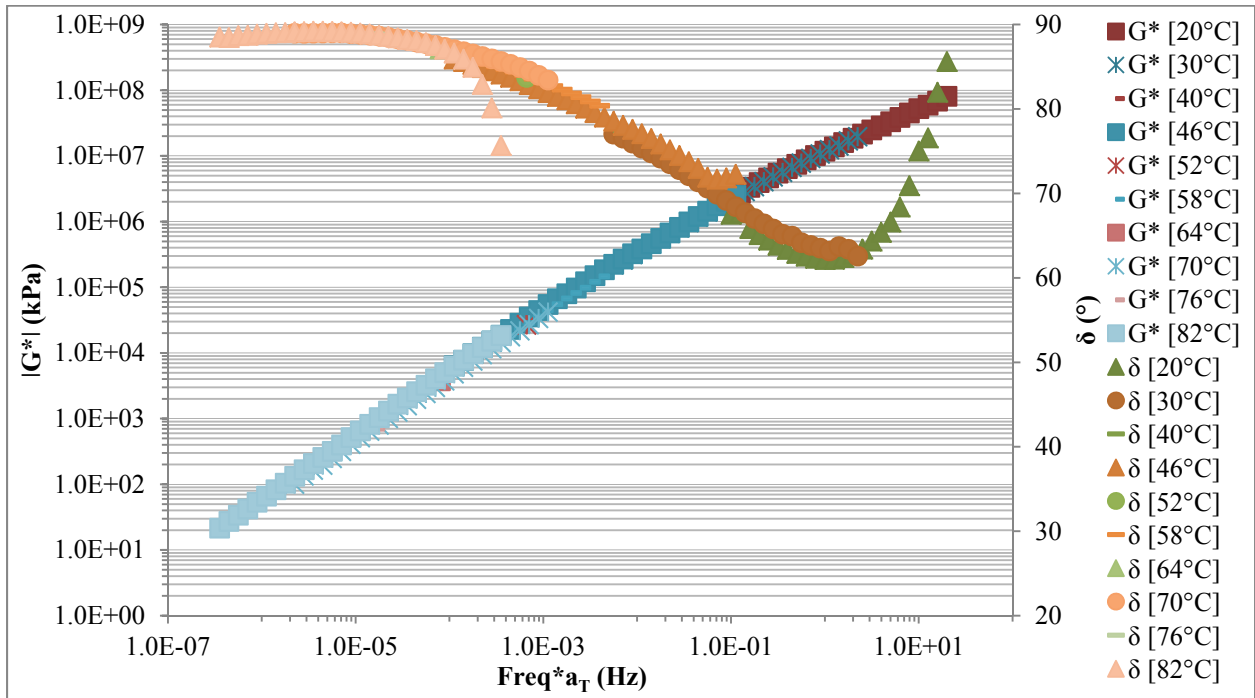


Figure 5.45: Master Curves, OR99-U

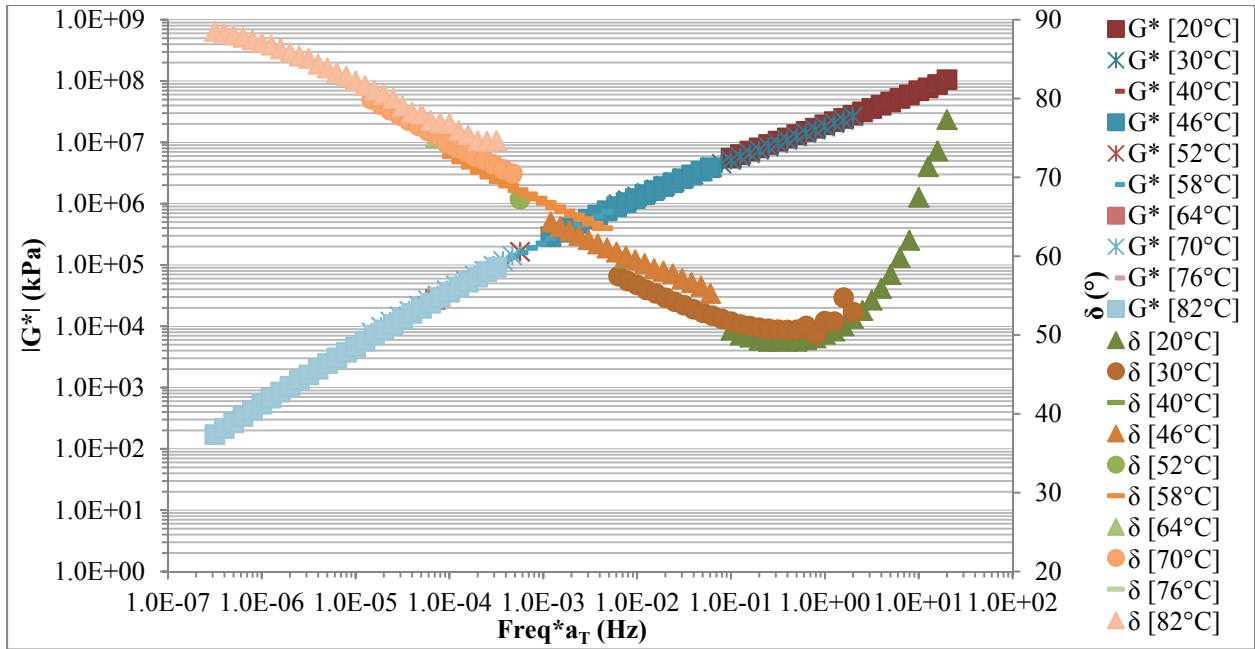


Figure 5.46: Master Curves, OR238-C

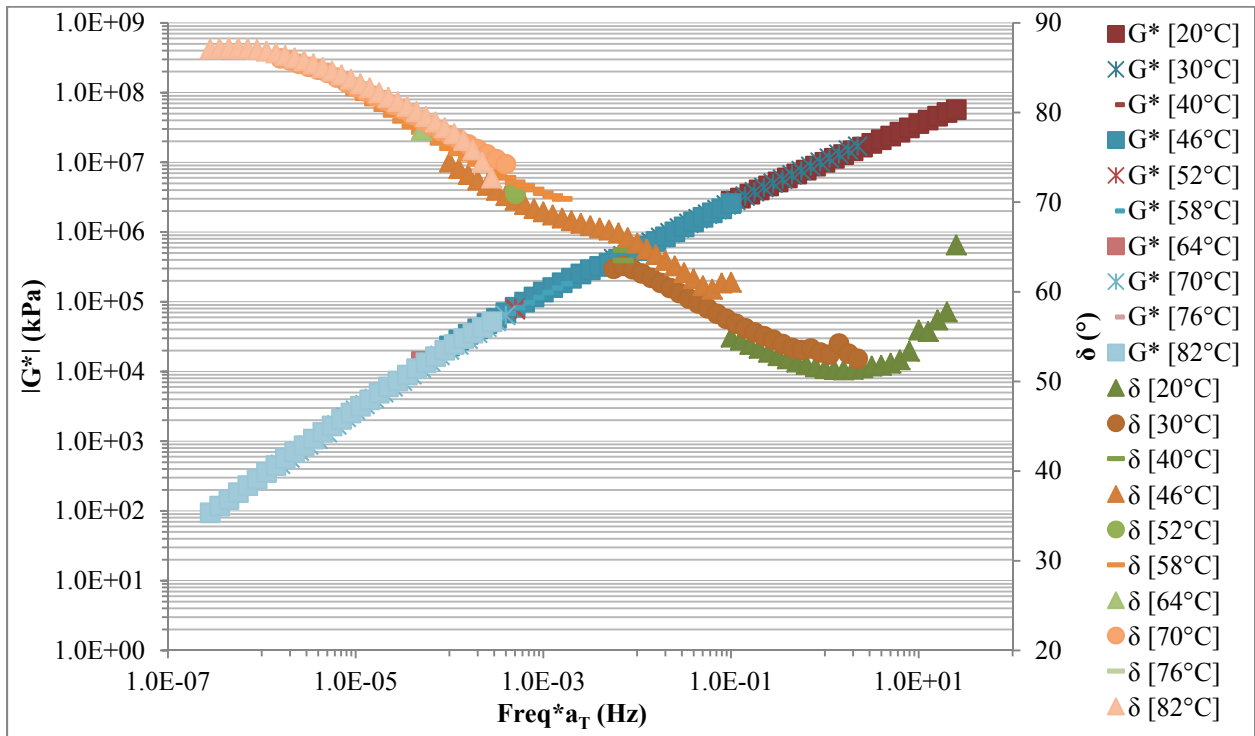


Figure 5.47: Master Curves, OR99W-C

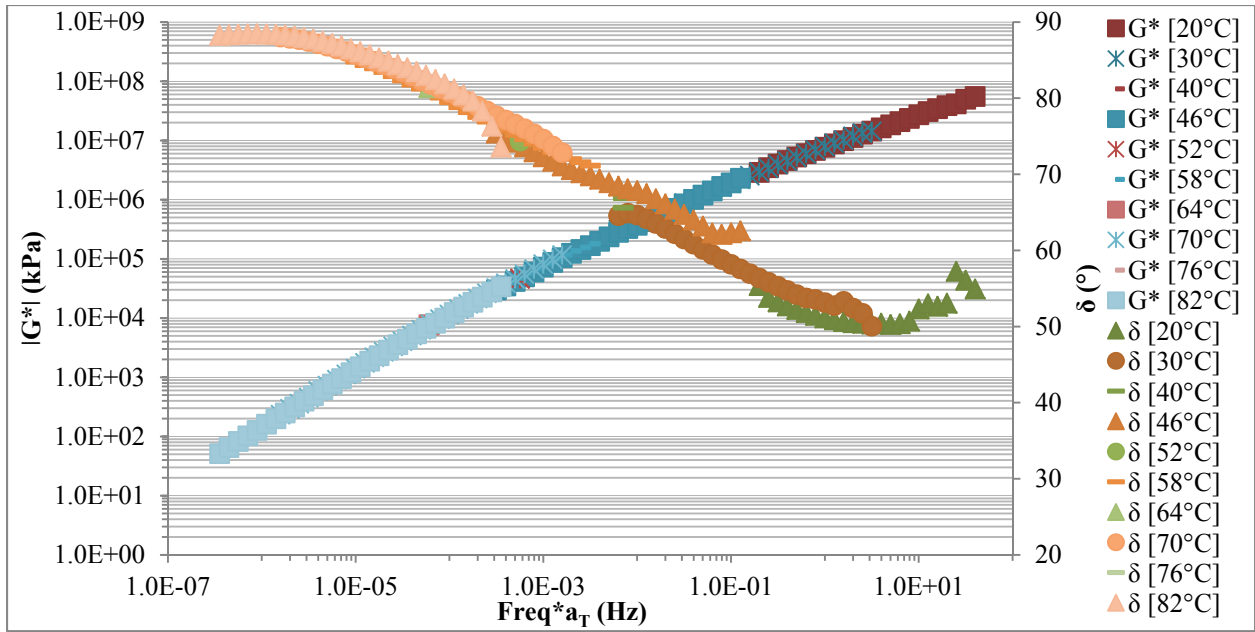


Figure 5.48: Master Curves, OR221-C

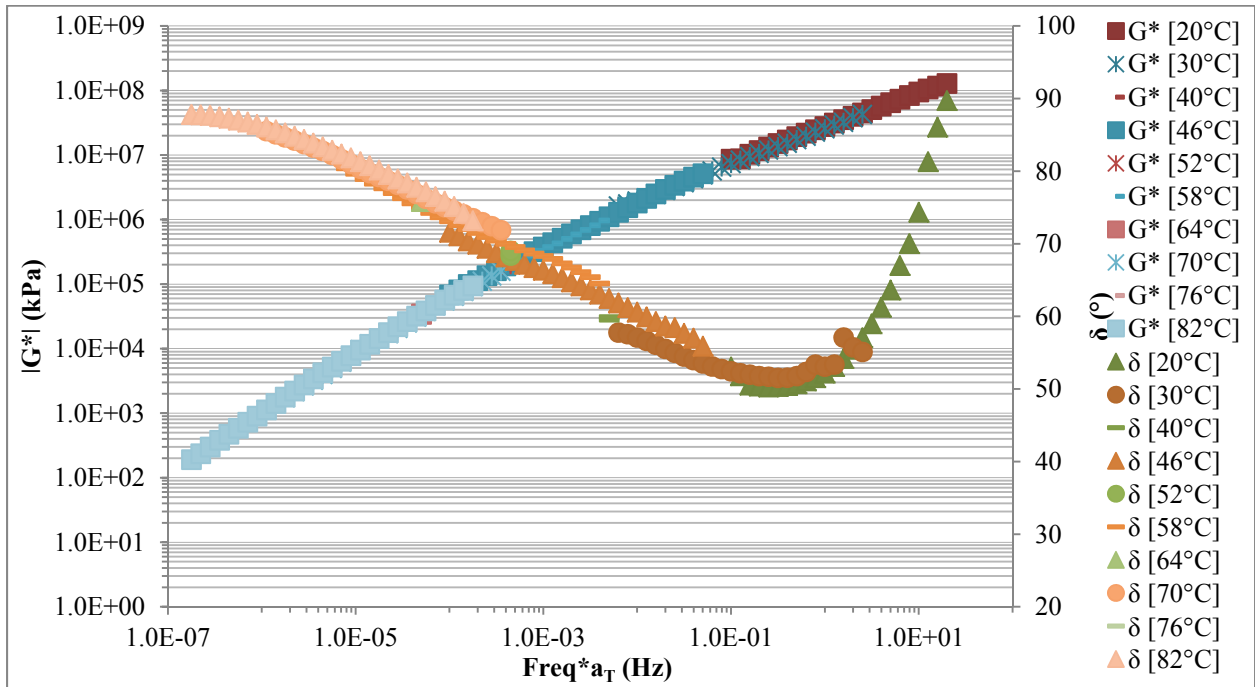


Figure 5.49: Master Curves, OR99EB-C

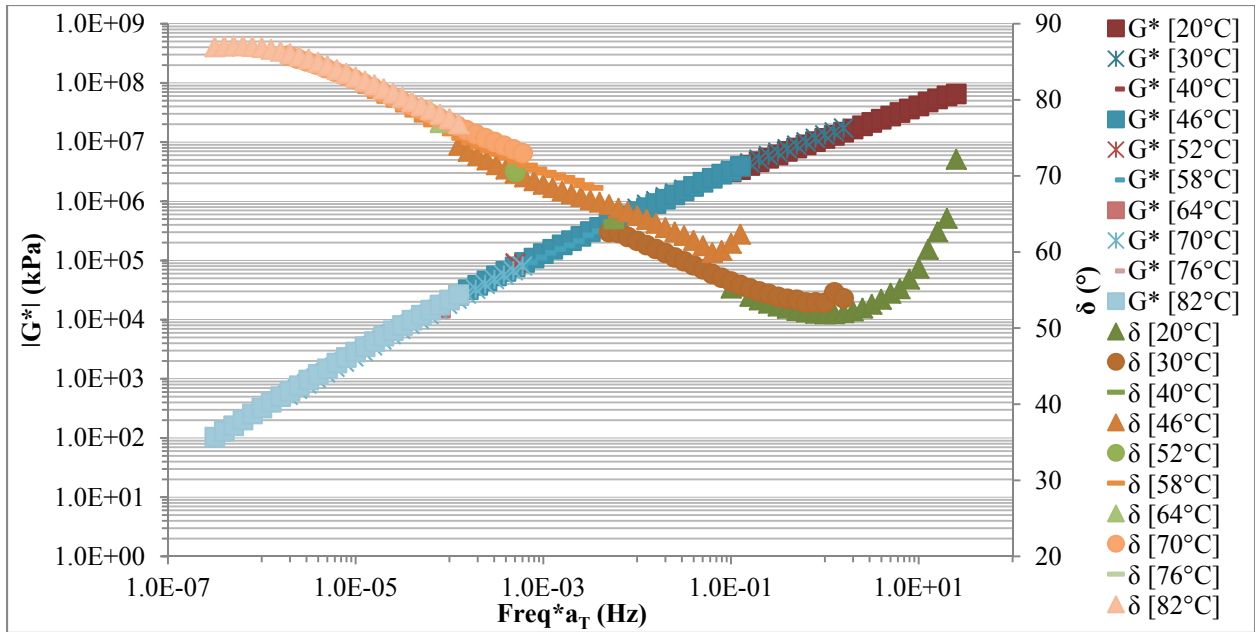


Figure 5.50: Master Curves, OR140-C

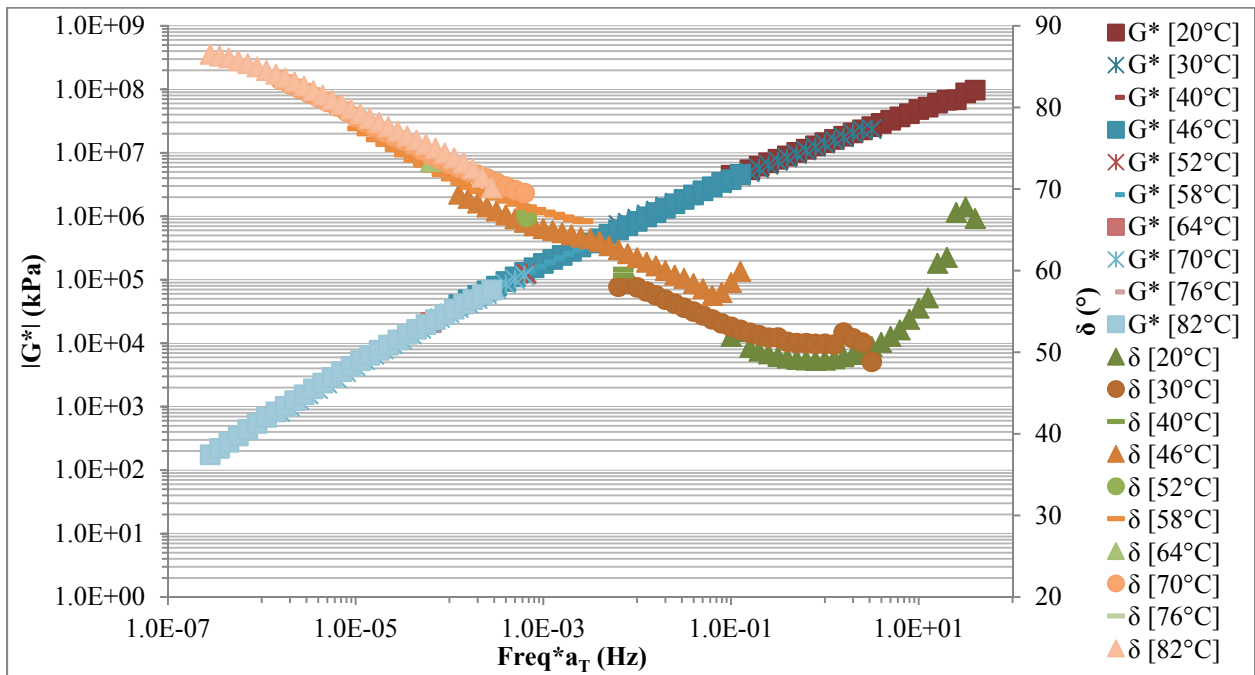


Figure 5.51: Master Curves, OR99*-C

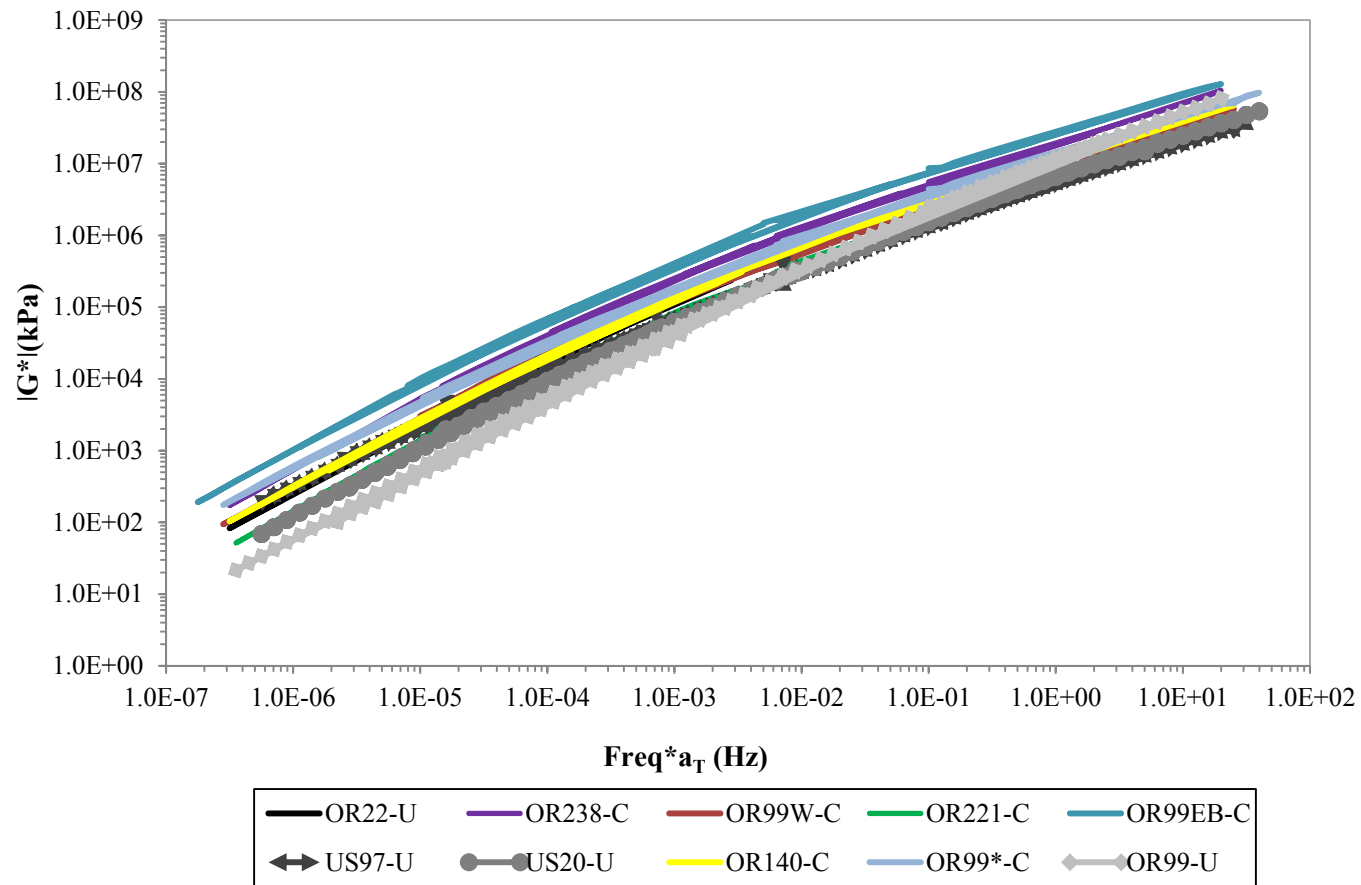


Figure 5.52: Complex Shear Modulus Master Curves

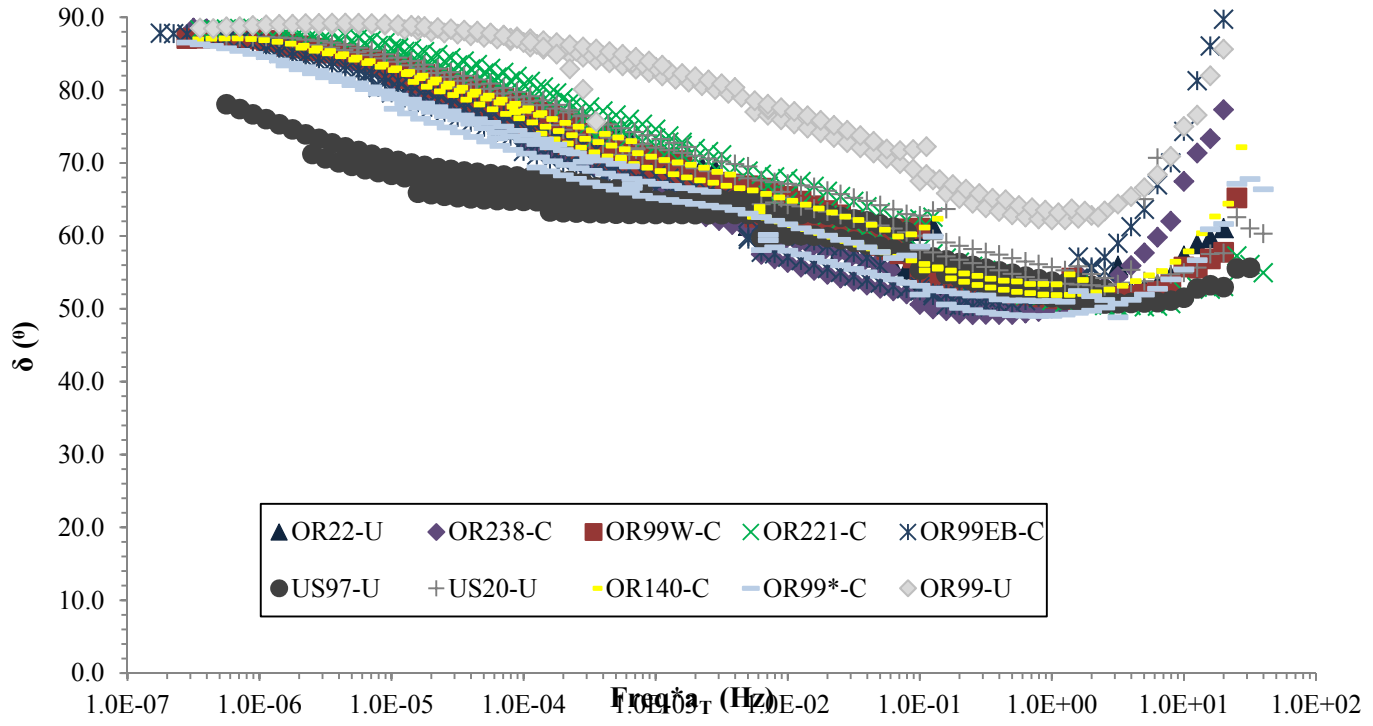


Figure 5.53: Master Curves for Phase Angle

5.2.4.4 BBR Test Results

BBR tests were conducted to evaluate binder low temperatures properties. For each temperature three replicate samples from each project were tested to determine two key properties: the stiffness (S) and the change in stiffness (m-value). Table 5.13 shows the average m-value and the average stiffness parameter S. The low critical temperatures of all the projects were determined from the m-value and stiffness (S) obtained from the two temperatures. Table 5.14 lists the low temperature performance grade for all the sections investigated in this study, determined from BBR tests. It could be observed that all the non-cracked sections except OR99-U exhibited better performance in resisting low temperature cracking than most of the top-down cracked sections. (except OR221-C). Table 5.15 shows the asphalt binder performance grade (PG grade) from laboratory testing along with original binder grade and % RAP content.

Table 5.13: BBR Test Results

OR22-U	Temp. (°C)				Temp. (°C)				US97-U
	-12		-18		-12		-18		
	m-value	S (MPa)	m-value	S (MPa)	m-value	S (MPa)	m-value	S (MPa)	
	0.35	226	0.25	378	0.37	120	0.28	250	
US20-U	Temp. (°C)				Temp. (°C)				OR99-U
	-12		-18		-12		-18		
	m-value	S (MPa)	m-value	S (MPa)	m-value	S (MPa)	m-value	S (MPa)	
	0.38	165	0.28	326	0.32	344	0.23	564	
OR238-C	Temp. (°C)				Temp. (°C)				OR99W-C
	-6		-12		-12		-18		
	m-value	S (MPa)	m-value	S (MPa)	m-value	S (MPa)	m-value	S (MPa)	
	0.34	124	0.29	250	0.32	244	0.25	421	
OR221-C	Temp. (°C)				Temp. (°C)				OR99EB-C
	-12		-18		-6		-12		
	m-value	S (MPa)	m-value	S (MPa)	m-value	S (MPa)	m-value	S (MPa)	
	0.33	184	0.29	295	0.32	206	0.27	370	
OR140-C	Temp. (°C)				Temp. (°C)				OR99*-C
	-12		-18		-6		-12		
	m-value	S (MPa)	m-value	S (MPa)	m-value	S (MPa)	m-value	S (MPa)	
	0.32	176	0.25	408	0.35	167	0.30	224	

Table 5.14: Low Temperature Performance Grade (PG)

OR22-U	US97-U	US20-U	OR99-U	OR238-C	OR99W-C	OR221-C	OR99EB-C	OR140-C	OR99*-C
BBR Failure Temp. (°C)									
-15	-17	-17	-11	-11	-14	-17	-8	-14	-8
Continuous Low Temp. Performance Grade (PG)									
-25	-27	-27	-21	-21	-24	-27	-18	-24	-18

Table 5.15: PG Grade and % Rap

OR22-U	US97-U	US20-U	OR99-U	OR238-C	OR99W-C	OR221-C	OR99EB-C	OR140-C	OR99*-C
76-25	76-27	76-27	64-21	82-21	76-24	70-27	82-18	76-24	82-18
Laboratory PG grade									
70-22	70-28 ER	70-28	70-22	PBA-5H	70-22	PBA-5	70-22	64-28	70-22
Original Mix Design PG grade									
20	20	N/A	30	20	20	N/A	25	20	30
% RAP									

5.2.5 Aggregate Gradation and Binders

Gradation analysis on the recovered aggregate was conducted in accordance with the standard procedure AASHTO T 27-93. Figure 5.54 shows the gradation curves of the all the projects. It could be observed that gradation curves of all the projects are identical except one non-cracked section, US20-U. No significant difference could be observed among the projects with respect to aggregate gradation that would impact cracking. Figures 5.55 illustrates % passing #200 sieve obtained from original mix design.

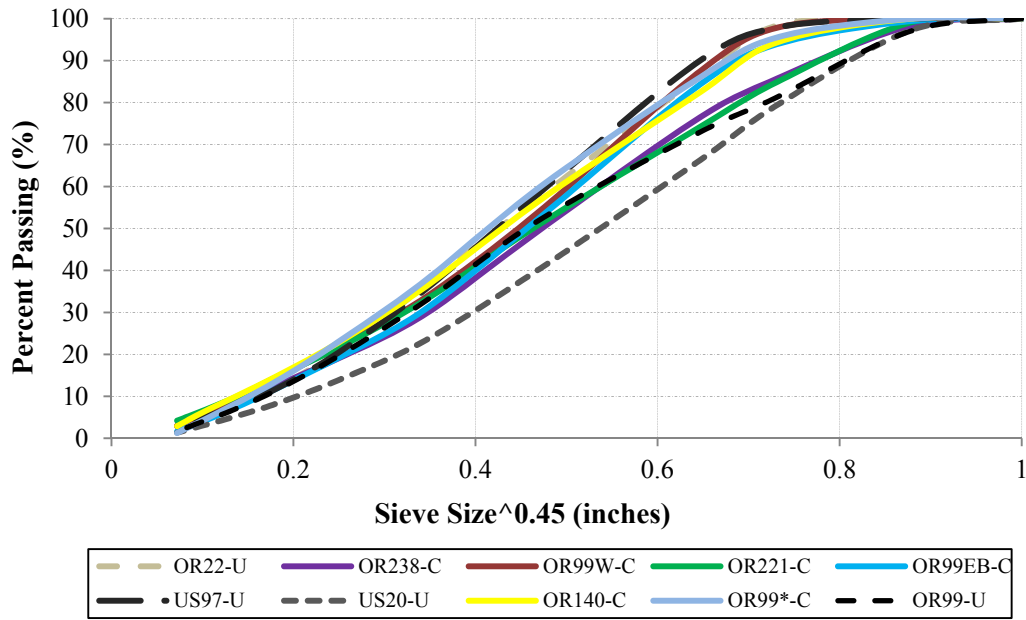


Figure 5.54: Gradation Analysis

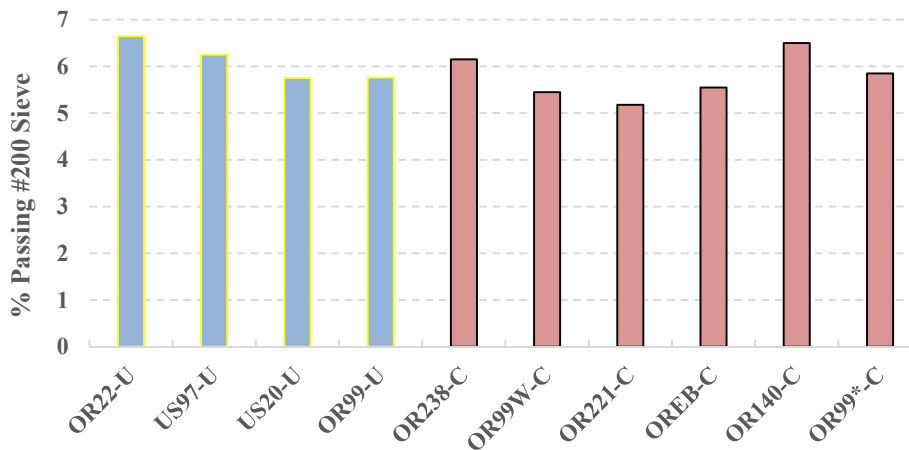


Figure 5.55: Original Mix Design % Passing #200 Sieve

Percent binder content by weight of the sections investigated in this study are illustrated in Figure 5.56 and were determined without a fines correction. Among top-down cracked sections, a maximum binder content of 6.6% was found with section OR140-C followed by 5.7% with OR221-C and the lowest value of 4.6% with OR238-C. A binder content of just over 5% was

found with the remaining top-down cracked sections. Among non-cracked sections, section US97-U showed highest binder content of 5.4% whereas a lowest value of 4.1% was found with US20-U. On average, top-down cracked sections exhibited slightly higher binder content compared to non-cracked sections. It is important to point out that loss of fines during the ignition oven process may have contributed some errors in the data.

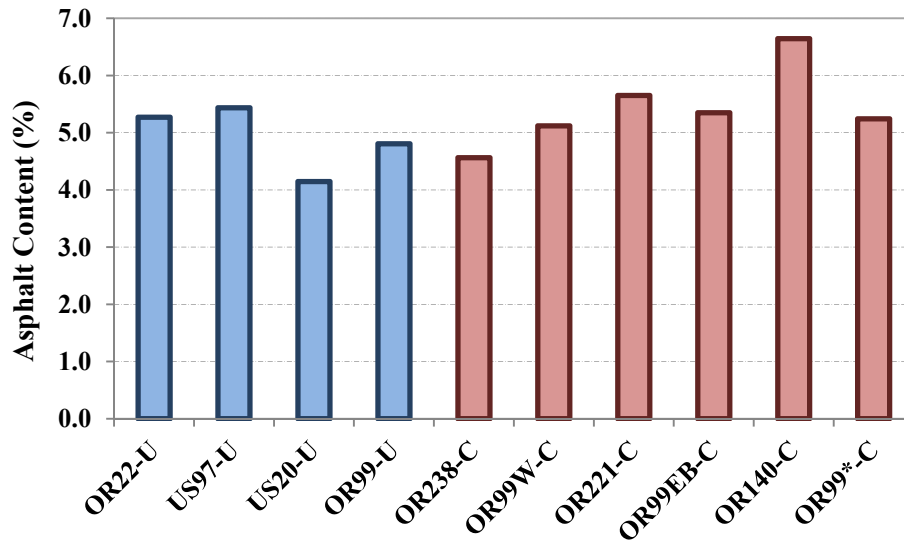


Figure 5.56: Binder Content by Weight

6.0 SUMMARY, CONCLUSION AND RECOMMENDATIONS

Recently the Oregon Department of Transportation (ODOT) has identified hot mix asphalt concrete (HMAC) pavements that have displayed top-down cracking within three years of construction. The objective of the study was to evaluate the top-down cracked pavement sections and compare the results with the non-cracked pavement sections. Research involved evaluating six surface cracked pavements and four non-cracked pavement sections. The research included extensive field and laboratory investigations of the 10 pavement sections by conducting distress surveys, falling weight deflectometer (FWD) testing, dynamic cone penetrometer (DCP) testing, and coring from the cracked and non-cracked pavement sections. Cores were then subjected to a full laboratory-testing program to evaluate the HMAC mixtures and binder rheology. The laboratory investigation included dynamic modulus, indirect tensile (IDT) strength, and specific gravity testing on the HMAC cores, binder rheological tests on asphalt binder and aggregate gradation analysis.

6.1 SUMMARY AND CONCLUSIONS

Based on the literature review, and the field and laboratory investigations, the following conclusions are drawn:

- Visual distress survey indicated that all the six sites exhibiting longitudinal wheel path cracking and transverse cracking were identified as top-down cracked pavements which was confirmed by examining cores. The only means to differentiate top-down cracking from bottom-up cracking is taking cores on the cracked areas.
- FWD tests were conducted to evaluate the structural capacity of top-down cracked pavements and pavement sections without top-down cracking. FWD tests indicated that top-down cracked pavements were structurally sound, even some of the sections with top-down cracking showed better structural capacity compared to non-cracked sections.
- Two backcalculation software programs were employed in the study to estimate backcalculated layer moduli. The study found a good correlation for AC moduli between Elmod and BAKFAA while no consistent correlation for base and subgrade moduli were observed between the two software packages.
- DCP tests were carried out on the aggregate base materials to evaluate the variations in density (strength) of both top-down cracked pavements and non-cracked pavements. Like the FWD test results, no significant differences in density variations of the aggregate bases were observed between pavements with and without top-down cracking. Only one section (OR99EB-C) of the six top-down cracked pavement sections was found to be displaying high variability in density.

- Top-down cracking initiation and propagation were found to be independent of pavement cross-section or the AC thickness.
- Dynamic modulus testing was conducted on the extracted cores to evaluate the mixture stiffness of both top-down cracked and non-cracked areas. Cores from all the top-down cracked pavement sections except OR140-C exhibited higher dynamic modulus (stiffer) values than that of non-cracked pavement sections.
- Indirect tensile (IDT) strength test results indicated that AC mixtures from all four non-cracked pavement areas exhibited fairly high IDT strength and low variability in IDT strength. Three top-down cracked pavement sections displayed low IDT strength and very high variability in IDT strength. All top-down cracked pavement sections except OR99EB-C showed much higher variability in IDT strength compared to non-cracked pavement areas.
- Air voids analysis results indicated that all six top-down cracked sections showed much higher variability in AC density compared to the four non-cracked pavement areas, like the IDT strength test results.
- Asphalt binder rheological test results indicated that asphalt binders from all the top-down cracked sections except OR140-C showed higher complex shear modulus (stiffer binder) compared to non-cracked pavement sections.
- The literature review indicated that there was no conclusive evidence based on the structural capacity that would lead to top-down cracking. Top-down cracking can be caused by a number of contributors such as stiffer AC mixtures, mixture segregation, binder aging, low AC tensile strength, and stiffness differentials between pavement layers and poor bond under the wearing course or by combination of any.

6.2 RECOMMENDATIONS

Currently, no pavement design method is capable of predicting or analyzing top-down cracking phenomenon which could explain the universally conclusive reasoning for top-down cracking occurrence and progression. The literature review indicated a number of factors that could contribute to the top-down cracking initiation and propagation such as high tensile contact stresses generated on the road surface close to the tire edges, climatic conditions, aging, construction quality, low AC tensile strength, and differential stiffness between pavement layers. This study found that top-down cracked sections displayed higher variability in density and tensile strength, low tensile strength, and stiffer binder of mixtures when compared to non-cracked sections. While the structural capacity (thickness) of pavements was found to be a non-contributing factor to top-down cracking, the material properties and construction practices could be fine-tuned to reduce the occurrence of top-down cracking. The following recommendations could be made based on the literature review, and the field and laboratory investigations to prevent top-down cracking in terms of material selection, material properties, and construction practices:

- It is recommended that a tighter density specification be established to ensure uniformity for in-situ air voids. Based on the study, the in-situ air voids should be kept at or below 6%.

Although post-compaction of constructed pavements was not done as part of this study, the Oregon DOT would benefit from an increase in the percent G_{mm} to 92% which would result in lower in-situ air voids. It is recommended that this be considered in a shadow specification prior to placing in actual construction specifications.

- The study clearly showed that stiffer mixes are more prone top-down cracking. One simple approach would be to reduce the design air voids from 4% to 3.5% which would effectively increase the design binder content of mixes by about 0.25%. This would also be beneficial to the first recommendation in achieving a higher percent G_{mm} . Like the first recommendation, this should be implemented on a shallow specification basis
- Top-down cracked sections found to be possessing relatively stiffer binder and mixtures compared to non-cracked sections. However, the careful selection of binder grade is recommended to ensure a delicate balance between rutting and fatigue cracking. It is important to point out that OR99 the Junction City section, had two sections, one OR99-U (non-cracked section) and the other one OR99*-C with top-down cracking. Section OR99*-C was found to displaying stiffer binder than section OR99-U. Section OR99*-C was found to better rut resistant than section OR99-C but was more susceptible to top-down cracking. The research team suggests lowering the low temperature binder grade by one grade as this would reduce the overall mix stiffness.
- Asphalt mixtures with higher tensile strength and low variability in tensile strength should be used. Tensile strength testing or another performance test could be developed as part of the mixture design and selection process and integrated into quality control and quality assurance testing. This would facilitate the need for developing criteria and would be best implemented on a shadow project basis.
- It is recommended that non-uniformities in the material properties be prevented along with prevention of segregation during construction. Segregation could be caused by areas within pavements and created by paving operations as indicated in the literature review. The Colorado Department of Transportation established a segregation specification in 2003 which led paving equipment manufacturers taking initiative to develop an anti-segregation kit so that existing paving equipment could be retrofitted.

6.3 RECOMMENDATIONS FOR FUTURE STUDY

Based on the results and conclusions of this study, the following recommendations can be made:

- It is important to differentiate between top-down cracking and classical bottom-up cracks because preventive and rehabilitation actions for top-down cracked pavements are much different than those of bottom-up cracked sections. Thus, it is recommended top-down cracking identification criteria be implemented in the Pavement Management System (PMS) database. The research team understand that the Oregon DOT currently records the difference in terms of top-down cracking (longitudinal cracking) or fatigue cracking.
- In this study, IDT strength tests were conducted at only one temperature due to the nature of the tests (destructive tests) and limitation on the number of cores. It is recommended that

cores be tested at different temperatures to evaluate the tensile strength as well as moisture susceptibility.

- A more in-depth study could be done to evaluate the effects of aging on the properties of the asphalt mixes.

7.0 REFERENCES

- Ali, H.A., and A. Lopez. Statistical Analyses of Temperature and Moisture Effects on Pavement Structural Properties Based on Seasonal Monitoring Data. *Transportation Research Record*, Issue 1540, 1996, pp. 48-55.
- Baladi, G.Y., M. Schorsch, and T. Svasdisnat. *Determination of Top-Down Cracks in Bituminous Pavements*. Publication MDOT-PRCE-MSU-2003-110. MDOT, Michigan Department of Transportation, MI, 2002.
- Baladi, G.Y., M. Schorsch, and C. Chang. Effects of Segregation on the Initiation and Propagation of Top-Down Cracks. . 82st Transportation Research Board Annual Meeting. Proceedings CD-Room. Washington, D.C., 2003.
- Birgisson, B., B. Sangpetngam, and R.Roque. Predicting Viscoelastic Response and Crack Growth in Asphalt Mixtures with the Boundary Element Method. In *Transportation Research Record: Journal of the Transportation Research Board*, No. 1789, Transportation Research Board of the National Academies, Washington, D.C., 2002, pp129–135.
- Chen, D-H, J. Bilyeu, H-H Lin, and M. Murphy. Temperature Correction on Falling Weight Deflectometer Measurements. In *Transportation Research Record: Journal of the Transportation Research Board*, No. 1716, Transportation Research Board of the National Academies, Washington, D.C., 2000, pp. 30-39.
- Dai, S.T., D. Van Deusen, M. Beer, D. Rettner, and G. Cochran. Investigation of Flexible Pavement Response to Truck Speed and FWD Load through Instrumented Pavements. Proceedings, 8th International Conference on Asphalt Pavements, University of Washington, Seattle, WA, 1997, pp. 141-160.
- Dauzats, M., and A. Rampal. Mechanism of Surface Cracking in Wearing Courses. Proceedings, 6th International Conference Structural Design of Asphalt Pavements, The University of Michigan, Ann Arbor, MI, 1987, pp. 232-247.
- De Beer, M., C. Fisher, and F.J. Jootse. Determination of Pneumatic Tyre/Pavement Interface Contact Stresses Under Moving Loads and Some Effects on Pavements With Thin Asphalt Surfacing Layers. Proceedings, 8th International Conference on Asphalt Pavements, University of Washington, Seattle, WA, 1997, pp. 179-227.
- Deepika, C., and V.K. Chakravarthi. Evaluation of Properties of Soil Subgrade Using Dynamic Cone Penetration Index-A Case Study. *International Journal of Engineering Research and Development*, Vol. 4, No. 4, 2012, pp. 7-15.
- Emery, J.J. Evaluation and Mitigation of Asphalt Pavement Top-Down Cracking. Annual Conference of the Transportation Association of Canada Charlottetown, Prince Edward Island, 2006.
- Ese, D., J. Myre, P. Noss, and E. Vaernes. The Use of Dynamic Cone Penetrometer (DCP) for Road Strengthening Design in Norway. Proceedings. The Fourth International Conference on the Bearing Capacity of Roads and Airfields, 1995.

Freitas, E.F., P. Pereira, L. Picado-Santos, and T. Papagiannakis. Construction Quality, Temperature and Rutting Effect on Top-Down Cracking Initiation. In *Transportation Research Record: Journal of the Transportation Research Board*, No. 1929, Transportation Research Board of the National Academies, Washington, D.C., 2005, pp. 174-182.

Gerritsen, A.H., C.A.P.M. van Gurp, J.P.J. van der Heide, A.A.A. Molenaar, and A.C. Pronk. Prediction and Prevention of Surface Cracking in Asphaltic Pavements. 6th International Conference Structural Design of Asphalt Pavements, The University of Michigan, Ann Arbor, MI, 1987, pp. 378-391.

Harmelink, D., T. Aschenbrener, and S. Shuler. Top-Down Cracking in Asphalt Pavements: Causes, Effects, and Cures. *Journal of Transportation Engineering*, Vol. 134, No. 1, 2008.

Kim, Y.R. and Y.C. Lee. Interrelationships among Stiffness of Asphalt-Aggregate Mixtures. *Journal of the Association of Asphalt Paving Technologists*, Vol. 64, 1995, pp. 575-609.

Kim, J., R. Roque, and T. Byron. Viscoelastic Analysis of Flexible Pavements and Its Effects on Top-Down Cracking. *Journal of Materials in Civil Engineering*, Vol. 21, No. 7, 2009.

Kim, Y.R., Y. Seo, M. King, and M. Momen. Dynamic Modulus Testing of Asphalt Concrete in Indirect Tension Mode. In *Transportation Research Record: Journal of the Transportation Research Board*, No. 1891, Transportation Research Board of the National Academies, Washington, D.C., 2004, pp. 163-173.

Kim, Y.R., and B.S. Underwood. Determination of Depth of Surface Cracks in Asphalt Pavements. In *Transportation Research Record: Journal of the Transportation Research Board*, No. 1853, Transportation Research Board of the National Academies, Washington, D.C., 2003, pp.143-149.

Lippert, D.L. *A Review of Cracking on Full Depth Bituminous Pavement (Longitudinal Cracking)*. Internal Report. Illinois Department of Transportation, 1993.

Lukanen, E.O., Stubstad, R. and Briggs, R. *Temperature Predictions and Adjustment Factors for Asphalt Pavement*. Publication FHWA-RD-98-085. Federal Highway Administration Turner-Fairbank Highway Research Center, 6300 Georgetown Pike, McLean, VA, 2000.

McGennis, R.B, S. Shuler, and H.U. Bahia. *Background of SUPERPAVE Asphalt Binder Test Methods*. Publication FHWA-SA-94-069. FHWA, U.S. Department of Transportation, 1994.

Myers, L.A., R. Roque, and B. Ruth. Mechanisms of Surface-Initiated Longitudinal Wheel Path Cracks in High-Type Bituminous Pavements. *Journal of the Asphalt Paving Technologists*, Vol. 67, 1998, pp. 401-432.

Myers, L.A., R. Roque, and B. Birgisson. Propagation Mechanisms for Surface-Initiated Longitudinal Wheel Path Cracks. In *Transportation Research Record: Journal of the Transportation Research Board*, No. 1778, Transportation Research Board of the National Academies, Washington, D.C., 2001, pp. 113-122.

Nunn, M. Design of Long-Life Roads for Heavy Traffic. Proceedings, Industry Conference, Australian Asphalt Pavement Association, Surfers Paradise, Queensland, Australia, 1998.

Ozer, H., I.L. Al-Qadi, and C.A. Duarte. Effects of Non-Uniform and Three Dimensional Contact Stresses on the Near-Surface Cracking Problem. 90th Transportation Research Board Annual Meeting. Proceedings CD-Room. Washington, D.C., 2011.

Park, S.W. and Y.R. Kim. Temperature Correction of Backcalculated Moduli and Deflections using Linear Viscoelasticity and Time-Temperature Superposition. In *Transportation Research Record: Journal of the Transportation Research Board*, No. 1570, Transportation Research Board of the National Academies, Washington, D.C., 1997, pp. 108-117.

Pellinen, T.K., G. Rowe, and K. Biswas. *Evaluation of Surface (Top Down) Longitudinal Wheel Path Cracking*. Publication FHWA/IN/JTRP-2004/06. Joint Transportation Research Program, Indiana Department of Transportation and Purdue University, West Lafayette, IN, 2004. doi: 10.5703/1288284313216

Roque, R., B. Birgisson, C. Drakos, and B. Dietrich. Development and Field Evaluation of Energy-Based Criteria for Top-Down Cracking Performance of Hot Mix Asphalt. *Asphalt Paving Technology*, No. 73, 2004, pp. 229–260.

Roque, R., B. Birgisson, L. Myers, Z. Zhang, and C.A. Drakos. *Evaluation of Surface-Initiated Longitudinal Wheel Path Cracking*. Final Report for FDOT No. C5978 Contract, University of Florida, Gainesville, FL, 2006.

Sridhar, R., K.S. Reddy, S.S. Kumar, S. Bose, and B.B. Pandey. Analysis of Top-Down Cracking Behavior of Asphalt Pavements. 87th Transportation Research Board Annual Meeting. Proceedings CD-Room. Washington, D.C., 2008.

Svasdisant, T., M. Achorsch, G.Y. Baladi, and S. Pinyosunun. Mechanistic Analysis of Top-Down Cracking in Asphalt Pavements. 81st Transportation Research Board Annual Meeting. Proceedings CD-Room. Washington, D.C., 2002.

Uhlmeyer, J.S., K. Willoughby, L.M. Pierce, and J. P. Mahoney. Top-Down Cracking in Washington State Asphalt Concrete Wearing Courses. In *Transportation Research Record: Journal of the Transportation Research Board*, No. 1730, Transportation Research Board of the National Academies, Washington, D.C., 2000, pp. 110-116.

Von Quintus, H.L., and Moulthrop, J.S. *Mechanistic-Empirical Pavement Design Guide Flexible Pavement Performance Prediction Models: Volume II-Reference Manual*. No. FHWA/MT-07-008/8158-2. Montana Department of Transportation. Research Programs. Helena, MT, 2007.

Wang, L.B., L.A. Myers, L.N. Mohammad, and Y.R. Fu. A Micromechanics Study on Top-Down Cracking. In *Transportation Research Record: Journal of the Transportation Research Board*, No. 1853, Transportation Research Board of the National Academies, Washington, D.C., 2003, pp. 121-133.

Wang, J., B. Birgisson, and R. Roque. Windows-Based Top-Down Cracking Design Tool for Florida: Using Energy Ratio Concept. In *Transportation Research Record: Journal of the Transportation Research Board*, No. 2037, Transportation Research Board of the National Academies, Washington, D.C., 2007, pp. 86-96.

Wang, H. and Al-Qadi, I.L. Near-Surface Pavement Failure under Multiaxial Stress State in Thick Asphalt Pavement. In *Transportation Research Record: Journal of the Transportation Research Board*, No. 2154, Transportation Research Board of the National Academies, Washington, D.C., 2010, pp. 91-99.

Webster, S.L., R.H. Grau, and T.P. Williams. *Description and Application of Dual Mass Dynamic Cone Penetrometer*. Instruction Report GL-92-3, U.S. Army Engineer Research and

Development Center, Waterways Experiment Station, Vicksburg, MS, 1992.

Witczak, M., and M. El-Basyouny. Development of the Fatigue Cracking Models for the 2002 Design Guide. 84th Transportation Research Board Annual Meeting. Proceedings CD-Room. Washington, D.C., 2005.

Wu, S. *DCP Field Application*. Internally circulated report, North Carolina Department of Transportation, 1987.

APPENDIX A – FWD DEFLECTION DATA

OR22-U

FWD Station	Force (lb)	Deflection (mils)						
		D1	D2	D3	D4	D5	D6	D7
1	9132	14.04	10.74	9.81	7.79	6.27	3.84	1.75
2	9188	12.49	9.61	8.90	7.25	6.03	3.86	1.67
3	9286	13.28	10.03	9.28	7.49	6.05	3.74	1.61
4	9283	13.49	10.64	9.80	7.78	6.24	3.69	1.54
5	9246	12.53	9.88	9.14	7.44	6.17	3.87	1.61
6	9246	12.56	9.81	9.10	7.33	5.98	3.74	1.57
7	9191	12.48	9.58	8.90	7.14	5.76	3.47	1.50
8	9199	11.90	9.30	8.74	6.96	5.57	3.27	1.47
9	9267	11.32	8.75	8.18	6.67	5.51	3.51	1.61
10	9275	11.41	8.91	8.33	6.78	5.59	3.58	1.66
11	9362	11.09	9.23	8.58	7.18	6.06	4.09	2.03
12	9191	13.42	10.22	9.46	7.69	6.29	4.07	2.04
13	9183	12.93	9.88	9.13	7.31	5.98	3.82	1.88
14	9188	14.56	11.36	10.63	8.65	7.13	4.74	2.46
15	9119	14.54	11.66	10.82	8.89	7.40	5.04	2.71
16	9219	14.15	11.56	10.89	8.97	7.46	5.00	2.55
17	9111	11.96	9.66	9.14	7.78	6.72	4.82	2.52
18	9172	13.43	10.92	10.26	8.67	7.41	5.32	2.78
19	9156	13.67	10.81	10.14	8.48	7.17	4.99	2.57
20	9156	13.31	10.13	9.63	8.13	6.91	4.96	2.59
21	9040	13.29	10.27	9.69	8.09	6.96	4.91	2.63
22	9148	12.96	10.17	9.57	7.92	6.67	4.59	2.41
23	9135	12.57	9.61	8.97	7.41	6.18	4.14	1.89

US97-U

FWD Station	Force (lb)	Deflection (mils)						
		D1	D2	D3	D4	D5	D6	D7
2	9640	10.83	8.87	8.21	6.71	5.63	3.70	1.47
3	9577	9.80	8.16	7.61	6.35	5.40	3.64	1.45
4	9680	9.63	8.06	7.54	6.23	5.28	3.48	1.25
5	9609	11.39	9.30	8.67	7.03	5.84	3.81	1.33
6	9601	11.68	9.40	8.65	7.01	5.82	3.71	1.31
7	9664	11.97	9.83	9.03	7.35	6.15	4.11	1.64
8	9572	13.26	10.73	9.89	7.99	6.67	4.45	1.91
9	9644	11.05	9.24	8.58	7.09	6.04	4.18	1.91
10	9799	9.04	7.18	6.58	5.19	4.27	2.63	0.82
11	9810	8.26	6.41	5.87	4.61	3.79	2.31	0.69
12	9810	7.76	6.04	5.57	4.40	3.61	2.19	0.63
13	9842	8.69	6.94	6.34	5.09	4.13	2.52	0.76
14	9664	10.06	7.81	7.08	5.63	4.56	2.79	0.89

US20-U

FWD Station	Force (lb)	Deflection (mils)						
		D1	D2	D3	D4	D5	D6	D7
2	9493	6.96	5.12	4.62	3.61	2.91	1.79	0.69
3	9572	6.86	5.02	4.59	3.81	3.26	2.35	1.28
4	9421	11.19	8.74	8.12	6.75	5.82	4.05	1.92
5	9545	9.61	7.41	6.92	5.82	5.02	3.54	1.75
6	10049	6.61	5.39	5.07	4.30	3.78	2.81	1.43
7	9998	6.61	5.72	5.36	4.70	4.00	3.03	1.56
8	9969	7.25	5.96	5.60	4.82	4.09	2.93	1.29
9	9919	7.62	6.20	5.85	4.99	4.41	3.26	1.61
10	9898	8.58	7.19	6.93	5.89	5.34	3.99	1.57
11	9675	10.15	8.49	8.20	7.14	6.32	4.74	2.48
12	9752	9.26	7.77	7.37	6.33	5.53	4.04	2.02
13	9723	8.43	6.92	6.48	5.57	4.77	3.41	1.52

OR99-U

FWD Station	Force (lb)	Deflection (mils)						
		D1	D2	D3	D4	D5	D6	D7
2	9469	6.07	5.13	4.81	4.09	3.57	2.62	1.41
3	9413	7.49	5.61	5.11	4.17	3.56	2.46	1.25
4	9445	7.73	6.39	5.98	4.98	4.23	2.99	1.55
5	9342	8.80	7.48	6.96	5.76	4.90	3.45	2.13
6	9302	8.02	6.67	6.23	5.05	4.32	3.06	1.87
7	9331	5.30	4.46	4.19	3.57	3.11	2.32	1.53
8	9339	6.38	5.17	4.76	3.97	3.43	2.55	1.65
9	9302	6.56	5.29	4.91	4.02	3.42	2.51	1.68
10	9382	6.28	5.31	4.96	4.19	3.61	2.67	1.73
11	9434	7.74	6.42	5.95	4.98	4.23	3.00	1.78
12	9294	7.40	6.17	5.75	4.78	4.07	2.91	1.70
13	9270	8.57	6.56	6.08	5.03	4.28	3.09	1.83
14	9291	7.06	6.00	5.68	4.89	4.26	3.19	1.87
15	9315	6.63	5.80	5.53	4.86	4.33	3.32	1.98
16	9283	7.61	6.34	6.02	5.28	4.67	3.50	1.97
17	9442	7.67	6.38	6.05	5.31	4.71	3.58	2.04
18	9474	6.28	5.51	5.27	4.69	4.18	3.19	1.77
19	9350	8.89	7.17	6.56	5.58	4.74	3.39	1.77

OR238-C

FWD Station	Force (lb)	Deflection (mils)						
		D1	D2	D3	D4	D5	D6	D7
2	9429	5.97	4.29	3.80	2.68	1.98	1.01	0.37
3	9421	6.93	4.76	4.12	2.81	2.00	1.02	0.36
4	9397	6.42	4.86	4.33	3.31	2.57	1.58	0.68
5	9386	6.83	5.00	4.30	3.01	2.15	1.10	0.55
6	9382	7.98	4.92	4.09	2.71	2.02	1.17	0.55
7	9450	6.32	4.67	4.09	2.94	2.26	1.35	0.64
8	9382	6.61	4.86	4.24	3.07	2.34	1.38	0.69
9	9323	7.63	5.25	4.58	3.26	2.49	1.44	0.63
10	9434	6.47	4.92	4.38	3.28	2.56	1.50	0.61
11	9402	6.54	5.28	4.79	3.74	2.98	1.76	0.69
12	9537	6.40	4.44	3.92	3.03	2.39	1.48	0.65
13	9525	7.46	5.14	4.38	3.17	2.46	1.50	0.72
14	9501	6.63	4.97	4.35	3.21	2.51	1.51	0.70
15	9493	6.83	4.63	3.98	2.83	2.19	1.35	0.65
16	9382	8.47	5.48	4.66	3.26	2.41	1.38	0.72
17	9461	7.14	4.77	4.12	2.97	2.28	1.39	0.66
18	9466	5.80	4.42	3.99	3.06	2.44	1.50	0.65
19	9370	6.92	5.22	4.58	3.27	2.49	1.40	0.64
20	9501	5.77	4.38	3.93	3.02	2.39	1.44	0.68
21	9374	5.97	4.74	4.22	3.17	2.47	1.47	0.66

OR99W-C

FWD Station	Force (lb)	Deflection (mils)						
		D1	D2	D3	D4	D5	D6	D7
2	9664	8.94	7.02	6.52	5.29	4.41	3.01	1.55
3	9532	8.71	6.72	6.26	5.18	4.38	3.03	1.55
4	9505	8.21	6.69	6.24	5.16	4.38	3.02	1.56
5	9334	7.50	6.26	5.89	4.99	4.33	3.08	1.65
6	9609	8.54	6.89	6.41	5.40	4.67	3.27	1.72
7	9763	8.66	7.18	6.69	5.57	4.76	3.31	1.61
8	9556	8.35	6.80	6.34	5.23	4.46	3.13	1.56
9	9474	8.30	6.71	6.21	5.15	4.38	3.09	1.61
10	9561	9.38	6.46	6.08	5.11	4.34	3.14	1.70
11	9763	7.91	6.56	6.11	5.07	4.35	3.20	1.70
12	9633	7.31	6.10	5.70	4.85	4.23	3.11	1.71
13	9358	8.24	6.67	6.26	5.33	4.63	3.37	1.85
14	9683	7.88	6.59	6.19	5.30	4.64	3.41	1.83
15	9803	7.82	6.34	5.98	5.13	4.50	3.35	1.81
16	9699	7.48	6.15	5.82	5.05	4.46	3.31	1.83
17	9656	6.96	6.09	5.79	4.96	4.38	3.20	1.77
18	9934	7.08	5.65	5.31	4.53	3.95	2.94	1.58
19	9529	7.32	5.74	5.41	4.63	4.09	2.99	1.63
20	9704	7.43	6.06	5.63	4.83	4.20	3.07	1.62
21	10120	7.72	5.95	5.57	4.76	4.13	3.06	1.66
22	9776	7.79	6.22	5.84	5.08	4.48	3.36	1.81
23	9834	5.88	4.43	4.14	3.56	3.05	2.36	1.38
24	10104	5.59	4.22	3.93	3.39	3.02	2.30	1.34
25	9953	5.48	4.33	4.04	3.51	3.09	2.35	1.37
26	9890	6.45	4.85	4.55	3.91	3.45	2.56	1.50
27	9553	5.47	4.49	4.20	3.68	3.27	2.51	1.45
28	9548	6.66	5.19	4.91	4.30	3.85	3.00	1.65
29	9537	7.17	6.06	5.80	4.89	4.29	3.26	1.38
30	9747	8.61	6.68	6.22	5.31	4.61	3.43	1.76

OR221-C

FWD Station	Force (lb)	Deflection (mils)						
		D1	D2	D3	D4	D5	D6	D7
2	9720	7.51	5.49	4.93	3.78	3.01	1.78	0.75
3	9421	9.20	6.74	6.08	4.61	3.83	2.38	0.96
4	9577	7.69	5.72	5.10	3.93	3.15	1.85	0.73
5	9529	8.08	6.10	5.48	4.19	3.32	1.91	0.72
6	9358	8.52	6.01	5.28	3.91	3.01	1.58	0.68
7	9490	8.22	5.82	5.10	3.80	2.96	1.61	0.67
8	9517	7.33	5.23	4.67	3.52	2.74	1.61	0.70
9	9410	8.41	5.71	5.14	3.81	2.96	1.63	0.68
10	9477	7.99	5.54	4.69	3.41	2.65	1.39	0.62
11	9513	7.45	5.07	4.44	3.30	2.50	1.36	0.62
12	9501	8.94	5.96	5.07	3.54	2.63	1.39	0.64
13	9501	9.78	6.92	6.04	4.36	3.37	1.86	0.67
14	9532	9.17	6.43	5.51	3.82	2.81	1.51	0.66
15	9426	11.29	8.11	6.94	4.88	3.70	1.98	0.73
16	9389	10.78	8.07	7.03	4.89	3.67	1.91	0.71
17	9485	9.11	6.80	5.98	4.50	3.55	2.04	0.70
18	9723	9.07	7.06	6.42	5.00	4.06	2.43	0.86
19	9532	9.76	7.39	6.59	5.03	3.98	2.27	0.80
20	9307	11.14	8.13	7.36	5.45	4.35	2.46	0.75
21	9291	13.07	9.79	8.43	6.10	4.52	2.20	0.69
22	9442	13.21	9.50	8.20	5.86	4.49	2.37	0.76
23	9469	12.24	9.23	8.29	6.31	4.92	2.74	0.89
24	9358	12.45	9.28	8.24	6.11	4.85	2.69	0.83
25	9382	11.02	8.12	7.24	5.45	4.31	2.49	0.80
26	9593	11.52	8.33	7.28	5.51	4.29	2.40	0.80

OR99EB-C

FWD Station	Force (lb)	Deflection (mils)						
		D1	D2	D3	D4	D5	D6	D7
2	9842	2.04	1.51	1.57	1.48	1.37	1.28	1.03
3	9879	2.35	1.82	1.80	1.70	1.61	1.43	1.06
4	10033	2.53	1.93	1.85	1.69	1.54	1.37	1.06
5	9911	2.09	1.80	1.70	1.63	1.46	1.37	1.06
6	9863	2.07	1.51	1.48	1.43	1.37	1.27	1.00
7	9914	3.06	2.23	2.11	1.86	1.71	1.45	1.04
8	9922	2.81	2.07	1.96	1.76	1.56	1.39	1.03
9	9898	2.91	2.24	2.18	2.02	1.88	1.65	1.13
10	9866	3.00	2.43	2.29	2.06	1.88	1.61	1.16
11	9799	3.22	2.54	2.43	2.20	2.02	1.72	1.18
12	10006	3.02	2.51	2.44	2.29	2.15	1.89	1.20
13	10252	3.48	2.49	2.39	2.23	2.06	1.78	1.30
14	10065	2.80	1.93	1.85	1.74	1.65	1.49	1.20
15	9942	5.16	2.88	2.57	2.17	1.94	1.69	1.28
16	10041	2.75	2.05	2.01	1.89	1.81	1.62	1.28
17	10128	2.60	1.96	1.89	1.79	1.71	1.56	1.20
18	10001	3.11	2.32	2.25	2.12	2.01	1.84	1.33
19	9998	3.60	2.46	2.33	2.13	1.99	1.74	1.29
20	10057	3.28	2.28	2.20	1.99	1.83	1.61	1.20
21	10030	2.94	2.13	2.09	1.96	1.85	1.65	1.24
22	10033	3.34	2.39	2.20	2.09	1.94	1.68	1.22
23	9858	3.38	2.21	2.17	2.04	1.92	1.66	1.19
24	9823	4.54	3.20	3.02	2.57	2.16	1.86	1.18
25	9961	3.49	2.16	2.09	1.96	1.83	1.63	1.23
26	9858	2.85	1.98	1.93	1.84	1.74	1.55	1.16
27	9942	3.33	1.99	1.92	1.79	1.68	1.48	1.12

OR140-C

FWD Station	Force (lb)	Deflection (mils)						
		D1	D2	D3	D4	D5	D6	D7
2	10200	9.33	7.11	6.61	5.44	4.61	3.15	1.37
3	10081	7.42	6.02	5.61	4.54	3.77	2.38	0.79
4	9966	6.35	4.97	4.60	3.64	2.96	1.81	0.63
5	9990	6.17	4.87	4.44	3.54	2.87	1.80	0.62
6	9906	8.71	7.12	6.72	5.70	4.94	3.56	1.80
7	9942	10.15	8.62	8.13	7.06	6.20	4.57	2.43
8	9990	9.00	7.45	6.96	5.87	5.08	3.56	1.69
9	10014	9.13	7.55	7.11	6.08	5.22	3.69	1.74
10	9966	9.97	8.30	7.79	6.50	5.59	3.85	1.85
11	9882	10.15	8.34	7.86	6.60	5.60	3.83	1.78
12	9911	9.80	8.07	7.54	6.30	5.36	3.68	1.76
13	9934	8.22	6.70	6.18	5.02	4.17	2.71	1.18
14	9823	9.36	7.41	6.97	5.75	4.80	3.21	1.33
15	9930	9.75	7.52	6.95	5.58	4.65	3.08	1.43
16	9930	10.38	8.33	7.75	6.33	5.33	3.54	1.63
17	9961	9.33	7.53	7.02	5.78	4.82	3.19	1.49
18	9895	12.26	10.35	9.73	8.20	7.07	5.00	2.39

FWD Station	Force (lb)	Deflection (mils)						
		D1	D2	D3	D4	D5	D6	D7
2	9664	8.94	7.02	6.52	5.29	4.41	3.01	1.55
3	9532	8.71	6.72	6.26	5.18	4.38	3.03	1.55
4	9505	8.21	6.69	6.24	5.16	4.38	3.02	1.56
5	9334	7.50	6.26	5.89	4.99	4.33	3.08	1.65
6	9609	8.54	6.89	6.41	5.40	4.67	3.27	1.72
7	9763	8.66	7.18	6.69	5.57	4.76	3.31	1.61
8	9556	8.35	6.80	6.34	5.23	4.46	3.13	1.56
9	9474	8.30	6.71	6.21	5.15	4.38	3.09	1.61
10	9561	9.38	6.46	6.08	5.11	4.34	3.14	1.70
11	9763	7.91	6.56	6.11	5.07	4.35	3.20	1.70
12	9633	7.31	6.10	5.70	4.85	4.23	3.11	1.71
13	9358	8.24	6.67	6.26	5.33	4.63	3.37	1.85
14	9683	7.88	6.59	6.19	5.30	4.64	3.41	1.83
15	9803	7.82	6.34	5.98	5.13	4.50	3.35	1.81
16	9699	7.48	6.15	5.82	5.05	4.46	3.31	1.83
17	9656	6.96	6.09	5.79	4.96	4.38	3.20	1.77
18	9934	7.08	5.65	5.31	4.53	3.95	2.94	1.58
19	9529	7.32	5.74	5.41	4.63	4.09	2.99	1.63
20	9704	7.43	6.06	5.63	4.83	4.20	3.07	1.62
21	10120	7.72	5.95	5.57	4.76	4.13	3.06	1.66
22	9776	7.79	6.22	5.84	5.08	4.48	3.36	1.81
23	9834	5.88	4.43	4.14	3.56	3.05	2.36	1.38
24	10104	5.59	4.22	3.93	3.39	3.02	2.30	1.34
25	9953	5.48	4.33	4.04	3.51	3.09	2.35	1.37
26	9890	6.45	4.85	4.55	3.91	3.45	2.56	1.50
27	9553	5.47	4.49	4.20	3.68	3.27	2.51	1.45
28	9548	6.66	5.19	4.91	4.30	3.85	3.00	1.65
29	9537	7.17	6.06	5.80	4.89	4.29	3.26	1.38
30	9747	8.61	6.68	6.22	5.31	4.61	3.43	1.76

APPENDIX B – BACKCALCULATED STIFFNESS MODULUS

FWD Station	Backcalculated Modulus (ksi)					
	Elmod			BAKFAA		
	AC	Base	Subgrade	AC	Base	Subgrade
1	567	23	23	880	9	24
2	619	17	25	874	8	26
3	620	13	26	865	6	28
4	796	12	27	1098	6	28
5	761	13	27	1052	6	29
6	721	14	29	965	8	28
7	829	11	31	1084	6	31
8	800	22	26	1135	10	26
9	876	18	27	1240	8	27
10	627	25	24	1376	8	23
11	649	20	23	856	12	20
12	688	26	23	839	13	22
13	592	17	19	798	10	18
14	738	14	19	649	33	14
15	764	15	19	1054	7	18
16	830	30	19	743	57	15
17	759	26	18	1091	14	16
18	788	21	19	1054	14	17
19	719	36	19	951	28	16
20	622	42	18	747	39	15
21	781	28	20	1087	16	18
22	1157	16	25	1127	13	21

US97-U

FWD Station	Backcalculated Modulus (ksi)					
	Elmod			BAKFAA		
	AC	Base	Subgrade	AC	Base	Subgrade
1	438	39	19	651	15	28
2	398	35	14	573	9	32
3	486	29	19	314	63	20
4	532	35	15	791	6	49
5	365	35	13	559	7	36
6	330	29	17	503	9	35
7	359	18	28	509	10	28
8	309	20	24	438	12	23
9	407	25	25	625	13	24
10	503	35	19	703	9	55
11	464	55	19	293	74	31
12	545	50	21	317	80	33
13	652	45	17	981	9	59
14	570	40	17	819	12	43

US20-U

FWD Station	Backcalculated Modulus (ksi)					
	Elmod			BAKFAA		
	AC	Base	Subgrade	AC	Base	Subgrade
1	402	65	28	505	15	59
2	469	36	14	639	3	46
3	331	110	43	388	99	36
4	265	34	24	316	67	22
5	344	49	23	405	15	22
6	387	92	27	319	146	28
7	615	33	34	879	12	32
8	495	51	23	468	59	25
9	410	53	31	263	77	32
10	417	39	25	406	72	20
11	400	28	25	341	80	19
12	520	25	21	775	7	21
13	442	34	30	423	71	23

FWD Station	Backcalculated Modulus (ksi)					
	Elmod			BAKFAA		
	AC	Base	Subgrade	AC	Base	Subgrade
1	793	45	32	1034	142	28
2	1426	45	37	1165	147	28
3	636	75	38	635	77	32
4	933	45	32	1399	13	31
5	919	32	27	1227	17	24
6	918	40	31	935	68	24
7	1601	76	41	1460	177	32
8	1070	85	36	1251	94	30
9	1477	51	36	1165	79	31
10	1236	80	35	1619	60	30
11	662	74	27	1235	33	27
12	1089	41	32	1419	26	28
13	670	68	30	810	61	25
14	1187	69	28	1737	34	25
15	1506	69	27	2246	27	24
16	1085	81	26	1215	101	21
17	1074	74	26	1346	74	22
18	1590	82	28	1672	139	23
19	988	81	37	801	65	23

FWD Station	Backcalculated Modulus (ksi)					
	Elmod			BAKFAA		
	AC	Base	Subgrade	AC	Base	Subgrade
Station	E1(EM)	E2(EM)	E3(EM)	E1(BF)	E2(BF)	E3(BF)
1	860	70	30	1207	13	105
2	1147	94	28	819	111	53
3	799	88	27	1040	22	84
4	1247	36	61	1686	21	58
5	1026	72	26	1289	22	69
6	531	91	38	519	65	57
7	1131	68	37	1407	28	62
8	981	64	38	1219	29	59
9	628	80	32	779	36	53
10	1186	71	28	956	100	40
11	1490	19	61	2043	10	66
12	651	137	32	648	99	47
13	593	91	34	725	43	52
14	749	86	32	985	32	55
15	630	104	38	766	50	58
16	486	80	32	588	36	54
17	692	97	38	688	75	50
18	1388	58	41	1783	25	60
19	988	58	31	730	76	44
20	1436	78	37	1130	113	44
21	1433	61	33	1038	104	41

OR99W-C

FWD Station	Backcalculated Modulus (ksi)					
	Elmod			BAKFAA		
	AC	Base	Subgrade	AC	Base	Subgrade
1	527	35	21	619	11	33
2	429	28	18	513	7	34
3	465	29	19	554	7	35
4	491	24	21	400	61	22
5	211	57	31	199	92	24
6	540	28	17	647	6	35
7	523	26	16	630	4	38
8	491	26	19	576	7	33
9	500	29	19	589	7	33
10	278	53	26	295	47	25
11	543	19	30	482	67	21
12	573	23	31	526	66	22
13	512	16	29	697	5	34
14	553	17	30	730	7	30
15	573	19	30	757	7	30
16	715	18	30	603	68	21
17	643	23	29	1043	4	42
18	733	27	33	693	70	24
19	727	36	31	975	14	29
20	821	22	31	1127	6	34
21	729	29	32	941	15	29
22	746	31	29	740	63	22
23	835	68	39	986	55	33
24	996	60	40	1164	54	34
25	1001	54	39	1239	38	33
26	713	70	35	802	68	29
27	1233	39	36	1631	16	33
28	881	48	30	1105	35	26
29	912	13	35	1420	2	210
30	252	87	28	235	139	22

FWD Station	Backcalculated Modulus (ksi)					
	Elmod			BAKFAA		
	AC	Base	Subgrade	AC	Base	Subgrade
1	312	64	30	400	28	51
2	466	68	28	645	23	50
3	360	64	21	320	64	29
4	476	71	22	407	79	33
5	441	53	24	612	16	47
6	375	56	22	485	18	54
7	403	58	24	407	79	33
8	446	68	31	587	28	51
9	355	67	25	494	22	51
10	368	72	27	463	28	57
11	437	80	32	551	36	56
12	365	59	27	441	24	59
13	374	53	21	501	17	49
14	383	53	22	473	18	61
15	341	41	16	431	12	48
16	413	29	19	491	10	54
17	462	72	16	671	14	48
18	625	48	17	418	65	28
19	486	52	16	690	11	46
20	416	39	16	561	10	42
21	333	31	13	426	8	45
22	323	31	15	417	10	42
23	416	34	14	589	7	43
24	405	30	15	548	8	41
25	428	35	20	590	11	41
26	365	37	20	484	13	41

FWD Station	Backcalculated Modulus (ksi)					
	Elmod			BAKFAA		
	AC	Base	Subgrade	AC	Base	Subgrade
1	1304	1541	25	1886	831	41
2	1251	3879	23	1589	2373	40
3	686	2254	24	762	1644	40
4	1134	2197	25	828	1149	43
5	1143	3593	25	1485	1262	42
6	747	1710	26	808	20461	24
7	450	1093	25	487	743	42
8	844	1229	26	1093	696	44
9	972	1112	23	1227	681	37
10	1040	592	27	1151	455	40
11	1074	748	25	434	8740	19
12	1247	629	30	624	8972	18
13	1145	963	25	1298	751	33
14	831	2702	23	898	2148	38
15	301	847	29	319	644	41
16	1210	2183	21	1409	1443	35
17	1120	1470	23	975	2241	36
18	943	2801	22	759	8089	21
19	890	1099	26	956	886	35
20	1050	1663	22	758	7717	23
21	1682	1560	22	1890	1100	35
22	1035	1276	22	1135	888	37
23	1103	1440	22	1182	1076	37
24	959	398	27	1144	283	37
25	850	1749	23	907	1366	38
26	899	2402	22	961	2022	37
27	803	2051	24	851	1641	40

FWD Station	Backcalculated Modulus (ksi)					
	Elmod			BAKFAA		
	AC	Base	Subgrade	AC	Base	Subgrade
1	347	59	21	336	54	26
2	491	38	20	351	68	31
3	425	47	31	604	7	87
4	495	53	26	495	16	26
5	313	51	28	527	9	21
6	360	35	22	338	67	22
7	337	39	28	337	79	21
8	363	40	26	532	6	28
9	377	35	25	308	78	20
10	363	27	26	331	72	20
11	352	41	26	652	7	43
12	517	62	17	609	7	34
13	362	29	31	280	60	25
14	311	38	31	534	7	29
15	350	33	27	648	7	33
16	399	37	29	636	4	23

FWD Station	Backcalculated Modulus (ksi)		
	BAKFAA		
	AC	Base	Subgrade
1	394	53	20
2	471	71	17
3	534	64	14
4	584	149	14
5	661	107	15
6	793	81	15
7	737	97	15
8	663	118	15
9	402	98	15
10	546	64	15
11	674	14	18
12	626	82	15
13	395	51	15
14	844	100	15
15	722	106	15
16	871	94	14
17	475	134	15
18	845	80	15
19	889	89	15
20	728	150	15
21	876	111	16
22	941	97	16
23	915	76	16
24	1357	116	16
25	962	123	18

APPENDIX C – DYNAMIC MODULUS TEST RESULTS DATA

OR22-U

Temp, °C	Freq, Hz	Dynamic Modulus (Mpa)			
		Sample1	Sample 2	Sample 3	Sample 4
4	25	12076	12994	13942	12318
4	10	12063	12140	12716	14146
4	5	11902	12504	12605	10768
4	1	10185	11601	10753	10944
4	0.5	9288	11011	9518	9755
4	0.1	7966	8716	8013	7769
21	25	6913	7589	7540	7991
21	10	7640	7974	8159	8747
21	5	5542	6208	6540	6634
21	1	3580	4197	4030	4287
21	0.5	2820	3462	3220	3460
21	0.1	1677	2125	1936	2126
37	25	1587	2157	2004	2184
37	10	1480	2302	2125	1862
37	5	1458	1844	1555	1329
37	1	636	986	713	644
37	0.5	555	792	574	484
37	0.1	180	313	259	229

US97-U

Temp, °C	Freq, Hz	Dynamic Modulus (Mpa)			
		Sample 1	Sample 2	Sample 3	Sample 4
4	25	10332	3808	12257	10813
4	10	9932	10722	10798	10766
4	5	8972	8640	10543	9588
4	1	7728	7959	8555	7898
4	0.5	6978	8136	7616	7195
4	0.1	5122	6353	5728	5744
21	25	5898	5777	4842	4989
21	10	5749	6367	5819	4949
21	5	4773	4677	4205	3703
21	1	2917	2653	2312	2102
21	0.5	2359	2035	1755	1586
21	0.1	1459	1135	1072	882
37	25	1761	1488	1188	1454
37	10	1510	1337	1264	1192
37	5	1183	964	839	856
37	1	601	512	378	440
37	0.5	440	362	280	316
37	0.1	232	198	121	185

US20-U

Temp, °C	Freq, Hz	Dynamic Modulus (Mpa)			
		Sample1	Sample 2	Sample 3	Sample 4
4	25	11785	12943	15603	13025
4	10	14238	13752	15423	13316
4	5	13574	12555	11557	10693
4	1	11017	10714	10677	10312
4	0.5	9863	9938	10465	9610
4	0.1	8699	8122	8417	7797
21	25	8295	6719	7868	6881
21	10	7722	7268	7904	7342
21	5	6844	6202	5989	5873
21	1	4569	4271	3956	3442
21	0.5	3857	3479	3219	2839
21	0.1	2494	2148	2124	1702
37	25	2749	2171	2103	2065
37	10	2514	2317	2104	1949
37	5	2112	1833	1660	1388
37	1	1124	907	804	762
37	0.5	870	724	634	649
37	0.1	477	385	284	302

OR99-U

Temp, °C	Freq, Hz	Dynamic Modulus (Mpa)			
		Sample1	Sample 2	Sample 3	Sample 4
4	25	14980	12949	11518	13864
4	10	17436	12036	12011	13198
4	5	15787	11420	11055	13259
4	1	12850	11797	10370	12332
4	0.5	12580	10744	9608	10714
4	0.1	8735	8669	7975	10196
21	25	7591	7885	6817	3848
21	10	10653	10018	5835	7959
21	5	8706	7507	6956	7421
21	1	4269	5000	4341	4121
21	0.5	2913	3975	3063	3180
21	0.1	1570	2694	1026	1669
37	25	1049	1900	848	895
37	10	669	1463	1047	645
37	5	751	1370	619	511
37	1	340	985	267	595
37	0.5	222	748	164	390
37	0.1	61	357	49	137

OR238-C

Temp, °C	Freq, Hz	Dynamic Modulus (Mpa)				
		Sample1	Sample 2	Sample 3	Sample 4	Sample 5
4	25	13500	13094	12619	11688	14754
4	10	15732	16209	11766	14350	12267
4	5	13443	13919	12143	13056	12540
4	1	11818	12620	10446	13127	11875
4	0.5	11499	11807	9926	12132	11175
4	0.1	10474	10394	8217	11950	9821
21	25	9412	8842	6605	10063	8868
21	10	10220	9569	7809	10522	8099
21	5	8396	7906	6035	8853	7817
21	1	6926	5191	4391	7688	5311
21	0.5	6231	4209	3657	7163	4335
21	0.1	4595	2632	2454	5210	2840
37	25	4884	2301	2558	4956	3209
37	10	4773	2375	2657	5583	3561
37	5	3463	1798	2055	4808	2605
37	1	2243	876	986	3036	1299
37	0.5	2071	744	845	2516	1056
37	0.1	1254	384	473	1082	519

OR99W-C

Temp, °C	Freq, Hz	Dynamic Modulus (Mpa)					
		Sample1	Sample 2	Sample 3	Sample 4	Sample 5	Sample 6
4	25	8432	8726	10089	10719	12845	13171
4	10	13008	16274	16422	10776	12351	11764
4	5	14493	14435	14512	10360	14572	12981
4	1	12690	12458	12799	9045	12947	10350
4	0.5	12475	11480	11839	7770	10203	9575
4	0.1	10398	9419	10561	7260	9972	8106
21	25	10148	8092	8652	6967	9156	7255
21	10	9368	7872	8793	7562	10157	7763
21	5	8577	6423	7163	6145	8567	6343
21	1	7098	4271	5291	3910	7287	4687
21	0.5	6284	3491	4486	3187	6664	4010
21	0.1	4762	2104	2942	1900	5533	2670
37	25	4426	1701	3753	1961	5084	2366
37	10	5278	1839	4344	2176	3950	2147
37	5	4103	1345	3067	1674	4208	1435
37	1	2476	686	1480	825	2797	960
37	0.5	2204	521	1065	683	2572	733
37	0.1	1201	246	525	334	1531	368

OR221-C

Temp, °C	Freq, Hz	Dynamic Modulus (Mpa)					
		Sample1	Sample 2	Sample 3	Sample 4	Sample 5	Sample 6
4	25	11978	12290	11173	13358	11655	10421
4	10	11726	14362	11587	14288	11250	13572
4	5	10451	12483	10495	12201	10722	12965
4	1	9270	11333	9880	13116	9749	10518
4	0.5	8358	10727	9331	12507	8803	10247
4	0.1	6908	8585	7973	11716	7335	8731
21	25	6267	6509	7114	9607	6689	7974
21	10	6787	7241	6965	9134	7137	8312
21	5	5369	5558	6018	9089	5441	6742
21	1	3429	3454	4305	7446	3485	4425
21	0.5	2756	2798	3539	6565	2816	3600
21	0.1	1715	1877	2346	5381	1650	2279
37	25	1554	1738	3281	5765	1797	1903
37	10	1198	1931	3502	5414	2128	2235
37	5	1180	1344	2595	4506	1430	1611
37	1	712	637	1676	2682	753	849
37	0.5	610	466	1511	2550	630	653
37	0.1	314	213	873	1433	281	327

OR99EB-C

Temp, °C	Freq, Hz	Dynamic Modulus (Mpa)							
		Sample 1	Sample 2	Sample 3	Sample 4	Sample 5	Sample 6	Sample 7	Sample 8
4	25	10455	10241	6517	12539	13608	2585	14743	14710
4	10	11221	17786	12665	13534	14653	14331	17098	15777
4	5	11948	15221	11645	10747	13869	10207	16191	11581
4	1	10545	14827	10586	11968	12842	9928	16475	12834
4	0.5	9791	14263	10321	12452	12339	10442	11701	11905
4	0.1	7762	12488	9100	10797	11139	9599	11061	10434
21	25	7552	10287	8468	8899	9722	9200	6783	8678
21	10	8054	10895	7589	8478	9548	8657	9366	8813
21	5	6357	8931	7465	7775	8389	7859	10003	7092
21	1	4534	6419	5570	5493	6604	6026	8638	5077
21	0.5	3850	5445	4982	4699	5854	5304	7812	4344
21	0.1	2815	3747	3377	3078	4169	3925	6042	2841
37	25	2682	4363	3606	4298	4221	4479	5954	2822
37	10	2736	4226	3528	4349	4510	4751	4619	2585
37	5	2014	2973	2741	3458	3846	3519	3931	2107
37	1	1049	1673	1532	2129	2315	2155	3053	1170
37	0.5	804	1014	1254	1779	1891	1722	2480	787
37	0.1	389	147	676	968	1017	925	1494	370

OR140-C

Temp, °C	Freq, Hz	Dynamic Modulus (Mpa)					
		Sample1	Sample 2	Sample 3	Sample 4	Sample 5	Sample 6
4	25	6890	10252	12845	12304	12911	11796
4	10	8941	10831	13289	10721	14461	10415
4	5	5712	8943	11898	10812	12021	9072
4	1	4610	8114	10619	8759	11957	8140
4	0.5	3781	7240	9557	7565	11364	7364
4	0.1	2645	6081	7572	5235	9864	5684
21	25	5141	4945	8016	5357	7558	4848
21	10	6787	6847	7576	6149	6926	5601
21	5	5226	5103	5728	5155	6020	4292
21	1	2847	3051	4450	2539	4064	2293
21	0.5	2588	2389	3573	1871	3421	1740
21	0.1	1561	1392	2249	930	2399	1031
37	25	629	1102	2755	942	3639	1098
37	10	541	1328	2771	1055	3651	843
37	5	578	1139	2107	704	2596	642
37	1	424	533	1127	354	1425	385
37	0.5	258	387	934	243	1079	266
37	0.1	143	214	433	111	593	146

OR99*-C

Temp, °C	Freq, Hz	Dynamic Modulus (Mpa)						
		Sample1	Sample 2	Sample 3	Sample 4	Sample 5	Sample 6	Sample 7
4	25	11038	11385	9137	9617	11086	12657	11441
4	10	11292	11810	11036	9655	14951	12491	10802
4	5	10976	11498	10457	9196	14176	11374	10437
4	1	9680	10007	10064	8364	12070	10280	9229
4	0.5	9575	9546	9948	7853	10873	9828	8518
4	0.1	7848	8414	8535	6921	8630	7994	7070
21	25	7736	7601	8284	6322	6123	6843	6489
21	10	7285	7434	8408	6209	6525	6931	6823
21	5	6674	6419	7154	5493	5044	5799	5201
21	1	5261	4572	5994	4197	3272	4116	3512
21	0.5	4739	3884	5447	3614	2647	3498	2964
21	0.1	3524	2483	4147	2490	1537	2097	1781
37	25	3499	3367	3998	2713	2113	2443	2210
37	10	3235	3265	4186	2644	2157	2460	2093
37	5	2674	2385	3632	1959	1462	1639	1422
37	1	1456	1312	2622	1185	795	918	841
37	0.5	1294	1084	2414	973	665	723	698
37	0.1	658	578	1321	574	304	350	332

APPENDIX D – DSR FREQUENCY TEST RESULTS DATA

OR22-U

Freq (Hz)	20°C		30°C		46°C		58°C		70°C		82°C		Freq @ 1.6 Hz	
	δ	G* , Pa	δ	G* , Pa										
0.1	53.7	3.36E+06	61.38	5.09E+05	74.23	24380	81.89	2787	86.19	419.2	87.3	82.7	40°C	
0.1	55.4	3.42E+06	61.62	5.57E+05	73.55	29340	81.17	3614	85.94	511.6	87.3	103.8	δ	G* , Pa
0.2	52.7	4.12E+06	61.13	6.50E+05	72.93	35080	80.71	4283	85.59	648.1	87.4	129.8	62.54	5.80E+05
0.2	52.2	4.71E+06	60.56	7.60E+05	72.26	42510	80.11	5286	85.21	804.1	87.4	160.6	63.67	5.26E+05
0.3	51.8	5.37E+06	59.97	8.86E+05	71.63	50970	79.45	6547	84.87	971.7	87.3	199.3	52°C	
0.3	51.5	6.11E+06	59.37	1.03E+06	71.04	60790	78.85	7968	84.48	1204	87.2	247.8	δ	G* , Pa
0.4	51.2	6.96E+06	58.78	1.20E+06	70.5	72010	78.27	9609	83.99	1530	87	311.3	70.73	82670
0.5	50.9	7.92E+06	58.19	1.38E+06	70	84950	77.67	11780	83.49	1915	86.8	390.4	71	80900
0.6	50.7	8.99E+06	57.6	1.60E+06	69.5	1.00E+05	77	14500	82.97	2405	86.6	472.7	64°C	
0.8	50.6	1.02E+07	57.03	1.85E+06	69.05	1.18E+05	76.37	17770	82.46	2964	86.3	599.9	δ	G* , Pa
1.0	50.5	1.15E+07	56.5	2.13E+06	68.62	1.40E+05	75.75	21610	81.98	3609	85.9	773.6	77.94	12960
1.3	50.6	1.30E+07	55.96	2.47E+06	68.16	1.67E+05	75.18	26060	81.53	4337	85.5	973.2	77.94	12970
1.6	50.8	1.47E+07	55.43	2.85E+06	67.8	1.97E+05	74.63	31260	80.99	5337	85.1	1201	76°C	
2.0	51.0	1.66E+07	54.93	3.29E+06	67.44	2.32E+05	74.13	37160	80.44	6582	84.7	1480	δ	G* , Pa
2.5	51.3	1.87E+07	54.45	3.80E+06	67.13	2.71E+05	73.67	43810	79.83	8241	84.3	1870	83.29	2494
3.2	51.7	2.11E+07	54.05	4.37E+06	66.84	3.15E+05	73.12	53110	79.24	10210	83.8	2338	83.23	2548
4.0	52.4	2.39E+07	53.65	5.02E+06	66.63	3.59E+05	72.56	64620	78.63	12670	83.3	2891		
5.0	52.8	2.69E+07	53.24	5.75E+06	66.34	4.13E+05	72.02	78460	78.12	15260	82.9	3523		
6.3	53.3	3.07E+07	52.91	6.60E+06	65.74	4.89E+05	71.54	94020	77.57	18550	82.4	4347		
7.9	54.5	3.52E+07	52.75	7.57E+06	65.13	5.79E+05	71.12	1.11E+05	77.1	22020	82	5313		
10.0	57.3	4.08E+07	52.88	8.66E+06	64.48	6.90E+05	70.78	1.28E+05	76.59	26470	81.5	6434		
12.6	58.9	4.64E+07	52.47	9.85E+06	63.83	8.22E+05	70.42	1.49E+05	76.07	31980	81	7895		
15.9	59.7	5.22E+07	52.36	1.12E+07	63.14	9.77E+05	69.97	1.78E+05	75.53	38770	80.5	9610		
20.0	61.1	5.89E+07	52.22	1.27E+07	62.46	1.16E+06	69.61	2.07E+05	74.98	47030	80	11700		
25.1	67.1	5.97E+07	53.37	1.42E+07	61.91	1.37E+06	69.24	2.40E+05	74.45	56840	79.4	14380		
31.6	67.9	7.56E+07	52.77	1.65E+07	61.22	1.61E+06	68.88	2.72E+05	73.99	66960	78.8	17520		
39.8	67.1	8.39E+07	52.08	1.86E+07	60.51	1.88E+06	68.54	2.88E+05	73.48	79450	78.1	21620		
50.1	60.4	6.63E+07	50.78	1.93E+07	59.68	2.18E+06	68.14	2.84E+05	72.89	94580	77.4	26600		
63.1	82.5	8.49E+07	55.91	2.33E+07	59.73	2.55E+06	67.78	2.66E+05	72.31	1.11E+05	76.3	32220		
79.4	93.5	4.07E+07	66.2	2.03E+07	60.7	2.89E+06	67.27	2.46E+05	71.51	1.19E+05	74.8	39080		
100.0	131.5	5.49E+07	79.11	3.03E+07	61.34	3.46E+06	66.51	2.24E+05	70.54	1.13E+05	72.8	46850		

US97-U

Freq (Hz)	20°C		30°C		46°C		58°C		70°C		82°C		Freq @ 1.6 Hz	
	δ	G* , Pa	δ	G* , Pa										
0.1	55.4	1.46E+06	59.73	2.42E+05	63.36	17960	65.93	3638	71.24	784.2	78.1	196	40°C	
0.1	56.35	1.55E+06	60.11	2.70E+05	63.26	20950	65.73	4169	70.66	937.7	77.4	240.2	δ	G* , Pa
0.2	54.77	1.84E+06	60.06	3.14E+05	63.2	24710	65.52	4955	70.11	1123	76.7	292	61.04	3.02E+05
0.2	54.29	2.11E+06	60.11	3.45E+05	63.14	29030	65.32	5894	69.61	1337	76	351.7	61.77	2.85E+05
0.3	53.82	2.42E+06	60.05	3.93E+05	63.09	34020	65.16	6913	69.16	1590	75.3	425.4	52°C	
0.3	53.37	2.78E+06	59.82	4.59E+05	63.06	39880	65.04	8069	68.77	1890	74.6	518	δ	G* , Pa
0.4	52.98	3.18E+06	59.56	5.39E+05	63.03	46730	64.93	9485	68.38	2252	74	627.7	63.76	55250
0.5	52.6	3.62E+06	59.24	6.30E+05	63.01	54750	64.86	11180	68.05	2674	73.3	758.2	63.88	54380
0.6	52.26	4.13E+06	58.88	7.38E+05	63	64060	64.81	13210	67.76	3181	72.7	914.3	64°C	
0.8	51.89	4.70E+06	58.52	8.59E+05	63	74950	64.76	15580	67.49	3789	72.2	1096	δ	G* , Pa
1.0	51.58	5.35E+06	58.16	9.99E+05	63	87790	64.73	18370	67.27	4499	71.7	1313	65.63	12380
1.3	51.25	6.10E+06	57.79	1.16E+06	62.99	1.03E+05	64.72	21640	67.08	5337	71.2	1572	65.63	12430
1.6	51.05	6.94E+06	57.43	1.34E+06	62.99	1.20E+05	64.71	25400	66.93	6300	70.7	1875	76°C	
2.0	50.89	7.90E+06	57.05	1.55E+06	62.99	1.40E+05	64.72	29840	66.8	7447	70.3	2238	δ	G* , Pa
2.5	50.73	8.98E+06	56.67	1.79E+06	63	1.64E+05	64.73	35110	66.69	8804	70	2676	68.58	3376
3.2	50.76	1.02E+07	56.29	2.06E+06	63	1.90E+05	64.75	41200	66.6	10430	69.6	3200	68.54	3422
4.0	50.79	1.16E+07	55.9	2.38E+06	63.02	2.23E+05	64.78	48600	66.53	12390	69.3	3837		
5.0	50.87	1.31E+07	55.51	2.74E+06	63	2.66E+05	64.8	57300	66.48	14690	69.1	4579		
6.3	50.91	1.48E+07	55.15	3.17E+06	62.98	3.13E+05	64.82	67650	66.44	17400	68.9	5429		
7.9	51.14	1.69E+07	54.82	3.64E+06	63.01	3.58E+05	64.85	79590	66.42	20560	68.7	6436		
10.0	51.52	1.91E+07	54.43	4.21E+06	63.08	4.01E+05	64.88	93250	66.41	24260	68.5	7640		
12.6	52.79	2.18E+07	54.08	4.85E+06	62.89	4.62E+05	64.91	1.09E+05	66.4	28560	68.3	9081		
15.9	53.24	2.45E+07	53.75	5.57E+06	62.62	5.44E+05	64.92	1.27E+05	66.4	33660	68.2	10790		
20.0	52.98	2.79E+07	53.45	6.36E+06	62.29	6.42E+05	64.93	1.49E+05	66.39	39870	68	12840		
25.1	55.54	3.01E+07	53.59	7.24E+06	61.99	7.57E+05	64.92	1.75E+05	66.37	47370	67.9	15400		
31.6	55.63	3.61E+07	53.14	8.39E+06	61.59	8.98E+05	64.9	2.04E+05	66.34	56340	67.8	18270		
39.8	54.98	4.04E+07	52.64	9.56E+06	61.16	1.06E+06	64.85	2.40E+05	66.31	66510	67.6	21690		
50.1	50.74	3.87E+07	51.31	1.05E+07	60.56	1.25E+06	64.69	2.86E+05	66.24	78090	67.3	25790		
63.1	67.84	4.88E+07	54.77	1.24E+07	60.62	1.47E+06	64.74	3.31E+05	66.07	90620	66.7	30610		
79.4	78.94	3.11E+07	59.21	1.21E+07	60.9	1.69E+06	64.77	3.71E+05	65.8	1.06E+05	65.6	36560		
100.0	107.5	4.98E+07	65.89	1.64E+07	61.39	2.01E+06	64.92	4.07E+05	65.43	1.24E+05	63.9	43390		

US20-U

Freq (Hz)	20°C		30°C		46°C		58°C		70°C		82°C		Freq @ 1.6 Hz
	δ	G* , Pa	δ	G* , Pa									
0.1	58.07	1.66E+06	64.35	2.46E+05	75.2	13840	82.11	1874	86.2	306.3	87.1	68.87	40°C
0.1	57.74	1.81E+06	64.58	2.72E+05	74.58	16700	81.65	2227	85.84	393.7	87.3	85.91	δ G* , Pa
0.2	57.18	2.10E+06	64.28	3.17E+05	73.91	20380	80.96	2846	85.52	488.6	87.3	108	65.22 3.25E+05
0.2	56.73	2.44E+06	64.06	3.66E+05	73.25	24770	80.36	3501	85.2	596.9	87.3	137	66.03 2.96E+05
0.3	56.26	2.82E+06	63.73	4.26E+05	72.69	29440	79.83	4188	84.82	741.8	87.2	171.2	52°C
0.3	55.75	3.27E+06	63.33	5.01E+05	72.18	34770	79.27	5092	84.38	921.6	87.1	215.8	δ G* , Pa
0.4	55.27	3.77E+06	62.87	5.89E+05	71.63	41720	78.66	6234	83.91	1144	87	267.9	71.86 48660
0.5	54.8	4.35E+06	62.4	6.94E+05	71.07	50440	78.04	7661	83.41	1420	86.8	330.2	72.03 47670
0.6	54.36	5.02E+06	61.93	8.14E+05	70.56	60560	77.45	9382	82.9	1759	86.5	407.4	64°C
0.8	53.97	5.76E+06	61.43	9.56E+05	70.09	72400	76.84	11480	82.36	2182	86.2	506.1	δ G* , Pa
1.0	53.65	6.59E+06	61	1.12E+06	69.71	85200	76.24	13980	81.81	2696	85.8	638.9	78.04 8879
1.3	53.44	7.55E+06	60.5	1.31E+06	69.28	1.01E+05	75.67	16950	81.31	3262	85.4	807.3	78.02 8919
1.6	53.33	8.61E+06	60.03	1.53E+06	68.89	1.20E+05	75.13	20430	80.8	3968	84.9	1018	76°C
2.0	53.24	9.83E+06	59.57	1.77E+06	68.56	1.41E+05	74.62	24480	80.19	4963	84.5	1265	δ G* , Pa
2.5	53.08	1.12E+07	59.1	2.07E+06	68.23	1.66E+05	74.13	29310	79.55	6262	84	1545	82.95 1977
3.2	53.32	1.28E+07	58.64	2.41E+06	67.91	1.96E+05	73.58	35620	79.02	7595	83.5	1919	82.96 1982
4.0	53.58	1.46E+07	58.19	2.80E+06	67.63	2.32E+05	73.1	42890	78.47	9264	83	2383	
5.0	53.78	1.66E+07	57.77	3.26E+06	67.37	2.72E+05	72.59	52170	77.95	11200	82.5	2904	
6.3	54.26	1.90E+07	57.44	3.79E+06	67.15	3.16E+05	72.13	62520	77.49	13290	82	3567	
7.9	54.72	2.16E+07	56.94	4.38E+06	66.95	3.64E+05	71.77	73160	76.96	16050	81.5	4339	
10.0	54.96	2.46E+07	56.49	5.03E+06	66.69	4.22E+05	71.39	85520	76.43	19500	80.9	5363	
12.6	55.65	2.82E+07	56.11	5.81E+06	66.2	5.00E+05	71.01	1.01E+05	75.88	23810	80.3	6655	
15.9	57.51	3.22E+07	55.71	6.68E+06	65.73	5.92E+05	70.6	1.22E+05	75.3	29380	79.8	8120	
20.0	57.64	3.64E+07	55.27	7.70E+06	65.22	7.02E+05	70.21	1.46E+05	74.78	35470	79.2	10070	
25.1	62.56	4.06E+07	55.82	8.80E+06	64.8	8.33E+05	69.87	1.71E+05	74.25	42890	78.6	12170	
31.6	61.03	4.80E+07	54.77	1.02E+07	64.22	9.91E+05	69.54	1.99E+05	73.81	50360	78	14710	
39.8	60.31	5.36E+07	54.22	1.16E+07	63.65	1.17E+06	69.23	2.22E+05	73.3	60240	77.3	17920	
50.1	59.46	4.69E+07	53.34	1.25E+07	62.98	1.37E+06	68.83	2.41E+05	72.77	71220	76.5	21490	
63.1	68.78	6.17E+07	55.34	1.50E+07	62.79	1.63E+06	68.52	2.59E+05	72.2	85440	75.2	25910	
79.4	93.46	3.85E+07	65.06	1.50E+07	63.45	1.89E+06	68.2	2.67E+05	71.43	1.02E+05	73.5	32080	
100.0	117.9	5.30E+07	70.72	1.99E+07	63.7	2.26E+06	67.85	2.64E+05	70.65	1.20E+05	71.1	38840	

OR99-U

Freq (Hz)	20°C		30°C		46°C		58°C		70°C		82°C		Freq @ 1.6 Hz	
	δ	G* , Pa	δ	G* , Pa	δ	G* , Pa								
0.1	67.54	2.46E+06	77.02	2.20E+05	85.93	6404	88.3	671.8	88.97	100.5	88.5	21.58	40°C	
0.1	67.69	2.68E+06	76.55	2.60E+05	85.63	7753	88.19	843.7	88.96	133.9	88.5	27.25	δ	G* , Pa
0.2	65.84	3.33E+06	75.95	3.17E+05	85.29	9810	88.03	1055	88.97	164.2	88.7	33.89	77.35	2.70E+05
0.2	65.13	3.94E+06	75.38	3.81E+05	84.91	12250	87.85	1330	88.99	195.2	88.7	42.34	77.52	2.62E+05
0.3	64.47	4.65E+06	74.8	4.58E+05	84.52	15250	87.68	1673	89.02	247.5	88.9	53.52	52°C	
0.3	63.87	5.47E+06	74.17	5.53E+05	84.14	18700	87.47	2085	89.01	316.6	89	66.38	δ	G* , Pa
0.4	63.37	6.41E+06	73.51	6.67E+05	83.76	22930	87.25	2583	88.92	406.5	89	82.75	83.75	27100
0.5	62.91	7.48E+06	72.81	8.05E+05	83.34	28490	87.03	3233	88.85	514	89.1	104.2	83.79	26650
0.6	62.59	8.74E+06	72.1	9.72E+05	82.89	35470	86.79	4017	88.74	644.8	89.1	133	64°C	
0.8	62.33	1.02E+07	71.37	1.17E+06	82.41	44340	86.54	4983	88.63	798.5	89.2	167.4	δ	G* , Pa
1.0	62.19	1.19E+07	70.64	1.41E+06	81.95	54800	86.28	6271	88.49	1004	89.2	208.2	87.13	3786
1.3	62.22	1.38E+07	69.92	1.69E+06	81.49	67110	85.96	8041	88.32	1257	89.2	257.2	87.13	3796
1.6	62.41	1.60E+07	69.17	2.02E+06	81.1	79830	85.66	10060	88.14	1577	89.2	319.1	76°C	
2.0	62.82	1.86E+07	68.44	2.41E+06	80.62	97940	85.34	12540	87.94	1968	89.2	399.4	δ	G* , Pa
2.5	63.42	2.15E+07	67.73	2.87E+06	80.1	1.21E+05	85.05	15220	87.75	2417	89.1	514.5	88.81	703.3
3.2	64.36	2.49E+07	67.04	3.41E+06	79.57	1.51E+05	84.74	18590	87.56	2979	89	651.6	88.81	706.7
4.0	65.4	2.87E+07	66.41	4.05E+06	79.04	1.86E+05	84.4	22820	87.31	3766	88.9	819.8		
5.0	66.62	3.32E+07	65.81	4.80E+06	78.55	2.24E+05	84.01	28480	87.05	4803	88.8	1038		
6.3	68.4	3.87E+07	65.17	5.61E+06	78.07	2.69E+05	83.58	35910	86.79	6063	88.6	1312		
7.9	70.92	4.51E+07	64.96	6.66E+06	77.58	3.24E+05	83.15	44670	86.53	7544	88.4	1663		
10.0	75.03	5.26E+07	64.18	7.75E+06	77.08	3.85E+05	82.71	55240	86.23	9436	88.2	2076		
12.6	76.59	5.94E+07	63.86	9.11E+06	76.5	4.61E+05	82.28	67460	85.94	11620	88.1	2578		
15.9	81.98	6.84E+07	63.53	1.07E+07	75.86	5.57E+05	81.84	81570	85.64	14350	87.9	3231		
20.0	85.62	8.10E+07	63.19	1.25E+07	75.17	6.74E+05	81.4	98440	85.3	17690	87.5	4070		
25.1	91.84	7.61E+07	63.71	1.42E+07	74.5	8.17E+05	80.89	1.21E+05	84.93	21780	87.1	5032		
31.6	97.97	9.73E+07	63.4	1.69E+07	73.77	9.91E+05	80.38	1.47E+05	84.51	26960	86.6	6302		
39.8	98.94	1.12E+08	62.58	1.96E+07	72.97	1.20E+06	79.75	1.77E+05	84	33560	85.9	7782		
50.1	78.33	9.08E+07	59.68	2.09E+07	71.93	1.44E+06	79.11	1.90E+05	83.43	41970	84.9	9746		
63.1	114.7	9.60E+07	66.58	2.56E+07	71.7	1.75E+06	78.5	1.75E+05	82.65	53160	82.9	12130		
79.4	110.8	4.28E+07	75.89	2.19E+07	71.85	2.05E+06	77.54	1.39E+05	81.69	65530	80.1	15150		
100.0	145.7	4.89E+07	91.58	3.14E+07	72.26	2.50E+06	75.99	1.07E+05	80.57	79160	75.7	18520		

OR238-C

Freq (Hz)	20°C		30°C		46°C		58°C		70°C		82°C		Freq @ 1.6 Hz	
	δ	G* , Pa	δ	G* , Pa										
0.1	50.61	5.56E+06	57.47	9.83E+05							88.5	171.5	40°C	
0.1	49.99	6.35E+06	56.85	1.14E+06							88.4	214.9	δ	G* , Pa
0.2	49.74	7.21E+06	56.35	1.31E+06							88.1	267.6	58.77	1.05E+06
0.2	49.33	8.16E+06	55.71	1.50E+06							87.8	337.7	58.77	1.05E+06
0.3	49.2	9.27E+06	55.29	1.72E+06							87.5	428.8	52°C	
0.3	49.23	1.05E+07	54.73	1.98E+06							87.1	537.4	δ	G* , Pa
0.4	49.21	1.19E+07	54.23	2.27E+06							86.8	675.5	67.26	1.64E+05
0.5	49.21	1.34E+07	53.78	2.60E+06							86.3	846	67.27	1.64E+05
0.6	49.42	1.52E+07	53.27	2.98E+06							85.8	1052	64°C	
0.8	49.64	1.71E+07	52.82	3.42E+06							85.4	1304	δ	G* , Pa
1.0	50.11	1.94E+07	52.47	3.91E+06	64.33	2.92E+05	72.69	45050	79.9	7932	85.1	1616	75.07	27730
1.3	50.51	2.19E+07	52.06	4.47E+06	63.75	3.44E+05	72.01	54480	79.22	9833	84.4	1996	75.07	27690
1.6	51.16	2.47E+07	51.71	5.11E+06	63.2	4.05E+05	71.34	65710	78.52	12030	83.9	2470	76°C	
2.0	52.11	2.79E+07	51.34	5.82E+06	62.64	4.77E+05	70.7	79110	77.85	14670	83.3	3070	δ	G* , Pa
2.5	53.12	3.15E+07	51.14	6.62E+06	62.1	5.60E+05	70.08	94960	77.19	17960	82.8	3764	81.41	5408
3.2	54.42	3.57E+07	50.94	7.52E+06	61.56	6.56E+05	69.5	1.13E+05	76.54	21930	82.2	4610	81.42	5390
4.0	55.92	4.05E+07	50.8	8.52E+06	61.04	7.68E+05	68.95	1.35E+05	75.91	26660	81.7	5719		
5.0	57.67	4.59E+07	50.69	9.66E+06	60.51	8.97E+05	68.37	1.60E+05	75.25	32050	81.1	7145		
6.3	59.82	5.23E+07	50.66	1.10E+07	60.02	1.05E+06	67.84	1.89E+05	74.36	38660	80.6	8729		
7.9	62.02	5.98E+07	50.68	1.24E+07	59.52	1.22E+06	67.3	2.25E+05	73.76	46590	80	10710		
10.0	67.49	6.95E+07	51.16	1.42E+07	59.06	1.41E+06	66.77	2.67E+05	73.27	55960	79.1	13170		
12.6	71.37	7.77E+07	50.08	1.60E+07	58.4	1.64E+06	66.21	3.16E+05	72.64	67390	78.3	16290		
15.9	73.35	8.80E+07	51.77	1.80E+07	58.08	1.90E+06	65.67	3.74E+05	72.22	80710	78	19700		
20.0	77.32	1.05E+08	51.71	2.04E+07	57.76	2.20E+06	65.18	4.43E+05	71.66	97570	77.2	23850		
25.1	83.14	9.57E+07	54.75	2.31E+07	57.13	2.55E+06	64.7	5.25E+05	71.04	1.17E+05	76.9	29470		
31.6	88.05	1.31E+08	52.92	2.66E+07	56.65	2.95E+06	64.12	6.19E+05	70.49	1.41E+05	76.8	36090		
39.8	86.8	1.44E+08	52.51	2.95E+07	56.2	3.39E+06	63.55	7.30E+05	69.98	1.70E+05	75.9	43620		
50.1	63.05	1.11E+08	49.82	3.02E+07	55.28	3.87E+06	62.99	8.57E+05	69.41	2.04E+05	75.4	52650		
63.1	107.2	1.18E+08	60.23	3.69E+07							74.6	63580		
79.4	102.9	4.62E+07	73.34	2.73E+07							74.6	78410		
100.0	145.9	6.68E+07	87.35	4.32E+07							74.7	92280		

OR99W-C

Freq (Hz)	20°C		30°C		46°C		58°C		70°C		82°C		Freq @ 1.6 Hz	
	δ	G* , Pa	δ	G* , Pa										
0.1	54.95	2.77E+06	62.57	4.15E+05	74.47	23350	82.11	3026	86.04	466.7	87.1	94.42	40°C	
0.1	54.61	3.07E+06	62.89	4.56E+05	73.75	28300	81.6	3695	85.81	575.3	87.2	117.4	δ	G* , Pa
0.2	54.14	3.51E+06	62.52	5.28E+05	73.08	34280	80.99	4536	85.43	720.8	87.2	146.1	63.49	5.15E+05
0.2	53.7	4.02E+06	62.05	6.14E+05	72.46	40990	80.36	5567	85.1	879.8	87.2	183.8	64.66	4.66E+05
0.3	53.25	4.59E+06	61.55	7.17E+05	71.87	48950	79.72	6950	84.77	1067	87.1	230.8	52°C	
0.3	52.88	5.26E+06	61	8.38E+05	71.32	58280	79.07	8482	84.43	1323	87	285.9	δ	G* , Pa
0.4	52.52	5.99E+06	60.44	9.79E+05	70.73	69910	78.45	10350	83.9	1712	86.8	357.3	70.97	80130
0.5	52.17	6.82E+06	59.86	1.14E+06	70.21	83610	77.82	12610	83.37	2194	86.7	448.1	71.33	76890
0.6	51.9	7.77E+06	59.26	1.34E+06	69.73	99320	77.2	15230	82.82	2776	86.4	562.8	64°C	
0.8	51.64	8.84E+06	58.7	1.56E+06	69.28	1.18E+05	76.6	18430	82.35	3361	86.1	699.4	δ	G* , Pa
1.0	51.44	1.01E+07	58.16	1.81E+06	68.92	1.38E+05	76.02	22130	81.86	4105	85.8	862.5	78.04	13840
1.3	51.33	1.14E+07	57.56	2.11E+06	68.57	1.61E+05	75.44	26740	81.39	4953	85.4	1077	78.02	13870
1.6	51.3	1.30E+07	56.99	2.45E+06	68.24	1.88E+05	74.83	32460	80.87	6034	85	1346	76°C	
2.0	51.36	1.47E+07	56.46	2.84E+06	67.93	2.18E+05	74.26	39320	80.36	7305	84.6	1660	δ	G* , Pa
2.5	51.52	1.66E+07	55.95	3.28E+06	67.64	2.52E+05	73.71	47480	79.78	9021	84.2	2061	83.12	2834
3.2	51.72	1.88E+07	55.48	3.78E+06	67.37	2.89E+05	73.21	56910	79.2	11110	83.7	2550	83.13	2821
4.0	51.81	2.11E+07	55.06	4.35E+06	67.13	3.22E+05	72.72	68040	78.58	13770	83.2	3177		
5.0	52.05	2.39E+07	54.66	5.02E+06	66.89	3.58E+05	72.21	82110	77.97	16940	82.8	3925		
6.3	52.42	2.71E+07	54.19	5.75E+06	66.57	4.09E+05	71.81	96840	77.45	20360	82.2	4905		
7.9	53.39	3.14E+07	53.76	6.61E+06	66.06	4.63E+05	71.4	1.15E+05	77	23980	81.7	6036		
10.0	55.74	3.61E+07	53.5	7.58E+06	65.44	5.44E+05	70.99	1.36E+05	76.46	28920	81.2	7323		
12.6	55.58	4.06E+07	53.68	8.75E+06	64.79	6.31E+05	70.68	1.57E+05	75.9	35320	80.7	8928		
15.9	56.86	4.60E+07	53.24	1.00E+07	64.16	7.34E+05	70.35	1.81E+05	75.35	42970	80.1	11000		
20.0	57.75	5.19E+07	53.01	1.15E+07	63.5	8.58E+05	69.97	2.10E+05	74.8	52190	79.6	13380		
25.1	65.23	5.72E+07	54.23	1.31E+07	62.9	1.01E+06	69.58	2.33E+05	74.25	63600	79	16390		
31.6	62.49	6.75E+07	53.12	1.50E+07	62.15	1.19E+06	69.16	2.51E+05	73.74	75520	78.3	20180		
39.8	61.34	7.44E+07	52.54	1.71E+07	61.47	1.40E+06	68.83	2.60E+05	73.31	86370	77.7	24460		
50.1	58.67	5.97E+07	51.89	1.78E+07	60.68	1.63E+06	68.35	2.63E+05	72.76	97750	76.9	29670		
63.1	72.8	8.35E+07	54.81	2.17E+07	60.28	1.89E+06	67.91	2.61E+05	72.19	1.06E+05	75.8	35640		
79.4	93.94	4.48E+07	66.67	2.04E+07	60.98	2.16E+06	67.22	2.56E+05	71.43	1.07E+05	74.4	42870		
100.0	125.8	5.65E+07	77.14	2.80E+07	61.08	2.57E+06	66.52	2.34E+05	70.21	1.02E+05	72.7	51700		

OR221-C

Freq (Hz)	20°C		30°C		46°C		58°C		70°C		82°C		Freq @ 1.6 Hz	
	δ	G* , Pa	δ	G* , Pa										
0.1	56.07	2.13E+06	64.57	3.12E+05	78.49	12910	84.8	1496	88.02	233.9	88.3	51.58	40°C	
0.1	65.07	1.36E+06	64.9	3.44E+05	77.58	16620	84.32	1875	87.87	293.7	88.3	65.16	δ	G* , Pa
0.2	61.85	2.01E+06	64.66	3.90E+05	77.13	18920	83.9	2290	87.7	359.7	88.4	82.53	65.61	3.61E+05
0.2	55.38	2.90E+06	64.17	4.52E+05	76.17	24560	83.43	2844	87.43	453.8	88.5	102.4	66.86	3.25E+05
0.3	53.83	3.48E+06	63.55	5.34E+05	75.41	29860	82.88	3602	87.14	588.6	88.5	127.2	52°C	
0.3	53.23	4.02E+06	62.88	6.29E+05	74.82	35080	82.31	4471	86.84	725.3	88.4	161.8	δ	G* , Pa
0.4	52.72	4.61E+06	62.19	7.42E+05	74.21	41640	81.76	5477	86.48	910.6	88.4	200	74.37	46620
0.5	52.25	5.26E+06	61.51	8.73E+05	73.6	49760	81.23	6656	86.14	1121	88.3	250.4	74.53	45760
0.6	51.86	6.00E+06	60.82	1.03E+06	72.96	59940	80.67	8085	85.74	1404	88.2	316.2	64°C	
0.8	51.47	6.82E+06	60.13	1.20E+06	72.3	72750	80.07	9920	85.31	1751	88	396.4	δ	G* , Pa
1.0	51.14	7.73E+06	59.46	1.41E+06	71.71	87480	79.45	12170	84.86	2183	87.8	491.1	81.38	7715
1.3	50.88	8.77E+06	58.81	1.64E+06	71.1	1.06E+05	78.8	15030	84.4	2701	87.5	614.5	81.39	7685
1.6	50.66	9.95E+06	58.18	1.90E+06	70.62	1.25E+05	78.14	18540	83.94	3324	87.2	770.2	76°C	
2.0	50.51	1.13E+07	57.56	2.21E+06	70.2	1.45E+05	77.52	22600	83.46	4072	86.9	953.9	δ	G* , Pa
2.5	50.44	1.28E+07	56.96	2.55E+06	69.81	1.68E+05	76.91	27380	82.93	5067	86.5	1201	85.81	1544
3.2	50.34	1.45E+07	56.39	2.94E+06	69.37	1.98E+05	76.31	33180	82.35	6366	86.1	1509	85.82	1540
4.0	50.44	1.64E+07	55.83	3.39E+06	68.9	2.37E+05	75.75	39620	81.8	7875	85.7	1874		
5.0	50.28	1.84E+07	55.29	3.90E+06	68.46	2.82E+05	75.16	47510	81.27	9602	85.3	2324		
6.3	50.37	2.09E+07	54.75	4.50E+06	68.11	3.26E+05	74.6	57130	80.77	11480	84.9	2878		
7.9	50.71	2.37E+07	54.21	5.18E+06	67.87	3.69E+05	74.03	68750	80.17	14150	84.4	3554		
10.0	52.31	2.73E+07	53.77	5.96E+06	67.47	4.27E+05	73.44	83400	79.57	17390	84	4394		
12.6	52.98	3.08E+07	53.57	6.88E+06	66.8	5.07E+05	72.9	1.00E+05	78.95	21440	83.5	5442		
15.9	52.68	3.46E+07	53.16	7.89E+06	66.13	6.04E+05	72.43	1.17E+05	78.33	26340	83	6717		
20.0	53.07	3.89E+07	52.75	9.02E+06	65.41	7.17E+05	71.99	1.36E+05	77.7	32150	82.5	8211		
25.1	57.26	4.17E+07	53.33	1.02E+07	64.74	8.50E+05	71.58	1.56E+05	77.15	38620	81.9	10040		
31.6	56.08	5.00E+07	52.45	1.18E+07	64	1.01E+06	71.13	1.80E+05	76.61	45670	81.2	12440		
39.8	54.95	5.54E+07	51.75	1.34E+07	63.21	1.20E+06	70.66	1.96E+05	76.01	54970	80.4	15380		
50.1	50.42	4.90E+07	50.04	1.43E+07	62.29	1.41E+06	70.17	1.91E+05	75.33	67270	79.6	18560		
63.1	67.59	6.43E+07	54.2	1.70E+07	62.12	1.67E+06	69.82	1.71E+05	74.64	81730	78.3	22670		
79.4	83.89	3.68E+07	61.79	1.58E+07	62.32	1.93E+06	69.04	1.46E+05	73.73	98540	76.3	27840		
100.0	114.5	5.61E+07	69.57	2.21E+07	62.57	2.31E+06	67.96	1.26E+05	72.85	1.16E+05	73.6	33890		

OR99EB-C

Freq (Hz)	20°C		30°C		46°C		58°C		70°C		82°C		Freq @ 1.6 Hz	
	δ	G* , Pa	δ	G* , Pa										
0.1	53.04	8.64E+06	57.77	1.63E+06	71.6	68370	80.38	7987	85.51	1120	87.8	191	40°C	
0.1	51.82	8.77E+06	57.55	1.75E+06	71.1	81600	79.63	10170	85.08	1414	87.8	235.3	δ	G* , Pa
0.2	50.54	1.03E+07	57.09	1.94E+06	70.39	99240	78.91	12450	84.66	1742	87.7	299.2	59.53	1.49E+06
0.2	50.41	1.18E+07	56.62	2.17E+06	69.95	1.14E+05	78.28	14950	84.21	2155	87.5	380.3	59.88	1.43E+06
0.3	50.27	1.34E+07	56.09	2.47E+06	69.38	1.35E+05	77.64	18050	83.74	2649	87.3	472.6	52°C	
0.3	50.35	1.52E+07	55.53	2.83E+06	68.76	1.62E+05	76.96	21980	83.26	3243	87	584.7	δ	G* , Pa
0.4	50.47	1.71E+07	55	3.25E+06	68.2	1.92E+05	76.26	26830	82.78	3985	86.8	725.2	68.37	2.13E+05
0.5	50.71	1.94E+07	54.46	3.74E+06	67.71	2.27E+05	75.56	32880	82.23	4933	86.5	903.9	69.04	1.99E+05
0.6	51.11	2.19E+07	53.98	4.31E+06	67.18	2.70E+05	74.89	40010	81.64	6163	86.1	1126	64°C	
0.8	51.56	2.47E+07	53.52	4.95E+06	66.73	3.20E+05	74.24	48340	81	7715	85.7	1417	δ	G* , Pa
1.0	52.2	2.78E+07	53.1	5.68E+06	66.37	3.76E+05	73.65	57910	80.35	9644	85.3	1776	75.82	34420
1.3	53.09	3.14E+07	52.75	6.49E+06	65.89	4.39E+05	73.09	68860	79.74	11840	84.8	2213	75.87	34260
1.6	54.2	3.54E+07	52.44	7.38E+06	65.33	5.15E+05	72.55	81580	79.19	14290	84.4	2742	76°C	
2.0	55.47	4.00E+07	52.17	8.38E+06	64.75	6.02E+05	72	97530	78.66	17040	83.9	3407	δ	G* , Pa
2.5	57.07	4.50E+07	51.97	9.47E+06	64.21	6.98E+05	71.47	1.17E+05	78.11	20550	83.4	4228	82.06	6122
3.2	58.98	5.09E+07	51.77	1.06E+07	63.66	8.10E+05	70.93	1.40E+05	77.49	25070	82.9	5212	82.03	6183
4.0	61.26	5.77E+07	51.69	1.20E+07	63.08	9.44E+05	70.42	1.68E+05	76.85	30880	82.4	6385		
5.0	63.64	6.49E+07	51.53	1.35E+07	62.47	1.11E+06	69.99	1.97E+05	76.2	37980	81.8	7802		
6.3	67.01	7.38E+07	51.55	1.52E+07	61.84	1.30E+06	69.55	2.32E+05	75.59	46340	81.3	9528		
7.9	70.02	8.37E+07	51.77	1.74E+07	61.22	1.53E+06	69.08	2.77E+05	75.06	55070	80.8	11690		
10.0	74.35	9.50E+07	52.34	1.96E+07	60.6	1.81E+06	68.64	3.28E+05	74.57	64740	80.2	14400		
12.6	81.3	1.06E+08	53.36	2.27E+07	59.93	2.13E+06	68.3	3.75E+05	74.07	77210	79.6	17790		
15.9	86.07	1.18E+08	53.08	2.57E+07	59.29	2.51E+06	67.92	4.27E+05	73.53	92120	78.9	21890		
20.0	89.73	1.29E+08	53.37	2.92E+07	58.67	2.94E+06	67.29	5.00E+05	72.97	1.11E+05	78.4	26400		
25.1	99.44	1.11E+08	57.1	3.21E+07	58.45	3.40E+06	66.73	5.87E+05	72.42	1.34E+05	77.8	31930		
31.6	104.1	1.52E+08	55.75	3.80E+07	57.67	3.97E+06	66.08	6.89E+05	71.87	1.58E+05	77.2	38660		
39.8	102.8	1.70E+08	55.1	4.25E+07	57	4.57E+06	65.39	8.13E+05	71.42	1.75E+05	76.5	46930		
50.1	73.42	1.23E+08	51.09	4.05E+07	55.89	5.16E+06	64.51	9.67E+05	70.94	1.83E+05	75.9	56760		
63.1	117.1	1.23E+08	65.04	5.09E+07	57	6.00E+06	64.15	1.15E+06	70.38	1.88E+05	75.2	67610		
79.4	108.8	4.59E+07	79.27	3.29E+07	59.9	6.43E+06	64.16	1.35E+06	69.52	1.84E+05	74.2	80150		
100.0	147.7	5.06E+07	108.3	4.82E+07	62.47	8.02E+06	64.24	1.62E+06	68.45	1.70E+05	73.2	94170		

OR140-C

Freq (Hz)	20°C		30°C		46°C		58°C		70°C		82°C		Freq @ 1.6 Hz	
	δ	G* , Pa	δ	G* , Pa										
0.1	55.25	3.15E+06	62.61	4.92E+05	74.03	25930	81.12	3471	85.82	528.9	87	103.9	40°C	
0.1	55.5	3.42E+06	62.5	5.49E+05	73.24	32280	80.46	4450	85.4	666.8	87.1	129.5	δ	G* , Pa
0.2	54.17	4.04E+06	61.98	6.47E+05	72.67	38050	79.83	5424	85.05	819.5	87.1	161.7	63.34	6.01E+05
0.2	53.69	4.65E+06	61.47	7.57E+05	72.09	45390	79.33	6424	84.65	1020	87.1	201.8	63.95	5.64E+05
0.3	53.27	5.33E+06	60.92	8.82E+05	71.46	54910	78.69	7945	84.17	1268	87	255.5	52°C	
0.3	52.9	6.10E+06	60.4	1.02E+06	70.89	65610	78.02	9841	83.71	1561	86.9	321.6	δ	G* , Pa
0.4	52.6	6.97E+06	59.87	1.18E+06	70.36	77960	77.36	12090	83.22	1918	86.6	403.1	70.51	90390
0.5	52.31	7.94E+06	59.3	1.37E+06	69.86	92620	76.74	14680	82.74	2358	86.4	500.1	70.72	88470
0.6	52.13	9.03E+06	58.79	1.59E+06	69.36	1.10E+05	76.15	17720	82.21	2906	86.1	618.7	64°C	
0.8	51.95	1.02E+07	58.27	1.83E+06	68.89	1.31E+05	75.56	21390	81.65	3625	85.7	765.8	δ	G* , Pa
1.0	51.87	1.15E+07	57.73	2.12E+06	68.45	1.55E+05	74.97	25880	81.04	4524	85.4	955.2	77.05	15670
1.3	51.89	1.31E+07	57.13	2.47E+06	68.02	1.84E+05	74.38	31490	80.47	5600	84.9	1193	76.99	15950
1.6	52.02	1.47E+07	56.63	2.87E+06	67.63	2.17E+05	73.81	38120	79.89	6885	84.5	1484	76°C	
2.0	52.25	1.67E+07	56.14	3.32E+06	67.28	2.57E+05	73.31	45330	79.36	8346	84	1851	δ	G* , Pa
2.5	52.63	1.89E+07	55.67	3.84E+06	66.87	3.08E+05	72.87	53110	78.84	10070	83.5	2299	82.33	3162
3.2	53.14	2.15E+07	55.23	4.44E+06	66.55	3.63E+05	72.38	63400	78.3	12210	83	2839	82.33	3168
4.0	53.78	2.43E+07	54.84	5.11E+06	66.23	4.20E+05	71.87	76490	77.74	14870	82.5	3485		
5.0	54.58	2.77E+07	54.52	5.90E+06	65.75	4.91E+05	71.35	92610	77.17	18160	82	4277		
6.3	55.17	3.17E+07	54.12	6.73E+06	65.28	5.73E+05	70.86	1.12E+05	76.6	22220	81.5	5271		
7.9	56.44	3.64E+07	53.86	7.71E+06	64.8	6.67E+05	70.42	1.34E+05	76.03	27120	80.9	6498		
10.0	57.86	4.10E+07	53.74	8.83E+06	64.28	7.81E+05	70.07	1.56E+05	75.51	32730	80.3	8005		
12.6	60.35	4.79E+07	53.39	1.01E+07	63.76	9.18E+05	69.74	1.80E+05	74.97	39620	79.8	9816		
15.9	62.66	5.38E+07	53.4	1.16E+07	63.21	1.08E+06	69.36	2.13E+05	74.47	47620	79.2	11920		
20.0	64.42	6.07E+07	53.34	1.32E+07	62.63	1.28E+06	68.78	2.66E+05	73.98	56930	78.7	14540		
25.1	72.17	6.51E+07	54.71	1.48E+07	62.17	1.51E+06	68.41	3.11E+05	73.5	67350	78.1	17700		
31.6	71.03	7.96E+07	53.94	1.73E+07	61.51	1.79E+06	68.12	3.44E+05	73.01	80660	77.5	21560		
39.8	70.28	8.86E+07	53.41	1.96E+07	60.83	2.10E+06	67.88	3.63E+05	72.5	96760	76.8	26400		
50.1	60.99	7.16E+07	51.42	2.05E+07	59.92	2.45E+06	67.51	3.81E+05	71.94	1.15E+05	76.1	32260		
63.1	87.28	8.94E+07	57.85	2.49E+07	60.19	2.88E+06	67.34	3.98E+05	71.42	1.30E+05	75.1	38860		
79.4	96.94	4.29E+07	68.1	2.17E+07	61.14	3.25E+06	67.24	4.03E+05	70.75	1.39E+05	73.9	46810		
100.0	133.6	5.20E+07	84.02	3.13E+07	62.35	3.92E+06	67.06	3.75E+05	69.88	1.36E+05	72.3	56200		

OR99*-C

Freq (Hz)	20°C		30°C		46°C		58°C		70°C		82°C		Freq @ 1.6 Hz	
	δ	G* , Pa	δ	G* , Pa										
0.1	51.94	4.43E+06	58.04	7.28E+05	69.37	40670	77.43	5399	83.38	821.7	86.5	174.8	40°C	
0.1	52.51	4.57E+06	58.41	7.96E+05	68.85	48480	76.8	6545	82.85	994.5	86.3	221.1	δ	G* , Pa
0.2	50.58	5.41E+06	57.95	9.23E+05	68.3	57190	76.07	8040	82.31	1257	86.1	275.6	59.4	8.30E+05
0.2	50.13	6.17E+06	57.45	1.07E+06	67.81	67290	75.5	9571	81.76	1549	85.7	347.8	60.14	7.64E+05
0.3	49.79	7.00E+06	56.97	1.23E+06	67.31	79600	74.86	11500	81.24	1877	85.4	436.7	52°C	
0.3	49.49	7.94E+06	56.45	1.42E+06	66.84	93940	74.21	13970	80.68	2299	85	544.5	δ	G* , Pa
0.4	49.29	8.98E+06	55.96	1.64E+06	66.35	1.11E+05	73.57	16930	80.13	2799	84.5	679.5	66.58	1.27E+05
0.5	49.11	1.02E+07	55.46	1.89E+06	65.92	1.31E+05	72.95	20470	79.53	3469	84.1	831.4	67.01	1.22E+05
0.6	49.05	1.15E+07	54.99	2.17E+06	65.5	1.55E+05	72.35	24640	78.85	4329	83.6	1016	64°C	
0.8	48.99	1.29E+07	54.52	2.49E+06	65.16	1.82E+05	71.8	29350	78.19	5387	83.1	1244	δ	G* , Pa
1.0	49.03	1.45E+07	54.03	2.86E+06	64.91	2.10E+05	71.28	34940	77.59	6553	82.6	1539	73.39	21280
1.3	49.19	1.63E+07	53.55	3.29E+06	64.65	2.42E+05	70.76	41620	77.01	7926	82.1	1909	73.4	21180
1.6	49.44	1.83E+07	53.14	3.78E+06	64.39	2.82E+05	70.24	49850	76.45	9531	81.5	2363	76°C	
2.0	49.72	2.06E+07	52.76	4.33E+06	64.12	3.29E+05	69.73	59970	75.98	11200	80.9	2914	δ	G* , Pa
2.5	50.17	2.31E+07	52.41	4.96E+06	63.91	3.82E+05	69.28	71300	75.39	13660	80.4	3563	79.35	4389
3.2	50.7	2.60E+07	52.1	5.67E+06	63.56	4.43E+05	68.91	83260	74.78	16780	79.8	4326	79.36	4371
4.0	51.22	2.91E+07	51.8	6.47E+06	63.05	5.21E+05	68.55	96940	74.18	20570	79.2	5320		
5.0	51.94	3.28E+07	51.81	7.38E+06	62.57	6.09E+05	68.17	1.14E+05	73.62	24940	78.7	6481		
6.3	52.74	3.70E+07	51.29	8.39E+06	62.07	7.13E+05	67.79	1.36E+05	73.1	29880	78.2	7769		
7.9	54.03	4.16E+07	51.13	9.54E+06	61.59	8.35E+05	67.44	1.61E+05	72.61	35720	77.7	9338		
10.0	55.4	4.83E+07	51.14	1.09E+07	61.04	9.80E+05	67.13	1.88E+05	72.14	42320	77.1	11330		
12.6	56.66	5.27E+07	51.04	1.23E+07	60.58	1.15E+06	66.85	2.18E+05	71.76	49260	76.5	13840		
15.9	60.89	6.09E+07	51.06	1.40E+07	60.02	1.34E+06	66.55	2.55E+05	71.31	58940	76	16600		
20.0	61.63	6.77E+07	50.96	1.58E+07	59.45	1.58E+06	66.25	2.96E+05	70.81	71030	75.5	19680		
25.1	67.14	6.89E+07	52.43	1.75E+07	59.06	1.85E+06	66.04	3.36E+05	70.34	85550	75	23620		
31.6	67.8	8.83E+07	51.73	2.03E+07	58.41	2.17E+06	65.82	3.64E+05	69.89	1.01E+05	74.4	28650		
39.8	66.38	9.72E+07	51.19	2.29E+07	57.79	2.54E+06	65.58	3.95E+05	69.53	1.17E+05	73.8	34480		
50.1	54.78	7.71E+07	48.83	2.36E+07	56.95	2.92E+06	65.08	4.50E+05	69.09	1.33E+05	73.2	41630		
63.1	88.86	9.24E+07	57.57	2.85E+07	57.3	3.42E+06	64.65	5.27E+05	68.75	1.44E+05	72.5	48900		
79.4	91.27	4.34E+07	65.39	2.35E+07	58.54	3.81E+06	64.39	6.13E+05	68.23	1.52E+05	71.5	58380		
100.0	131.7	5.65E+07	83.42	3.51E+07	59.91	4.57E+06	64.25	7.21E+05	67.64	1.49E+05	70.2	69240		

APPENDIX E-CORE PICTURES OF TOP-DOWN CRACKED SECTIONS

OR238: Beg. Div. Hwy-JCT Hwy 063



OR221:N. Salem-Orchard Heights







OR 99W: Brutscher St-JCT Hwy 151







OR99: Junction City Section 1 (cracked)







OR140: Aspen Lake R-Boat Landing







APPENDIX F-CORES INFORMATION OF VISUAL OBSERVATION

OR238: Beg. Div. Hwy-JCT Hwy 063

<i>Cores Info</i>									
Cores No.	MP	Thickness (in)	Drilled on Crack	Comment				Avg. Thickness and Standard deviation	
1	38.148	8	Trans.	Cracking from top-down and upper 5 1/4" is delam				8.5" and 0.448"	
2	38.153	8.5	No	Upper 5 1/2" is delam					
3	38.16	8	Trans. And Long.						
4	38.163	8.25	No						
5	38.167	9	Long.						
6	38.17	9.25	No	Upper 2 1/2" is delam					
7	38.18	8.75	Long.	Upper 5 1/2" is delam					
8	38.183	8.25	No.	Upper 5 1/2" is delam					
9	38.191	8	Long.						
10	38.192	8.75	Trans.	Cracking from top-down and upper 5 1/2" is delam					

US97: NW Wimp Way-Terrebonne

<i>Cores Info</i>									
Cores No.	MP	Thickness (in)	Drilled on Crack	Comment				Avg. Thickness and Standard deviation	
1	114.355	8	No					8.35" and 1"	
2	114.364	8	No						
3	114.388	7	No						
4	114.402	9.25	No						
5	114.426	9.5	No						

US20: NE 11th ST-Purcell Blvd

<i>Cores Info</i>									
Cores No.	MP	Thickness (in)	Drilled on Crack	Comment				Avg. Thickness and Standard deviation	
1	1.835	9.5	No.					9.9" and 0.224"	
2	1.821	10	No.						
3	1.812	10	No.						
4	1.802	10	No.						
5	1.783	10	No.						

OR221:N. Salem-Orchard Heights

<i>Cores Info</i>									
Cores No.	MP	Thickness (in)	Drilled on Crack	Comment					Avg.Thickness and Standard deviation
1	18.595	9.5	Through Patch						8.63" and 0.637"
2	18.595	9.5	No.	Upper 2" is Delam					
3	18.61	9	Long.						
4	18.61	8.75	No.						
5	18.64	8.75	No.						
6	18.641	8.5	Long.	Delam in three parts (Upper 2" Middle 2-5" Lower 5-8.5")					
7	18.648	8.75	No.						
8	18.6485	8	Trans.	Cracking from top-down					
9	18.666	7.75	No.	Upper 2" is Delam					
10	18.667	7.75	Long.	Upper 2" is Delam					

OR22: Sublimity Intchg Sect (RW2-WB)

<i>Cores Info</i>									
Cores No.	MP	Thickness (in)	Drilled on Crack	Comment					Avg.Thickness and Standard deviation
1	13.079	10	No.	Upper 7" is Delam					9.55" and 0.326"
2	13.065	9.25	No.						
3	13.05	9.5	No.	Upper 6.5" is Delam					
4	13.036	9.75	No.	Upper 6" is Delam					
5	13.021	9.25	No.	Upper 6 1/4" is Delam					

OR 99W: Brutscher St-JCT Hwy 151

<i>Cores Info</i>									
Cores No.	MP	Thickness (in)	Drilled on Crack	Comment					Avg.Thickness and Standard deviation
1	22.248	12.75	Long.	Upper 8 3/4" is Delam					12.75" and 0.640"
2	22.249	12.75	No.	Upper 8 3/4" is Delam					
3	22.253	13	Long.	Delam in three parts (Upper 11 1/2" Middle 13 1/4-8 1/4" Lower 9 1/2-13")					
4	22.262	13.5	No.	Upper 9" is Delam					
5	22.268	12	Long.	Upper 4" (cracked and broken) is Delam					
6	22.268	12.5	No.	Upper 7" is Delam					
7	22.282	12.5	Long.						
8	22.286	12.25	No.						
9	22.299	12	Trans.	Upper 8 1/4" is Delam					
10	22.311	14	Long.						

OR99: Junction City Section 1 (cracked)

<i>Cores Info</i>									
Cores No.	MP	Thickness (in)	Drilled on Crack	Comment				Avg. Thickness and Standard deviation	
1	109.06	9	Trans.	Top-down and upper 2 1/2" (cracked and broken) is Delam				8.93" and 0.355"	
2	109.06	9.25	No.						
3	109.055	9.25	No.	Upper 2 1/2" is Delam					
4	109.054	8.5	Trans. And Long.	Upper 2" (cracked and broken) is Delam					
5	109.043	8.75	No.	Upper 2 1/4" is Delam					
6	109.035	8.5	Trans.	Top-down and Delam in three parts (Upper 2" Middle 2-4" Lower 4-8 1/2")					
7	109.033	8.5	Long.	Delam in three parts (Upper 2" (cracked and broken) Middle 2-4" Lower 4-8 1/2")					
8	109.025	9.5	Long.	Upper 2" is Delam					
9	109.016	9	Trans.	Top-down and upper 2" (cracked and broken) is Delam					
10	109.016	9	No.	Upper 2" is Delam					

OR99: Junction City Section1 (uncracked)

<i>Cores Info</i>									
Cores No.	MP	Thickness (in)	Drilled on Crack	Comment				Avg. Thickness and Standard deviation	
1	108.85	9.25	No.					10" and 1.744"	
2	108.85	9.75	No.						
3	108.859	8.5	No.						
4	108.908	12.5	No.						

OR140: Aspen Lake R-Boat Landing

<i>Cores Info</i>									
Cores No.	MP	Thickness (in)	Drilled on Crack	Comment					Avg. Thickness and Standard deviation
1	53.6	9.25	Long.	Upper 13/4" is Delam					9.50" and 0.275"
2	53.6	9.5	No.						
3	53.621	9.44	Long.						
4	53.621	9.5	No.						
5	53.641	9.5	Long.	Upper 2" is cracked and broken					
6	53.641	9.5	No.						
7	53.662	10	Long.						
8	53.662	9.75	No.						
9	53.676	9.25	Long.						
10	53.676	9	No.						

OR99EB: JCT Hwy 001-Comm. ST.

<i>Cores Info</i>									
Cores No.	MP	Thickness (in)	Drilled on Crack	Comment					Avg. Thickness and Standard deviation
1	2.013	6.5	Trans.	Top-down; Total Thickness 16.75" with CTB at bottom and upper 4.5" is Delam					8.2" and 0.880"
2	2.012	8	No.	Total Thickness 16.25" with CTB at bottom					
3	2.006	7.5	Trans.	Top-down; Total Thickness 13" with CTB at bottom and upper 4" is Delam and lower AC portion is (cracked and broken) Delam...Cracking in the lower portion of AC comes from the CBT (Reflective cracking from CBT)					
4	2.003	7.5	Long.	CBT at Bottom					
5	2.003	8	No.	CBT at Bottom and upper 4.5" is Delam					
6	1.994	8.5	Long.	CBT at Bottom and upper 4" is Delam					
7	1.993	9	No.	CBT at Bottom and upper 4" is Delam					
8	1.974	8.75	No.	CBT at Bottom					
9	1.974	9.5	Trans.	Cracking started from the top and going down to lower lift and in the lowr part of AC there is crcaking reflecting from CBT....the whole core is cracked and broken into pieces...					
10	1.975	8.75	No.	CBT at bottom and upper 2" is Delam					